TECHNISCHE UNIVERSITÄT WIEN

DISSERTATION

Predictive energy management of fuel cell vehicles with robustness against uncertainties

submitted for the degree of
DOCTOR TECHNICAE (DR.TECHN.)
at the
FACULTY OF MECHANICAL AND INDUSTRIAL ENGINEERING
of
TECHNISCHE UNIVERSITÄT WIEN
by

Sandro Kofler
Matriculation number: 01326082

Vienna, September 19, 2025

Sandro Kofler

This work was supported in part by the Climate and Energy Fund within the framework of the research projects *FC-IMPACT* and *FC4HD* and in part by the TU Wien Bibliothek within the framework of its Open Access Funding Program.

I confirm that the printing of this thesis requires the approval of the examination board.

Affidavit

I declare in lieu of oath that I wrote this thesis and carried out the associated research myself, using only the literature cited in this work. If text passages from sources are used literally, they are marked as such.

I confirm that this work is original and has not been submitted for examination elsewhere, nor is it currently under consideration for a thesis elsewhere.

I acknowledge that the submitted work will be checked using suitable state-of-the-art means (plagiarism detection software). On the one hand, this ensures that the submitted work was prepared according to the high-quality standards within the applicable rules to ensure good scientific practice at the TU Wien ("Code of Conduct"). On the other hand, a comparison with other student theses avoids violations of my personal copyright.

Vienna, September 19, 2025

Sandro Kofler

You may not control all the events that happen to you,
but you can decide not to be reduced by them.

Maya Angelou (1928–2014)

Abstract

The energy management strategy of a fuel cell vehicle is responsible for the power allocation between the fuel cell system (FCS) and a battery. The optimal power allocation strongly depends on the trip, which is why predictive information is highly valuable for an energy management strategy. In particular, long-term predictions that cover the entire trip allow for significant improvements in fuel efficiency. However, the accuracy of such long-term predictions is limited because of numerous influences that are inevitable in real-world driving, such as traffic, driver behavior, and weather.

This dissertation proposes a predictive energy management concept that is specifically designed to handle these uncertainties. The results are close-to-optimal fuel efficiency and increased FCS durability. The concept follows a two-stage approach: First, the long-term prediction is processed in an offline optimization before departure, which yields predictive control information. Then, a real-time strategy determines the power allocation considering the predictive control information while driving. The distinctive feature of the proposed concept is that the predictive control information is provided in the form of a map that expresses the optimal cost-to-go, i.e., the minimum amount of fuel required to reach the destination, as a function of the covered distance and the battery state of charge. Two real-time strategies that follow the cost-to-go-based concept are proposed.

The first strategy is based on the equivalent consumption minimization strategy (ECMS). The cost-to-go-based design allows the ECMS to adapt continuously to the actual conditions, which may considerably deviate from the long-term prediction. In this way, the ECMS is robust against unpredicted disturbances and achieves close-to-optimal fuel efficiency. In addition, a predictive fuel cell stack start/stop strategy is proposed. It is seamlessly integrated into the cost-to-go-based ECMS and exploits the long-term prediction to robustly minimize the number of stack starts/stops, which cause harmful operating conditions. As a result, the proposed start/stop strategy mitigates FCS degradation and increases its durability. The second strategy is based on model predictive control (MPC) and additionally considers accurate short-term predictions that are updated in real time. The short-term predictions allow the MPC-based strategy to reduce the dynamic load on the FCS and the associated degradation while preserving the efficiency benefits of the cost-to-go-based energy management.

The proposed energy management concept is complemented with an extensive experimental evaluation that validates the effectiveness of long-term predictions for improving fuel efficiency. The evaluation was conducted with a real fuel cell vehicle and focused on real-world driving on public roads. It revealed significant reductions in fuel consumption of more than 6 % compared to a nonpredictive strategy.

Kurzfassung

Die Energiemanagementstrategie eines Brennstoffzellenfahrzeugs ist für die Lastaufteilung zwischen dem Brennstoffzellensystem (FCS) und einer Batterie verantwortlich. Die optimale Lastaufteilung hängt stark von der Fahrt ab, weshalb Vorhersagen äußerst nützlich für das Energiemanagement sein können. Insbesondere Langzeitvorhersagen, die die gesamte Fahrt abdecken, ermöglichen eine erhebliche Verbesserung der Kraftstoffeffizienz. Allerdings ist die Genauigkeit solcher Langzeitvorhersagen aufgrund zahlreicher Einflüsse wie Verkehr, Fahrerverhalten und Wetter, die im realen Fahrbetrieb unvermeidbar sind, eingeschränkt.

Diese Dissertation führt ein prädiktives Energiemanagementkonzept ein, das speziell für den Umgang mit diesen Unsicherheiten ausgelegt ist. Dadurch werden eine nahezu optimale Kraftstoffeffizienz und eine Verlängerung der Lebensdauer des FCS erreicht. Das Konzept baut auf einem zweistufigen Ansatz auf: Zuerst wird die Langzeitvorhersage in einer Offline-Optimierung vor der Abfahrt verarbeitet. Daraus ergibt sich prädiktive Information, die dann von der Echtzeit-Strategie während der Fahrt berücksichtigt wird. Die Besonderheit des vorgestellten Konzepts besteht darin, dass die prädiktive Information in Form eines Kennfelds bereitgestellt wird. Das Kennfeld beschreibt die sogenannte optimale „Cost-to-go“, d. h. die benötigte Menge an Kraftstoff zum Erreichen des Ziels, in Abhängigkeit von der zurückgelegten Distanz und dem Ladezustand der Batterie. Zwei Echtzeit-Strategien, die auf dem Cost-to-go-Konzept aufbauen, werden vorgestellt.

Die erste Strategie basiert auf der „Equivalent Consumption Minimization Strategy“ (ECMS). Das Cost-to-go-basierte Design ermöglicht der Strategie eine kontinuierliche Anpassung an die tatsächlichen Bedingungen, die erheblich von der Langzeitvorhersage abweichen können. Dadurch ist die Strategie robust gegen unvorhergesehene Störungen und erreicht nahezu optimale Kraftstoffeffizienz. Darüber hinaus wird eine prädiktive Start/Stopp-Strategie für das FCS eingeführt. Sie ist nahtlos in die Cost-to-go-basierte ECMS integriert und nutzt die Langzeitvorhersage aus, um die Anzahl von schädlichen Start/Stopp-Vorgängen robust zu minimieren. Damit wird die Degradation des FCS reduziert und dessen Lebensdauer verlängert. Die zweite Strategie basiert auf einem modellprädiktiven Regler (MPC), der zusätzlich genaue Kurzzeitvorhersagen berücksichtigt. Dies erlaubt es dem MPC die dynamische Beanspruchung des FCS und die damit verbundene Degradation zu reduzieren, wobei die Effizienzvorteile des Cost-to-go-basierten Energiemanagements erhalten bleiben.

Das Konzept wird durch eine umfassende experimentelle Untersuchung ergänzt, die die Wirksamkeit von Langzeitvorhersagen zur Steigerung der Kraftstoffeffizienz bestätigt. Die Untersuchung wurde mit einem echten Brennstoffzellenfahrzeug durchgeführt und fokussierte sich auf den realen Fahrbetrieb im öffentlichen Verkehr. Das Ergebnis ist eine signifikante Senkung des Kraftstoffverbrauchs um mehr als 6 % im Vergleich zu einer nicht-prädiktiven Strategie.

Contents

List of figures xii

List of tables xiii

Nomenclature xiv

1 Overview 1
- 1.1 Motivation . . . 1
- 1.2 State of the art . . . 2
- 1.3 Objectives . . . 4
- 1.4 Scientific approach and outline . . . 5
- 1.5 Methodology . . . 8
  - 1.5.1 Control-oriented modeling . . . 8
  - 1.5.2 Cost-to-go-based predictive energy management . . . 11
  - 1.5.3 Minimization of stack start/stop actions . . . 17
  - 1.5.4 Combination of long-term and short-term predictions . . . 21
  - 1.5.5 Experimental validation with a real vehicle . . . 27
- 1.6 Scientific contributions . . . 30

Bibliography 33

2 Publications 39
- 2.1 Publication A . . . 41
- 2.2 Publication B . . . 49
- 2.3 Publication C . . . 63
- 2.4 Publication D . . . 75

List of scientific publications 89

List of figures

1 Schematic illustration of two-stage energy management showing alternatives of predictive control information and three different real-time EMSs 7
2 Hybrid powertrain consisting of the FCS, battery, traction motor, and auxiliary systems 9
3 Stack fuel consumption curve and the corresponding efficiency curve . . . 10
4 Optimal cost-to-go map and equivalence factor map resulting from the offline optimization of a long-term prediction 14
5 Comparison of the cost-to-go-based P-ECMS with the A-ECMS based on a real-world driving mission 16
6 Demonstration of the map-based start/stop control for a vehicle with a single-stack FCS 19
7 MPC combining the short-term prediction with the optimal cost-to-go . . 23
8 Typical profiles of the optimal cost-to-go and its partial derivative with respect to the SoC 25
9 Comparison of the equivalent number of FCS load cycles and the fuel consumption as a function of the short-term prediction horizon length . . 26
10 Experimental validation of the predictive SoC reference tracking with a fuel cell demonstrator vehicle of AVL List GmbH 27
11 Results of the experimental validation on the dynamometer testbed . . . 29

List of tables

1 Comparison of the map-based start/stop control with two benchmark methods. 21

Nomenclature

Abbreviations

A-ECMS	Adaptive ECMS
Alt.	Altitude
AS	Auxiliary systems
DP	Dynamic programming
ECMS	Equivalent consumption minimization strategy
EMS	Energy management strategy
FCS	Fuel cell system
M	Traction motor
MPC	Model predictive control(ler)
P-ECMS	Predictive ECMS
RP	Research problem
SoC	State of charge

Superscripts

$*$	Optimal
curr	Current
final	Final
idle	Idle limit
ind	Indication of map
init	Initial
max	Maximum
min	Minimum
prev	Previous

Greek letters

γ_0, γ_1	Parameters of cost-to-go model
ΔP_{st}	Stack power increment
Δt	DP sampling interval
δ	Correction coefficient of rotating mass
$\bar{\eta}_{\mathrm{FCS}}$	Mean FCS efficiency
η_{m}	Traction motor efficiency
θ	Road inclination angle
λ	Equivalence factor
$\bar{\lambda}$	Adapted equivalence factor
λ_{ad}	Adaption parameter
ξ	Battery SoC
ξ_{th}	SoC constraint threshold
ρ	Air density

Latin letters

A_{f}	Vehicle frontal area
c_{d}	Aerodynamic drag coefficient
c_{r}	Rolling friction coefficient
f	Battery SoC dynamics
g	Gravitational acceleration
H	Equivalent fuel consumption rate
H_{i}	Lower heating value of hydrogen
I_{b}	Battery current
J	Cost-to-go
$\hat{J}^*$	Optimal cost-to-go model
k	Index of current instant in MPC
L	Number of time grid points in DP
m	Vehicle mass
$\dot{m}_{\mathrm{FCS}}$	FCS fuel consumption rate
$\hat{\dot{m}}_{\mathrm{FCS}}$	Approximated FCS fuel consumption rate
$\dot{m}_{\mathrm{st}}$	Stack fuel consumption rate

$\dot{m}_\Omega$	Virtual fuel consumption rate for battery losses
N_{eq}	Equivalent number of FCS load cycles
N_{st}	Number of stacks
N_{p}	Number of samples in short-term prediction horizon
n_{st}	FCS state (number of active stacks)
$\mathcal{N}$	Set of possible FCS states
P_{aux}	Auxiliary power demand
P_{b}	Battery power
P_{el}	Electric power demand
P_{FCS}	FCS power
$\boldsymbol{P}_{\mathrm{FCS}}$	FCS power sequence in MPC
P_{m}	Traction motor power
P_{st}	Stack power
p	Start/stop penalty
$\mathcal{P}$	Feasible stack power range
Q_0	Battery capacity
R_{int}	Internal ohmic resistance
s	Position (covered distance)
T_{s}	MPC sampling time
t	Time
u_{st}	FCS state in next instant
V_{b}	Battery voltage
V_{OC}	Open-circuit voltage
v	Vehicle velocity
x_{st}	Current FCS state

Chapter 1

Overview

Predictions derived from static information along a planned route are highly valuable for improving the fuel efficiency of fuel cell vehicles. However, such predictions have only limited accuracy, and deviations from the actual conditions must be expected. This work proposes a predictive energy management concept that is specifically designed to deal with these uncertainties. The result is improved robustness, which benefits not only fuel efficiency but also the durability of the fuel cell system (FCS).

The findings are presented in the form of a cumulative dissertation. This chapter first provides an overview of the state of the art, specifies the objectives, and outlines the methodology of the proposed concept. Chapter 2 then consists of four full-length research articles that elaborate on the methods and an experimental validation in detail.

1.1 Motivation

The electrification of vehicles is one of the keys to the decarbonization of the transport sector. In this regard, it is encouraging that the market share of battery electric vehicles has steadily increased in recent years, particularly in the area of passenger vehicles [1]. While battery electric vehicles impress with their high energy efficiency [2], they cannot cover all areas of transport at this time [3, 4]. Especially when it comes to heavy loads and long trip distances, which are typical for long-haul freight transportation, hydrogen fuel cell technology provides a wider range of feasibility because of the high gravimetric energy density of hydrogen and the capabilities for fast refueling and higher payloads [5, 6, 7, 8]. Moreover, hydrogen is a suitable storage for intermittent renewable energy sources, which can help to avoid excessive stress on the electrical grid [9, 10]. Therefore, fuel cell vehicles are an excellent complement to purely battery-powered vehicles.

Fuel cell vehicles are commonly equipped with a hybrid powertrain consisting of the FCS and a battery. The battery is necessary for covering fast changes in the power demand, which are characteristic in automotive applications. Additionally, the battery offers the possibility to increase fuel efficiency by avoiding inefficient operating ranges of the FCS and recuperating braking energy. However, the actual performance in terms

of fuel efficiency strongly depends on the energy management strategy (EMS), which determines the power allocation between the two powertrain components. The optimal power allocation is driving mission-specific. Therefore, the performance of an EMS can be improved if predictions of the driving mission are available in advance. To achieve significant improvements in fuel efficiency, long prediction horizons that allow the EMS to schedule the use of battery energy throughout the trip are necessary.

1.2 State of the art

Various approaches have been proposed to benefit from long-term predictive information. At a basic level, predictive EMSs simply consider the length of the planned trip. While this information is advantageous for evenly discharging the battery in plug-in hybrid vehicles [11, 12], it does not allow for the specific adaptation of the use of battery energy to the driving mission. For this purpose, a prediction of the power demand is required. Simple power demand predictions can be derived from readily available static route information, such as the altitude profile, speed limits, and average segment speeds, if the route is determined in advance [13]. While such predictions are typically inaccurate, they provide the long prediction horizons required to actively involve the battery in the energy management.

Two-stage energy management schemes have shown to be an effective way for considering long-term power demand predictions. First, a reference trajectory for the battery state of charge (SoC) is optimized based on the long-term prediction before departure. Then, a suitable real-time EMS determines the power allocation such that the optimized SoC reference is tracked while driving. Computationally simple real-time methods directly determine the power allocation with control laws [14], logic rules [15], or fuzzy logic controllers [16] to track the optimized SoC reference. A well-established alternative for the real-time control is the optimization-based equivalent consumption minimization strategy (ECMS), which can be adapted to provide SoC reference tracking capabilities. For this purpose, a proportional-integral controller that considers the SoC feedback is used to determine the so-called equivalence factor [17, 18], which expresses a virtual fuel consumption for the use of battery energy and plays a central role in the ECMS.

Real-time EMSs can also be informed with short-term predictions that are updated in real time. Although their prediction horizon, typically in the range of tens of seconds, is too short to enable an active use of the battery, short-term predictions are interesting for preparing the energy management for upcoming transients, provided that they are accurate. Therefore, emerging prediction technologies that consider vehicle-to-vehicle and vehicle-to-infrastructure communication are particularly interesting for this task [19, 20, 21]. Besides current and past states of the own vehicle, the communication provides access to data of the traffic environment, e.g., the velocities of preceding vehicles, allowing for significant improvements in the prediction accuracy [22]. To include

short-term predictions in the two-stage energy management scheme, ECMS-based methods that continuously optimize the equivalence factor to ensure predictive SoC reference tracking have been proposed [23, 24, 25]. Another common approach is model predictive control (MPC), where the power allocation is determined such that an objective function, usually expressing fuel consumption or degradation, is minimized within the short-term horizon while tracking the SoC reference [26, 27, 28]. A particular advantage of MPC is that it allows for predictive consideration of powertrain constraints. In either case, however, the short prediction horizons may be too restrictive to considerably benefit from the improved accuracy when short-term predictions are combined with optimized SoC reference trajectories.

Tracking optimized SoC reference trajectories to consider long-term predictive information, with or without the inclusion of short-term predictions, has another drawback: The performance strongly depends on the accuracy of the long-term prediction, which is limited due to random disturbances that are inevitable in real-world driving, such as traffic, driver behavior, and weather. Tracking the optimized SoC reference provokes suboptimal behavior, which affects fuel efficiency in sections where the long-term prediction deviates from the actual conditions. A possible solution to this issue is an MPC that extends the prediction horizon until the end of the trip instead of tracking an optimized SoC reference [29]. However, the long prediction horizon can imply computational challenges for the real-time capability. An interesting alternative is replacing the optimized SoC reference trajectory with a map expressing the so-called optimal cost-to-go as the carrier of predictive information [30, 31, 32]. The optimal cost-to-go map describes the minimum fuel amount required to reach the destination as a function of the covered distance and the battery SoC. Thus, it provides information in the entire distance-SoC space and not just along an optimal path, which facilitates adaptions in the case of disturbances. However, cost-to-go-based approaches have only been proposed for conventional hybrid vehicles with internal combustion engines so far.

In addition to the power allocation between the FCS and the battery, an EMS must also decide on fuel cell stack shutdowns. Stack shutdowns are crucial to avoid overcharging the battery or wasting precious energy in driving missions with low or negative power demand, such as in urban areas or when descending. However, each stack start/stop event causes harmful operating conditions [33, 34, 35], which is why it is desirable to keep the number of starts/stops low. In the literature, fuel cell stack start/stop control can basically be divided into two groups: instantaneous methods [36, 37] and methods based on short-term predictions [38, 39]. Because instantaneous strategies alone cannot prevent infeasibly frequent start/stop events, they are usually combined with a minimum hold time for the stack state [38, 15] or a hysteresis [40, 41]. Nevertheless, neither these measures nor short-term predictions can reliably prevent inefficient start/stop actions, e.g., performing a stack shutdown shortly before entering a high-power section. Studies that investigated the optimal energy management of driving cycles with known power demand profiles successfully minimized the number of starts/stops by considering penalties for start/stop actions [42, 43], indicating that an optimization based on

the long-term prediction could be a solution here. However, blindly realizing real-time start/stop actions at the optimal positions according to the long-term prediction can provoke severe performance deterioration and infeasible operation in the presence of any uncertainties. Strategies that robustly exploit long-term predictions to minimize the number of starts/stops are not available.

Another important aspect due to the limited accuracy of long-term predictions is the actual performance benefit of predictive EMSs in practice. Considerable improvements thanks to long-term predictions have been demonstrated in simulation studies, but simulations can never fully replicate reality. More significant experimental evaluations with real vehicles are rare in the literature and focus on nonpredictive strategies [44, 45, 46, 47] and short-term predictive MPC [48]. The performance benefit of long-term predictions exploited in a two-stage scheme has not yet been validated in practical tests with real vehicles.

This concise overview of the state of the art reveals open research issues. First, the fuel efficiency of the established two-stage energy management approach, which is based on optimized SoC reference trajectories, suffers if the long-term prediction deviates from the actual conditions. Second, accurate short-term predictions from emerging intelligent transportation systems do not develop their full potential when combined with SoC reference trajectories. Third, current stack start/stop strategies cannot prevent inefficient start/stop actions that cause avoidable FCS degradation. Fourth, the performance benefit of exploiting long-term predictions remains unanswered in the real-world application.

1.3 Objectives

The overall objective of this work is to **exploit predictive information for the energy management of fuel cell vehicles to increase their fuel efficiency and durability**. This objective is translated into four research problems (RPs) that address the identified research gaps and are elaborated in the following:

RP.1 Robust exploitation of long-term predictions

How to exploit route-derived long-term predictions with limited accuracy in order to maximize fuel efficiency?

Predictions derived from static route information are easily available and cover the entire planned driving mission. However, their accuracy is limited due to various random influences, such as traffic, that are inevitable in the application. How can such long-term predictions be considered in the energy management to robustly maximize fuel efficiency?

RP.2 Minimization of the number of fuel cell stack starts/stops

How to use long-term predictions to minimize the number of fuel cell stack start/stop events while ensuring robustness?

Fuel cell stack start/stop events cause harmful operating conditions. In order to limit the associated degradation of the fuel cell stack, the number of start/stop events must be kept low. How can route-derived long-term predictions be exploited for this purpose while ensuring robustness and feasible operation?

RP.3 Consideration of short-term predictions

How to improve the energy management performance if accurate short-term predictions are available in addition to the long-term prediction?

Intelligent transportation systems offer the possibility to obtain accurate short-term predictions that are updated in real time. How can these short-term predictions be combined with the long-term prediction to improve the performance further?

RP.4 Experimental validation

Can significant improvements in fuel efficiency be achieved in the typical real-world application by considering long-term predictions?

As mentioned above, route-derived long-term predictions are affected by various random disturbances in the real-world application. Are significant improvements in fuel efficiency nevertheless possible?

1.4 Scientific approach and outline

Addressing the research problems specified above, this work proposes a predictive energy management concept for fuel cell vehicles. The scientific approach of the concept is outlined through its key elements below:

- **Route-derived long-term prediction:** Planning the route of a driving mission before departure gives access to static route information, i.e., legal speed limits and the altitude profile along the route. Based on this predictive information, a long-term prediction of the power demand can be derived. Such a prediction is highly valuable for the predictive energy management because it covers the entire driving mission and is available before departure.

- **Two-stage energy management:** Assuming that the route-derived long-term prediction is not updated while driving, the predictive energy management can be divided into two stages (see Fig. 1): (i) The long-term prediction is processed in an offline optimization before departure, yielding predictive control information for the real-time control. (ii) While driving, the real-time EMS determines the power allocation between the FCS and the battery considering the predictive control information and system measurements.

- **Optimal control methods:** Optimal control theory plays a crucial role in the exploitation of the available predictive information with respect to predefined objectives. Corresponding methods are applied in the offline optimization before departure as well as in the real-time energy management.

- **Control-oriented modeling:** The optimization-based methods rely on dynamic models of the vehicle and its powertrain. Simplified models focusing on the most relevant system characteristics are used to considerably speed up the optimizations and facilitate the real-time capabilities of the EMSs without compromising the overall performance.

- **Evaluation focused on real-world driving:** The performance of the developed predictive EMSs is evaluated focusing on real-world driving where unpredictable disturbances are inevitable. For this purpose, all EMSs were benchmarked against state-of-the-art methods in simulation studies based on measurements of various real driving cycles. The expectations from these studies were confirmed in an extensive experimental validation with a real fuel cell passenger vehicle.

The centerpiece of this dissertation is a predictive energy management concept that is specifically designed to handle the limited accuracy of route-derived long-term predictions by continuously adapting to the actual conditions. The distinctive feature of this concept is that the predictive control information resulting from the offline optimization is stored in the form of a 2-D map expressing the optimal cost-to-go, i.e., the minimum amount of fuel required to reach the destination, as a function of the covered distance and the battery SoC. Unlike commonly used SoC reference trajectories, the cost-to-go map also provides predictive control information if deviations from the initially optimal path occur due to random influences such as traffic. This allows the proposed EMSs to continuously adapt to the actual conditions, which improves their robustness against unpredicted disturbances. The contributions were published in four scientific publications, which are outlined in the following (see also Fig. 1):

- Publication A proposes a predictive ECMS that derives the equivalence factor, which expresses a virtual fuel consumption for using energy from the battery, from the optimal cost-to-go map. The approach allows the equivalence factor to take the optimal estimate according to the long-term prediction in each instant. In this

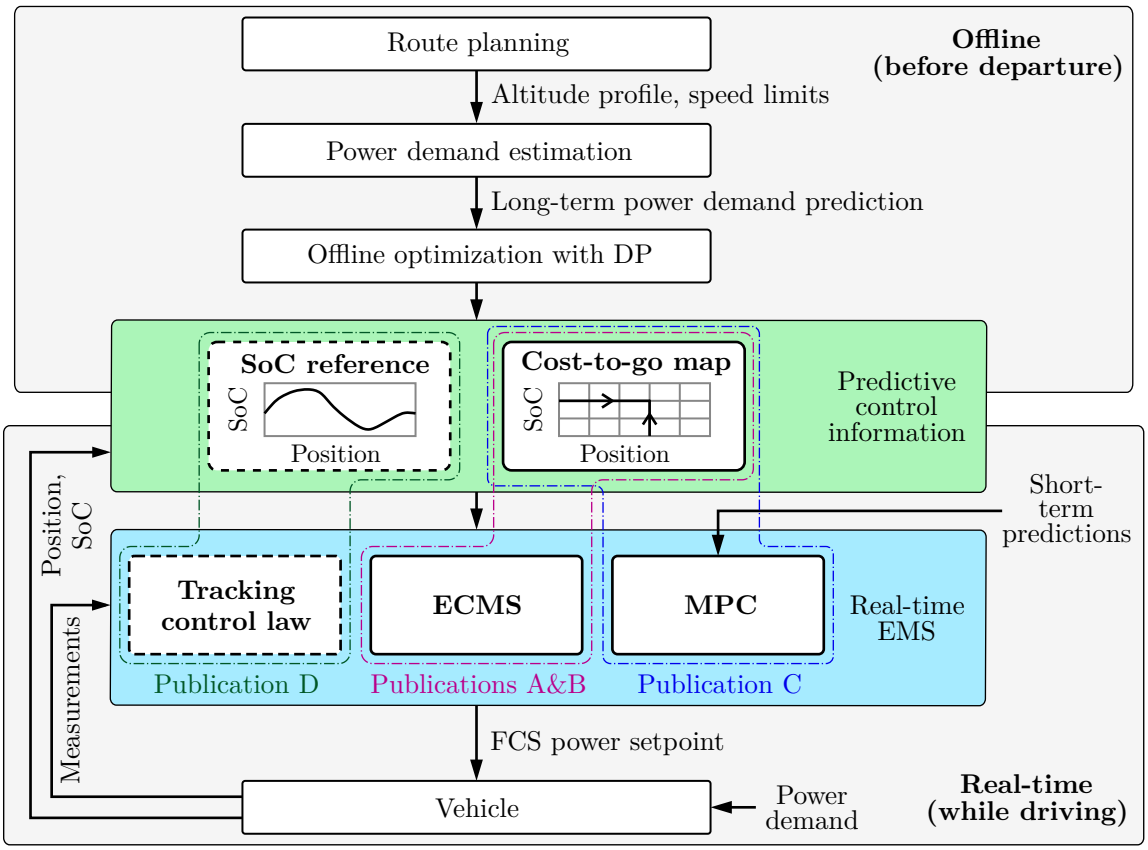

Figure 1: Schematic illustration of two-stage energy management showing alternatives of predictive control information and three different real-time EMSs. The outlines indicate the approaches proposed and investigated in this work.

way, the ECMS continuously adapts to the actual conditions, even if considerable disturbances occur. The method provides a solution to RP.1 and is described in more detail in Section 1.5.2.

- Publication B extends the predictive ECMS with a predictive stack start/stop control that robustly minimizes the number of start/stop actions for a planned driving mission. The start/stop control is based on a map expressing the optimal number of active stacks, which is determined in the offline optimization. The work addresses RP.2 and is discussed in Section 1.5.3.

- Publication C proposes a method that combines the long-term prediction with short-term predictions that are updated while driving. The method is based on an MPC that considers the short-term predictions within its prediction horizon and adds the cost-to-go that represents the long-term prediction as a terminal cost. The cost-to-go-based MPC addresses RP.3 and is outlined in Section 1.5.4.

- Publication D presents an extensive experimental evaluation of a two-stage EMS with a real fuel cell passenger vehicle. To validate the effectiveness of long-term predictions for improving fuel efficiency in general, the evaluation applies a simplified EMS that tracks an optimized SoC reference trajectory. The evaluation is based on several real driving tests, which were conducted on public roads, and reproducible chassis dynamometer tests. The study answers RP.4, and the key results are presented in Section 1.5.5.

1.5 Methodology

This section presents an overview of the methodology proposed in this dissertation. First, the control-oriented models of the vehicle and its powertrain are described in Section 1.5.1. Then, the cost-to-go-based predictive ECMS is outlined in Section 1.5.2, and the extension for the predictive stack start/stop control is described in Section 1.5.3. Section 1.5.4 presents the cost-to-go-based MPC. Finally, Section 1.5.5 summarizes the key results of the experimental validation with the real fuel cell vehicle. The corresponding research publications are included in full length in Chapter 2.

1.5.1 Control-oriented modeling

To exploit predictive information for optimizing the energy management, models of the relevant vehicle components are required. First, a model of the longitudinal vehicle dynamics is used to derive the long-term power demand prediction from static route information, i.e., the speed limits and the altitude profile along the route. Then, a model of the hybrid powertrain is used to conduct the offline optimization. The powertrain model is also an integral part of the proposed real-time EMSs.

In order to keep the computational complexities of the offline optimization and the real-time EMSs low, the vehicle dynamics and the powertrain are described with simple models focusing on the system characteristics that are most significant for optimizing the energy management. The low computational complexities ensure that the predictive control information is provided shortly after the route is defined and strongly facilitate the real-time implementation of the EMSs. Nevertheless, the simplified modeling does not compromise the overall performance because the accuracy of the long-term prediction is the most relevant limitation.

In the following, the model of the longitudinal vehicle dynamics is described first before the model of the hybrid powertrain is introduced.

Longitudinal vehicle dynamics

To derive the long-term power demand prediction from the speed limits and the altitude profile along the route, a model of the longitudinal vehicle dynamics is used. The model

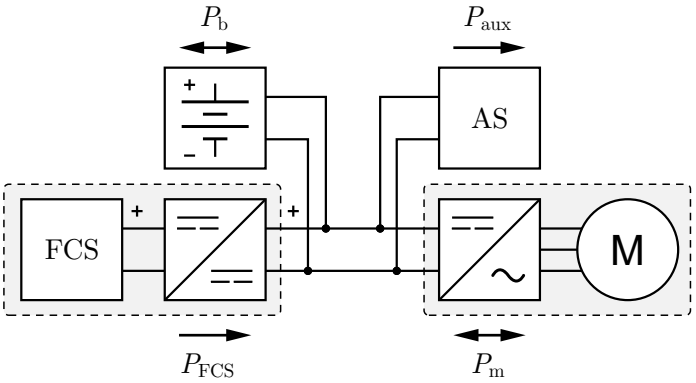

Figure 2: Hybrid powertrain consisting of the FCS, battery, traction motor (M), and auxiliary systems (AS). The arrows indicate the possible directions of the power flows. The figure is adapted from Publication C.

considers the traction force of the electric motor, aerodynamic drag, rolling friction, and gravitational force [49]

$$\delta m \frac{\mathrm{d}v}{\mathrm{d}t} = \eta_\mathrm{m}^{\operatorname{sgn} P_\mathrm{m}} \frac{P_\mathrm{m}}{v} - \frac{\rho A_\mathrm{f} c_\mathrm{d}}{2} v^2 - c_\mathrm{r} m g \cos\theta - m g \sin\theta \tag{1}$$

where δ denotes the correction coefficient of rotating mass, m the vehicle mass, v the vehicle velocity, t the time, η_m the efficiency of the traction motor, P_m the traction motor power, ρ the air density, A_f the frontal area of the vehicle, c_d the aerodynamic drag coefficient, c_r the rolling friction coefficient, g the gravitational acceleration, and θ the road inclination angle, which can be computed from the altitude profile.

With this model, a prediction of the traction motor power is derived from the speed limit-based prediction of the vehicle velocity and the altitude profile. The prediction of the overall electric power demand P_el is then computed by adding a prediction of the auxiliary power demand P_aux:

$$P_\mathrm{el} = P_\mathrm{m} + P_\mathrm{aux}. \tag{2}$$

The auxiliary power demand is challenging to predict over long prediction horizons. However, since its magnitude is relatively small compared with the traction power, a constant estimate of P_aux serves as a sufficient approximation.

Hybrid powertrain

The hybrid powertrain consists of the FCS and the battery (see Fig. 2). The overall system power, i.e., the sum of the FCS power P_FCS and the battery power P_b, satisfies the electric power demand of the vehicle

$$P_\mathrm{el} = P_\mathrm{FCS} + P_\mathrm{b} \tag{3}$$

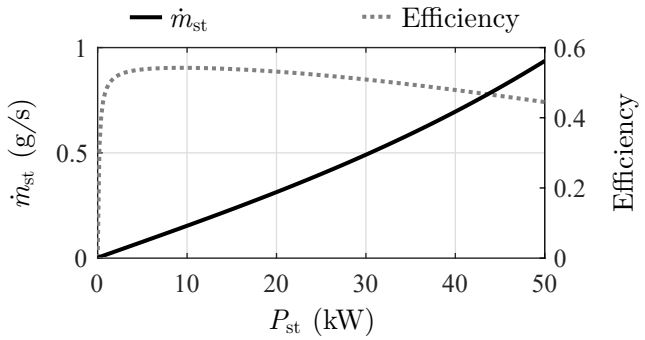

Figure 3: The stack fuel consumption curve and the corresponding efficiency curve of a fuel cell passenger vehicle. The figure is adapted from Publication B.

whereby the power allocation between the FCS and the battery is determined by the EMS. Both power sources are described with simple quasistatic models that focus on the most relevant characteristics from an energy management point of view. Besides the modeling, the specification of constraints plays an important role in preventing infeasible power requests and mitigating the degradation of the power sources.

In general, the FCS consists of N_{st} fuel cell stacks in parallel. The individual stacks are assumed to be identical and modeled with a polynomial curve describing the stack fuel consumption rate $\dot{m}_{st}(P_{st})$ as a strictly convex function of the stack net power P_{st} (see Fig. 3). This fuel consumption curve is fitted to measurement data and implicitly considers the power consumption of fuel cell-related auxiliaries such as the compressor. To prevent harmful operation, the stacks are only operated within $[P_{st}^{idle}, P_{st}^{max}]$, where P_{st}^{idle} denotes the lower idling power limit and P_{st}^{max} the upper power limit of the stack. Moreover, constraints on the stack power rate are specified in the form of minimum and maximum stack power increments per time step, i.e., ΔP_{st}^{min} and ΔP_{st}^{max}, respectively.

The FCS power and the FCS consumption rate $\dot{m}_{FCS}$ are the sum of the corresponding stack contributions. Assuming that all stacks contribute equally, the FCS power and the FCS consumption rate $\dot{m}_{FCS}$ can be computed with

$$P_{FCS} = n_{st} P_{st} \tag{4}$$
$$\dot{m}_{FCS} = n_{st} \dot{m}_{st}(P_{st}) \tag{5}$$

where $n_{st} \in \{0, 1, \ldots, N_{st}\}$ denotes the number of active stacks, which is also referred to as the "FCS state" in this work. Note that single-stack FCSs that remain active throughout the entire driving mission are assumed in the remainder of this work except for Section 1.5.3, where the predictive start/stop strategy is discussed. In the case of a constantly active single-stack FCS follows $n_{st} = 1$, which implies $P_{FCS} = P_{st}$ and $\dot{m}_{FCS} = \dot{m}_{st}$.

The battery is approximated with a steady-state equivalent circuit model [49] where

the battery voltage V_b varies linearly depending on the battery current I_b:

$$V_\mathrm{b} = V_\mathrm{OC} - R_\mathrm{int} I_\mathrm{b}. \tag{6}$$

The battery parameters V_OC and R_int denote the open-circuit voltage and the ohmic resistance, respectively, and are determined based on measurement data. Based on this approximation, the dynamics of the battery SoC ξ is a nonlinear function of the battery power

$$\dot{\xi} = f(P_\mathrm{b}) = -\frac{V_\mathrm{OC} - \sqrt{V_\mathrm{OC}^2 - 4P_\mathrm{b}R_\mathrm{int}}}{2Q_0 R_\mathrm{int}} \tag{7}$$

where Q_0 denotes the battery capacity. The battery can be operated within the feasible SoC range $[\xi^\mathrm{min}, \xi^\mathrm{max}]$, where ξ^min denotes the minimum SoC and ξ^max the maximum SoC. Additionally, the continuous battery power, which can be sustained over long periods of time, is constrained by an upper limit $P_\mathrm{b}^\mathrm{max}$ and a lower limit $P_\mathrm{b}^\mathrm{min}$. The latter is negative, i.e., the battery can be charged while driving.

1.5.2 Cost-to-go-based predictive energy management

Covering the entire planned driving mission, the long-term power demand prediction derived from static route information provides the long prediction horizon necessary to involve the battery actively in the energy management. However, the accuracy of the long-term prediction is limited due to various random influences that are hardly predictable, e.g., traffic, traffic regulation, driver behavior, and weather. Consequently, deviations from the long-term prediction must be expected in the real-world application.

The main idea of the proposed EMS is to adapt the energy management continuously to these unpredicted disturbances. For this purpose, the real-time EMS considers the predictive control information from the long-term prediction in a form that ensures flexibility for continuous adaptation: a 2-D map expressing the optimal cost-to-go. The optimal cost-to-go refers to the minimum amount of fuel required to reach the destination and varies depending on the position along the driving mission and the battery SoC. Unlike an optimized SoC reference trajectory, the cost-to-go map provides predictive control information within the entire position-SoC space. This gives the cost-to-go-based EMS the freedom to deviate from the initially optimal path regarding the prediction in order to respond to disturbances.

The proposed strategy follows a two-stage scheme: (i) Before departure, an optimization is conducted based on the long-term prediction, yielding the optimal cost-to-go map. (ii) While driving, the real-time EMS determines the optimal power allocation considering current system measurements and the optimal cost-to-go for the current position and SoC (see Fig. 1). The real-time strategy is based on the ECMS and considers the long-term information by deriving estimates of the optimal equivalence factor from the optimal cost-to-go. In this way, the ECMS continuously adopts the optimal power

allocation regarding the long-term prediction for the remainder of the driving mission, even if the system states considerably deviate from the initially optimal path because of disturbances that occurred in the past. The key advantages of the cost-to-go-based predictive ECMS can be summarized as follows:

- Robust minimization of fuel consumption
- Exploitation of the long-term prediction while continuously adapting to the actual conditions
- Harmful operation prevented with constraints
- No recurring offline optimizations after departure
- Low computational complexity and simple implementability

In the remainder of this section, the offline optimization and the cost-to-based predictive ECMS are described first. Then, the advantages of the predictive ECMS over a state-of-the-art approach are demonstrated in a numerical study. For more details, the reader is referred to Publication A.

Offline optimization with dynamic programming

The offline stage starts with the derivation of the long-term power demand prediction from the static route information based on the model of the longitudinal vehicle dynamics, as described in Section 1.5.1. The long-term power demand prediction is the input of the subsequent offline optimization, which determines the optimal power allocation between the FCS and the battery such that the fuel consumption J for the planned trip is minimized. The objective is formulated in discrete time assuming a single-stack FCS, i.e., $P_{\mathrm{FCS},l} = P_{\mathrm{st},l}$, and considering the relevant powertrain constraints in each time step $l = 1, \ldots, L-1$:

$$\begin{aligned} \min_{P_{\mathrm{FCS}}} J = \sum_{l=1}^{L-1} & \dot{m}_{\mathrm{FCS}}(P_{\mathrm{FCS},l})\Delta t_l \\ \text{s.t.} \quad & P_{\mathrm{st}}^{\mathrm{idle}} \leq P_{\mathrm{FCS},l} \leq P_{\mathrm{st}}^{\mathrm{max}}, \\ & P_{\mathrm{b}}^{\mathrm{min}} \leq P_{\mathrm{b},l} \leq P_{\mathrm{b}}^{\mathrm{max}}, \\ & \xi^{\mathrm{min}} \leq \xi_l \leq \xi^{\mathrm{max}}, \\ & \xi_1 = \xi^{\mathrm{init}}, \\ & \xi_L \geq \xi^{\mathrm{final}}. \end{aligned} \tag{8}$$

Here, $\Delta t_l = t_{l+1} - t_l$ denotes the time interval of the lth time step, $(L-1)$ the number of time steps, ξ^{init} the initial SoC, and ξ^{final} the minimum SoC at the destination. The FCS power is chosen as the decision variable, and the battery power takes the residual

power demand. In order to keep the dimension of the optimization problem low, a relatively rough sampling is chosen in the magnitude of one time step per kilometer on average. While the rough sampling reduces the computational complexity, it does not necessarily compromise the overall performance due to the limited accuracy of the long-term prediction. Moreover, the FCS power rate constraints can be neglected here because the time constants of the FCS dynamics are assumed to be much smaller than the time steps of the offline optimization.

To determine the optimal cost-to-go map for the real-time control, the optimization problem is solved with dynamic programming (DP). DP breaks down the problem into a series of subproblems, which are solved backward in time with discretized control input (P_{FCS}) and state (ξ). In each time step $l = (L-1), \ldots, 1$, the cost-to-go, i.e., the amount of fuel to reach the destination, is minimized for each ξ_l in the discrete SoC space

$$J_l^*(\xi_l) = \min_{P_{\mathrm{FCS},l}} \left(\dot{m}_{\mathrm{FCS}}(P_{\mathrm{FCS},l}) \Delta t_l + J_{l+1}^*(\xi_{l+1}) \right) \tag{9}$$

considering the constraints specified in Eq. (8). For more details regarding the DP implementation, the reader is referred to the literate, e.g., [50]. The algorithm yields the optimal cost-to-go J^* at each point in the discrete time-SoC space. A time-to-distance mapping based on the predicted velocity then gives the desired map $J^*(s, \xi)$ describing the optimal cost-to-go as a function of the covered distance s, i.e., the position along the trip, and the battery SoC. The description in the distance domain is used here because it is independent of the elapsed time, which is affected by deviations from the predicted velocity and vehicle standstills. Therefore, the distance-based description is advantageous for robust real-time control. An example of the optimal cost-to-go map is shown in the upper plot of Fig. 4.

The optimal cost-to-go cannot be considered directly in the ECMS. However, the equivalence factor λ, which expresses a virtual fuel consumption for the use of energy from the battery, can be derived from the optimal cost-to-go by computing the partial derivative with respect to the SoC [31, 32]:

$$\lambda(s, \xi) = \frac{\partial J^*(s, \xi)}{\partial \xi}. \tag{10}$$

This computation is performed numerically and finalizes the offline stage. The resulting 2-D map that describes the equivalence factor as a function of the covered distance and the SoC is stored and represents the predictive control information for the real-time control. An example of the equivalence factor map is shown in the lower plot of Fig. 4.

Real-time predictive ECMS

The ECMS determines the power allocation by minimizing the equivalent fuel consumption rate H, which does not only include the actual fuel consumption rate of the FCS

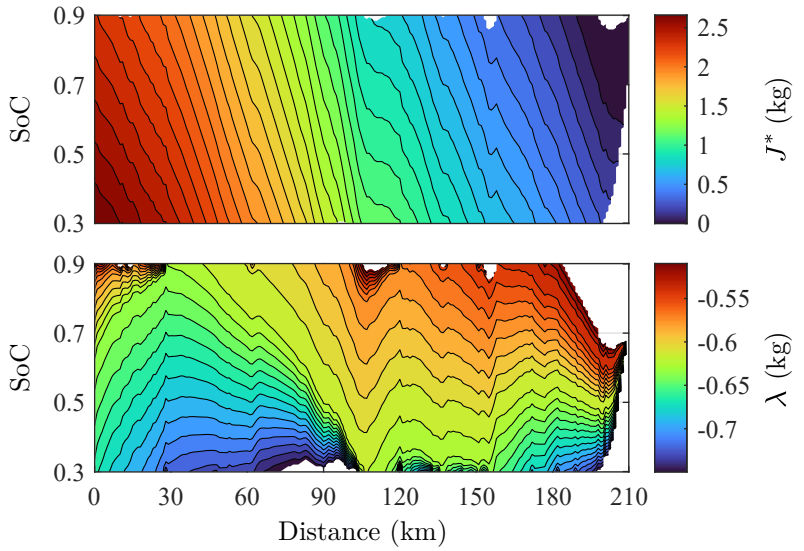

Figure 4: Optimal cost-to-go map (upper plot) and equivalence factor map (lower plot) resulting from the offline optimization of a long-term prediction. The figure is adapted from Publication C.

but also a virtual fuel consumption rate for using energy from the battery:

$$H(P_{\mathrm{FCS}}, \lambda, P_{\mathrm{el}}) = \dot{m}_{\mathrm{FCS}}(P_{\mathrm{FCS}}) + \lambda f(P_{\mathrm{el}} - P_{\mathrm{FCS}}). \tag{11}$$

The performance of the ECMS is strongly influenced by the choice of the equivalence factor. In theory, the ECMS can provide candidates for the globally optimal power allocation if the optimal equivalence factor is known, see [51]. However, the optimal equivalence factor strongly depends on the power demand profile of the driving mission and is therefore unknown in advance.

Considering the equivalence factor map resulting from the offline optimization, the proposed method provides the ECMS with a prediction-based estimate of the optimal equivalence factor. The estimate is continuously updated by linearly interpolating in $\lambda(s, \xi)$ based on the current position along the trip and SoC. In this way, the ECMS performs the optimal power allocation regarding the long-term prediction for the trip remainder in each instant and continuously adapts to the actual conditions.

Because the ECMS cannot consider SoC constraints directly, an indirect SoC constraint handling mechanism is included. The mechanism adapts the equivalence factor based on a quadratic formulation such that charging the battery is favored close to $\xi^{\min}$ and discharging the battery is favored close to $\xi^{\max}$:

$$\bar{\lambda} = \begin{cases} \lambda(s,\xi) + \lambda_{\mathrm{ad}} \left(\frac{\xi - \xi^{\max} + \xi_{\mathrm{th}}}{\xi_{\mathrm{th}}} \right)^2, & \xi > \xi^{\max} - \xi_{\mathrm{th}} \\ \lambda(s,\xi) - \lambda_{\mathrm{ad}} \left(\frac{-\xi + \xi^{\min} + \xi_{\mathrm{th}}}{\xi_{\mathrm{th}}} \right)^2, & \xi < \xi^{\min} + \xi_{\mathrm{th}} \\ \lambda(s,\xi), & \text{otherwise.} \end{cases} \tag{12}$$

Here, λ_{ad} and ξ_{th} are tuning parameters. With the adapted equivalence factor $\bar{\lambda}$, the ECMS determines the optimal FCS power in real time with

$$P^*_{\mathrm{FCS}} = \arg \min_{P_{\mathrm{FCS}} \in \mathcal{P}} H(P_{\mathrm{FCS}}, \bar{\lambda}, P_{\mathrm{el}}) \tag{13}$$

where the feasible stack power range $\mathcal{P}$ considers the specified constraints:

$$\begin{aligned} \mathcal{P} = \Big\{ P_{\mathrm{st}} \in \mathbb{R} : P_{\mathrm{st}}^{\mathrm{idle}} \leq P_{\mathrm{st}} \leq P_{\mathrm{st}}^{\mathrm{max}}, \\ \Delta P_{\mathrm{st}}^{\mathrm{min}} \leq P_{\mathrm{st}} - P_{\mathrm{st}}^{\mathrm{prev}} \leq \Delta P_{\mathrm{st}}^{\mathrm{max}}, \\ P_{\mathrm{b}}^{\mathrm{min}} \leq P_{\mathrm{b}} \leq P_{\mathrm{b}}^{\mathrm{max}} \Big\}. \end{aligned} \tag{14}$$

Here, $P_{\mathrm{st}}^{\mathrm{prev}}$ denotes the stack power in the previous control instance. To prevent infeasibility, the battery power constraint is implemented as a soft constraint.

Thanks to the strict convexity of the fuel consumption curve, H is also strictly convex in P_{FCS}. Consequently, the optimization problem in Eq. (13) has a unique solution, which ensures convergence and facilitates the application of computationally simple optimization algorithms. For the proof of the convexity of H, the reader is referred to Publication B.

Selected results

The cost-to-go-based predictive ECMS (P-ECMS) is qualitatively compared with the so-called adaptive ECMS (A-ECMS) in simulation. In this state-of-the-art approach, the equivalence factor is determined with a proportional-integral controller that tracks a SoC reference trajectory [18]. To ensure a fair comparison, the SoC reference trajectory of the A-ECMS is optimized based on the long-term prediction with the DP algorithm using the same settings as for the P-ECMS. This means that both methods are based on the same prediction and the same offline optimization but provide the predictive information in different forms to the real-time control.

The comparison is based on measurements of a real-world driving mission with a focus on highway driving (see Fig. 5). The long-term prediction gives a good estimate of the measured velocity but inevitably shows traffic-induced deviations. In particular, the highlighted roadworks section (shaded area) represents a considerable disturbance, where the prediction overestimates the power demand. Similar to the theoretically optimal solution, which is included in the SoC plot, the P-ECMS takes advantage of the lower power demand to charge the battery efficiently during the roadworks section. The energy stored in the battery is subsequently used to reduce the load on the FCS in the trip remainder, which increases the overall efficiency. In contrast, the A-ECMS reduces the FCS power during the roadworks section due to the decreasing SoC reference and only maintains the battery SoC. Consequently, the FCS is operated with higher power and thus less efficiently in the trip remainder. The last plot in Fig. 5 shows that the

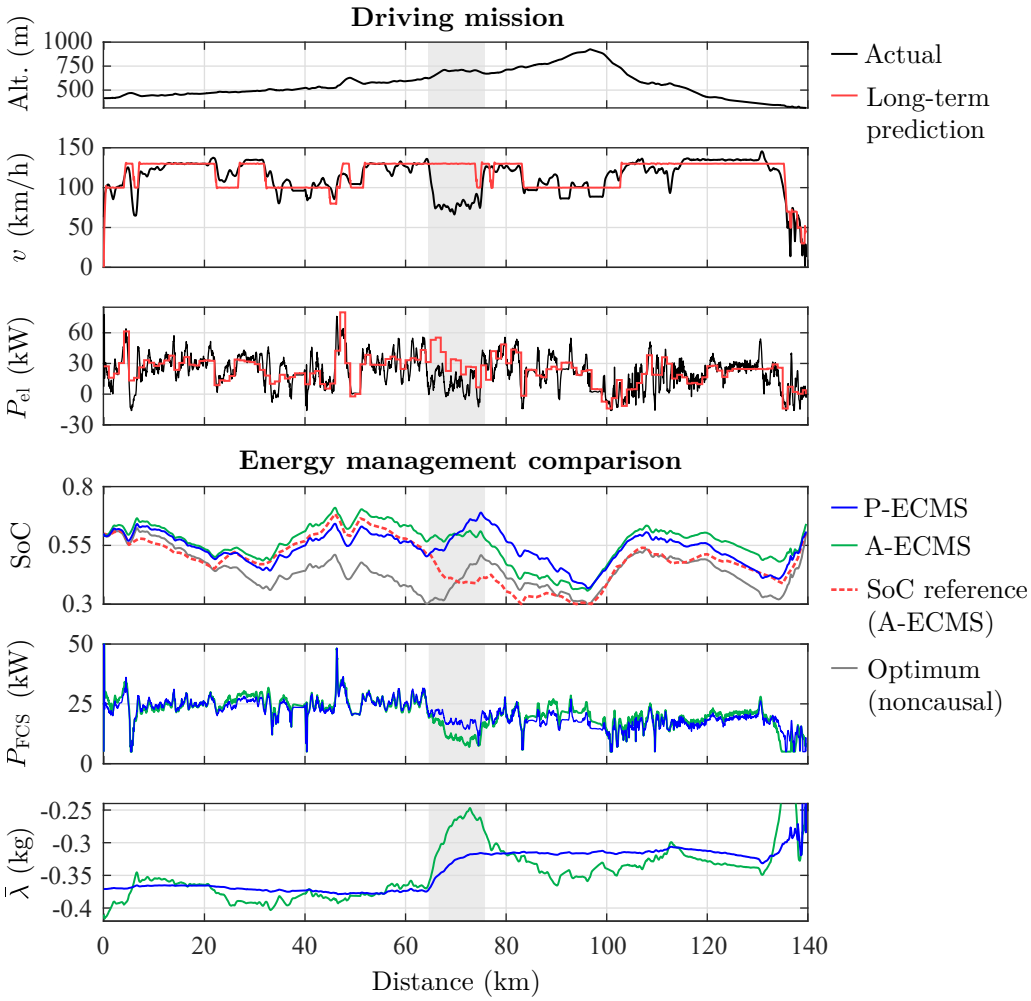

Figure 5: Comparison of the cost-to-go-based P-ECMS with the A-ECMS based on a real-world driving mission. The shaded areas highlight unpredicted roadworks. The figure is adapted from Publication A.

P-ECMS adapts the equivalence factor more smoothly and avoids fluctuations during disturbances, which also indicates an improvement in the energy management quality.

This comparison demonstrates the superior adaptability of the cost-to-go-based P-ECMS to unpredicted disturbances. The result is a 0.9 % reduction in fuel consumption compared with the A-ECMS for the investigated driving mission, which is remarkable considering that both methods are based on the ECMS and informed with the same long-term prediction. Moreover, the performance of the A-ECMS strongly depends on the tuning of the proportional-integral controller and the choice of the initial equivalence factor, whereby the optimal configuration is trip-dependent. The P-ECMS provides robust performance without the need for tuning.

1.5.3 Minimization of stack start/stop actions

So far, the FCS was assumed to be active throughout the entire driving mission. This assumption is not restrictive in driving missions with high and steady power demand, e.g., on highways, as observed in the numerical study above. However, many driving missions include sections with low or even negative power demand, e.g., when driving in urban areas or downhill. Here, temporarily shutting down the FCS or individual stacks benefits the efficiency as well as the durability of both powertrain components: Regarding the FCS, the fuel consumption and the power consumption of the auxiliaries are reduced, harmful low-power operation is avoided, and the FCS operation time is lowered. Regarding the battery, overcharging is prevented and the strain on the battery is reduced if the power demand is negative. However, each stack start/stop event is associated with harmful operating conditions, which is why unnecessary starts/stops must be avoided.

The key idea of the contribution presented in this section is to expand the concept of the cost-to-go-based energy management to stack start/stop control. Analogously to the equivalence factor map, the long-term prediction is exploited in the form of a 2-D map describing the optimal FCS state depending on the covered distance and the SoC. The real-time control performs start/stop actions based on this map but also considers system measurements to adapt to the actual conditions. The main advantages of the proposed stack start/stop control are:

- Coherent integration of start/stop control into the cost-to-go-based predictive energy management
- Robust minimization of the number of start/stop events
- Further reduction in fuel consumption
- Applicable to single and multi-stack FCSs

In the following, the computation of the optimal FCS state map and the real-time start/stop control are described. Then, the method is demonstrated in a numerical study, and the advantages over two benchmark strategies are analyzed. The in-depth description of the approach can be found in Publication B.

Offline optimization including start/stop actions

The offline optimization is again based on the long-term power demand prediction. Here, however, not only the individual stack power but also the FCS state, i.e., the number of active stacks, is included in the set of decision variables. The objective is to minimize

the fuel consumption for the planned trip considering a penalty p for start/stop actions:

$$\begin{aligned}\min_{n_{\mathrm{st}},P_{\mathrm{st}}} J = &\sum_{l=1}^{L-1} n_{\mathrm{st},l}\,\dot{m}_{\mathrm{st}}(P_{\mathrm{st},l})\Delta t_l + p|n_{\mathrm{st},l} - n_{\mathrm{st},l+1}| \\ \text{s.t.}\quad & n_{\mathrm{st},l} \in \{0,1,\dots,N_{\mathrm{st}}\}, \\ & P_{\mathrm{st}}^{\mathrm{idle}} \le P_{\mathrm{st},l} \le P_{\mathrm{st}}^{\mathrm{max}}, \\ & P_{\mathrm{b}}^{\mathrm{min}} \le P_{\mathrm{b},l} \le P_{\mathrm{b}}^{\mathrm{max}}, \\ & \xi^{\mathrm{min}} \le \xi_l \le \xi^{\mathrm{max}}, \quad l = 1,\dots,L-1, \\ & \xi_1 = \xi^{\mathrm{init}}, \quad n_{\mathrm{st},1} = 0, \\ & \xi_L \ge \xi^{\mathrm{final}}, \quad n_{\mathrm{st},L} = 0.\end{aligned} \tag{15}$$

The optimization problem is solved with DP. Due to the start/stop penalty, the DP algorithm must consider the FCS state as both a state and a decision variable. To distinguish between them in the following, x_{st} denotes the state, which is the *current* FCS state, and u_{st} denotes the decision variable, which is the FCS state in the *next instant*, i.e., $x_{\mathrm{st},l+1} = u_{\mathrm{st},l}$. The DP algorithm proceeds backward in time minimizing the cost-to-go at each step $l = (L-1),\dots,1$:

$$J_l^*(\xi_l, x_{\mathrm{st},l}) = \min_{u_{\mathrm{st},l},P_{\mathrm{st},l}} \Big(u_{\mathrm{st},l}\,\dot{m}_{\mathrm{st}}(P_{\mathrm{st},l})\Delta t_l + p|x_{\mathrm{st},l} - u_{\mathrm{st},l}| + J_{l+1}^*(\xi_{l+1}, u_{\mathrm{st},l}) \Big). \tag{16}$$

After a time-to-distance mapping, the algorithm yields two 3-D maps that express the information of interest depending on the position, the SoC, and the current FCS state: the optimal cost-to-go $J^*(s,\xi,x_{\mathrm{st}})$ and the optimal FCS state $u_{\mathrm{st}}^*(s,\xi,x_{\mathrm{st}})$. The former serves to derive the equivalence factor map according to Eq. (10). The latter represents optimal start/stop actions according to the long-term prediction. To have a more compact and memory-saving representation, $u_{\mathrm{st}}^*(s,\xi,x_{\mathrm{st}})$ is condensed in a 2-D map

$$\mathcal{N}^*(s,\xi) = \{n \in \mathcal{N} : \exists m \in \mathcal{N}\, u_{\mathrm{st}}^*(s,\xi,m) = n\} \tag{17}$$

with $\mathcal{N} = \{0,1,\dots,N_{\mathrm{st}}\}$. The resulting map describes the set of optimal FCS states $\mathcal{N}^*$ as a function of the position and SoC only.

An example of the FCS state map for a single-stack FCS is included in the SoC plot of Fig. 6. The map includes three possible cases: $\mathcal{N}^* = \{0\}$ indicates to stop the FCS, $\mathcal{N}^* = \{1\}$ to start the FCS, and $\mathcal{N}^* = \{0,1\}$ to remain in the current FCS state. The latter results from the start/stop penalty. In this case, the potential reduction in fuel consumption after a switching action would not compensate for the penalty, which is why maintaining the current FCS state is optimal.

Map-based real-time start/stop control

In each control instant, a nearest-neighbor interpolation in $\mathcal{N}^*(s,\xi)$ is performed to determine the set of optimal FCS states for the current position and SoC according

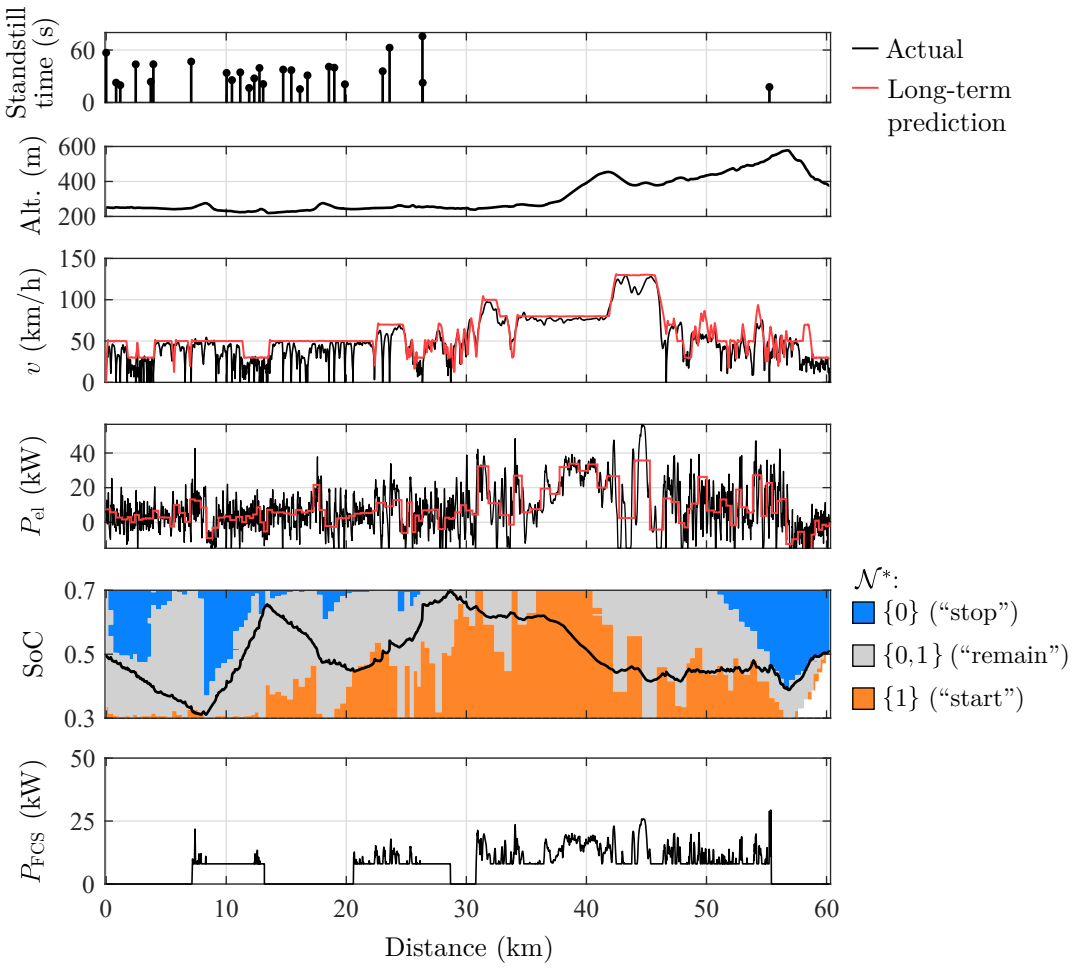

Figure 6: Demonstration of the map-based start/stop control for a vehicle with a single-stack FCS. The executed start/stop actions are visible in the FCS power. The figure is adapted from Publication B.

to the long-term prediction. If the current FCS state $n_{\mathrm{st}}^{\mathrm{curr}}$ is included in this set, no start/stop action is needed. Otherwise, the element of the set that is closest to the current FCS state is considered as the optimal FCS state indication $n_{\mathrm{st}}^{\mathrm{ind}}$. To prevent SoC constraint violations in the case of considerable deviations of the prediction, the optimal FCS state indication is overruled if the specified SoC constraints are reached: If $\xi \leq \xi_{\mathrm{min}}$, then $n_{\mathrm{st}}^{\mathrm{ind}} \geq 1$. If $\xi \geq \xi_{\mathrm{max}}$, then $n_{\mathrm{st}}^{\mathrm{ind}} = \min \mathcal{N}^*(s, \xi)$, i.e., the lowest number in the set of optimal FCS states is chosen.

However, the FCS state indication is not followed directly because the long-term prediction may deviate from the actual power demand. Instead, an instantaneous condition taking into account the actual power demand is evaluated based on the equivalent

fuel consumption rate, which is adapted for the consideration of the FCS state:

$$H(P_{\mathrm{st}}, n_{\mathrm{st}}, \lambda, P_{\mathrm{el}}) = n_{\mathrm{st}} \dot{m}_{\mathrm{st}}(P_{\mathrm{st}}) + \lambda f(P_{\mathrm{el}} - n_{\mathrm{st}} P_{\mathrm{st}}). \tag{18}$$

The indicated start/stop action is only realized if it implies a strict reduction in the equivalent fuel consumption rate, i.e.,

$$H^{\mathrm{ind}} < H^{\mathrm{curr}} \tag{19}$$

where H^{ind} and H^{curr} are the minimum equivalent fuel consumption rates for the corresponding FCS states:

$$H^{\mathrm{ind}} = \min_{P_{\mathrm{st}} \in \mathcal{P}} H(P_{\mathrm{st}}, n_{\mathrm{st}}^{\mathrm{ind}}, \bar{\lambda}^{\mathrm{ind}}, P_{\mathrm{el}}) \quad \text{and} \tag{20}$$

$$H^{\mathrm{curr}} = \min_{P_{\mathrm{st}} \in \mathcal{P}} H(P_{\mathrm{st}}, n_{\mathrm{st}}^{\mathrm{curr}}, \bar{\lambda}^{\mathrm{curr}}, P_{\mathrm{el}}). \tag{21}$$

Here, $\bar{\lambda}^{\mathrm{ind}}$ and $\bar{\lambda}^{\mathrm{curr}}$ denote the equivalence factor estimates corresponding to $n_{\mathrm{st}}^{\mathrm{ind}}$ and $n_{\mathrm{st}}^{\mathrm{curr}}$, respectively, which take into account the SoC constraint handling mechanism defined in Eq. (12). The consideration of this instantaneous start/stop condition suppresses inefficient start/stop actions in situations where the long-term prediction considerably deviates. For example, shutting down the FCS is prevented during an overtaking maneuver, and starting the FCS is suppressed while braking. The start/stop condition is therefore not only important to preserve efficiency but also to ensure smooth operation and safety. After determining the FCS state, the individual stack power is determined based on the ECMS as defined in Eq. (13).

Selected results

The map-based start/stop control is demonstrated for a passenger vehicle with a single-stack FCS in Fig. 6. The investigated real-world driving mission is characterized by considerable variations in the power demand and several traffic-induced vehicle standstills with varying standstill times. The standstills, which are not considered by the long-term prediction, make FCS start/stop actions unavoidable to prevent overcharging the battery.

Thanks to the optimal FCS state map, the start/stop control adapts the number of active stacks according to the long-term prediction depending on both the position along the trip and the SoC. For example, the FCS is not activated until the lower SoC constraint is approached at the beginning of the trip because the power demand is low and battery-only operation is efficient. After 30 km, however, an FCS start is executed with an almost fully charged battery because high power demand is predicted subsequently. Consequently, the predictive start/stop control not only minimizes the number of start/stop actions but also ensures high fuel efficiency.

To quantify these benefits, the map-based start/stop strategy is benchmarked against two alternative methods: (i) an instantaneous strategy that does not consider

Table 1: Comparison of the map-based start/stop control with two benchmark methods.

	Map-based	Instantaneous	Position-based
Number of starts/stops	**6**	40	2
Fuel consumption† (kg/100km)	**0.876**	0.884	0.985
Relative difference	**0 %**	+0.9 %	+12.5 %
Compliance with SoC constraints	**Yes**	No	No

†Takes into account deviations in the final SoC

predictions [37] and prevents infeasibly frequent starts/stops with a 60 s hold time [38], which is a state-of-the-art approach, (ii) a predictive strategy that performs starts/stops at optimized positions without considering actual system measurements [42]. The latter is referred to as position-based strategy and informed with the long-term prediction. The main results of the comparison are presented in Table 1. Compared with the instantaneous strategy, the proposed map-based strategy reduces the number of starts/stops from 40 to 6 for the investigated driving mission, which is a considerable improvement. Remarkably, the map-based strategy also achieves a 0.9 % reduction in fuel consumption and ensures feasible operation. In contrast, the instantaneous strategy causes a violation of the specified SoC constraints due to the hold time. The position-based strategy performs only two starts/stops. However, the low number of starts/stops comes at the expense of a significant 12.5 % increase in fuel consumption compared with the map-based strategy and a severe SoC constraint violation. The results confirm the superior performance and robustness of the proposed map-based start/stop control, which enables a reduction of FCS degradation while maintaining high fuel efficiency. For more details on this comparison, the reader is referred to Publication B.

1.5.4 Combination of long-term and short-term predictions

Emerging technologies in the field of intelligent transportation systems enable communication between individual vehicles and the infrastructure. In this way, information of the traffic environment is accessible, enabling accurate predictions that are updated in real time. Even though such predictions have relatively short prediction horizons, typically in the range of tens of seconds, their high accuracy makes them highly valuable for further improving the energy management performance.

The contribution presented in this section proposes how these real-time short-term predictions can be integrated into the cost-to-go-based two-stage energy management (see scheme in Fig. 1). The proposed EMS is an MPC that considers the short-term power demand prediction within its prediction horizon and includes the cost-to-go representing the long-term prediction as terminal cost at the end of the prediction horizon. The main benefits of the cost-to-go-based MPC are summarized below:

- Mitigation of FCS degradation through reduced transient operation

- Predictive consideration of powertrain constraints
- A linear MPC formulation ensuring convergence and low computational complexity
- Facilitation of predictive control at the FCS level

The remainder of this section first elaborates on how the short-term predictions are integrated into the cost-to-go-based energy management in more detail. Then, the powertrain and cost-to-go modeling for a linear MPC formulation is described, and the relation to the cost-to-go-based ECMS is discussed. Finally, selected results are shown. For further details on the cost-to-go-based MPC, the reader is referred to Publication C.

Real-time cost-to-go-based MPC

The EMS follows the cost-to-go-based two-stage approach. This means that an offline optimization is conducted based on the long-term prediction before departure, which yields the optimal cost-to-go map (see Section 1.5.2). The objective of the real-time MPC is to minimize the fuel consumption for the trip remainder in each control instant. While the optimal cost-to-go map already provides the minimum fuel consumption depending on the position and the SoC, its accuracy is limited due to the expected deviations of the long-term prediction. To improve the energy management performance, the MPC additionally considers accurate short-term predictions. For this purpose, the objective function of the MPC is split into two parts

$$J_k = \sum_{j=k}^{k+N_\mathrm{p}-1} \hat{m}_\mathrm{FCS}(P_{\mathrm{FCS},j}, P_{\mathrm{el},j}) T_\mathrm{s} + \hat{J}^*_{k+N_\mathrm{p}}(\xi_{k+N_\mathrm{p}}) \tag{22}$$

where T_s denotes the constant MPC sampling time and N_p determines the length of the short-term prediction horizon, which is $N_\mathrm{p}T_\mathrm{s}$. The first term considers the fuel consumption within the short-term prediction horizon. The formulation is based on a fuel consumption model $\hat{m}_\mathrm{FCS}$ that suits a linear MPC formulation, which is outlined in the following section. The second term describes the minimal fuel consumption $\hat{J}^*_{k+N_\mathrm{p}}$ for the trip remainder as a function of the SoC ξ_{k+N_p} at the end of the short-term prediction horizon. This information is available from the optimal cost-to-go map, which implicitly represents optimal paths for the trip remainder (see Fig. 7). In each control instant, the MPC determines the optimal FCS power sequence $\boldsymbol{P}^*_{\mathrm{FCS},k}$ of the single-stack FCS with

$$\begin{aligned} \boldsymbol{P}^*_{\mathrm{FCS},k} = \arg \min_{\boldsymbol{P}_{\mathrm{FCS},k}} \; & J_k \\ \text{s.t.} \; & P^\mathrm{idle}_\mathrm{st} \leq P_{\mathrm{FCS},k+n} \leq P^\mathrm{max}_\mathrm{st}, \\ & \Delta P^\mathrm{min}_\mathrm{st} \leq \Delta P_{\mathrm{FCS},k+n} \leq \Delta P^\mathrm{max}_\mathrm{st}, \\ & P^\mathrm{min}_\mathrm{b} \leq P_{\mathrm{b},k+n} \leq P^\mathrm{max}_\mathrm{b}, \\ & \xi^\mathrm{min} \leq \xi_{k+n} \leq \xi^\mathrm{max}, \\ & \xi^\mathrm{min}_{k+N_\mathrm{p}} \leq \xi_{k+N_\mathrm{p}} \leq \xi^\mathrm{max}_{k+N_\mathrm{p}} \end{aligned} \tag{23}$$

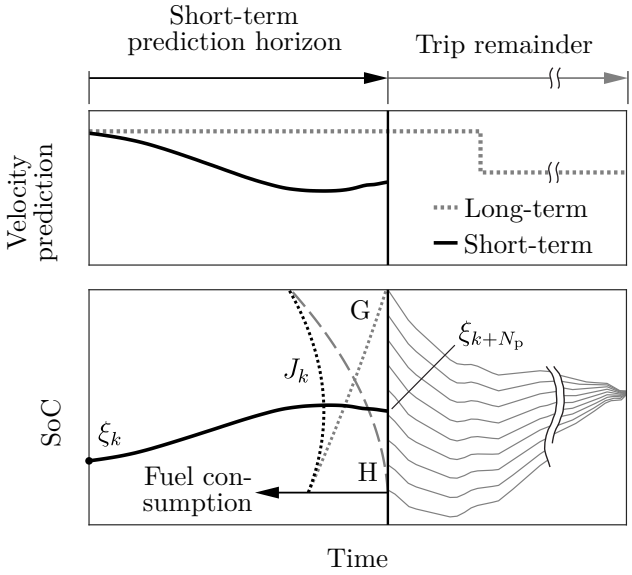

Figure 7: MPC combining the short-term prediction with the optimal cost-to-go. The lower plot illustrates the trade-off between the two terms of J_k, i.e., the fuel consumption within the short-term prediction horizon (H) and the optimal cost-to-go at its end (G), as a function of ξ_{k+N_p}. The optimal cost-to-go represent optimal paths for the trip remainder. The figure is adapted from Publication C.

for all $n = 0, \ldots, (N_\mathrm{p} - 1)$, where $\Delta P_{\mathrm{FCS},k} = P_{\mathrm{FCS},k} - P_{\mathrm{FCS},k-1}$. The constraints on the battery power, the SoC, and the terminal SoC are implemented as soft constraints to avoid infeasibility. The terminal set constraint determined by $[\xi^{\min}_{k+N_\mathrm{p}}, \xi^{\max}_{k+N_\mathrm{p}}]$ represents the feasible SoC range at the corresponding position according to the offline optimization. Following the receding horizon principle, only the first step $P^*_{\mathrm{FCS},k}$ is actually applied to the system. Then, the short-term prediction and the measurements are updated, and the optimization is repeated.

To lower the computational complexity of the optimization problem and ensure convergence, a linear MPC formulation is elaborated in the following. The linear MPC formulation is characterized by a linearized model and a quadratic objective function and turns the optimization problem into a quadratic programming (QP) problem, which can be solved efficiently with QP solvers. First, the linearization of the powertrain model is outlined before the cost-to-go modeling for the quadratic objective function is described.

Powertrain model for the linear MPC

To obtain the discrete-time state-space model for the linear MPC, the nonlinear battery SoC model of Eq. (7) is first linearized at the operating point $P_\mathrm{b} = 0\,\mathrm{W}$ and then discretized assuming a zero-order hold for the battery power. Considering $P_\mathrm{b} = P_\mathrm{el} - P_\mathrm{FCS}$

gives the linearized discrete-time SoC model as a function of the decision variable (P_{FCS}) and the predicted disturbance (P_{el}):

$$\xi_{k+1} = \xi_k + \frac{T_\mathrm{s}}{Q_0 V_{\mathrm{OC}}}(P_{\mathrm{FCS},k} - P_{\mathrm{el},k}). \tag{24}$$

The linearization of the battery model entails that ohmic battery losses are neglected. Seeking minimum fuel consumption, the linear MPC would therefore put too much load on the battery without further measures. To avoid this behavior, a physically motivated penalty for battery losses is included in the objective function. The penalty is based on a quadratic formulation that expresses a virtual fuel consumption rate $\dot{m}_\Omega$ for battery losses

$$\dot{m}_\Omega(P_{\mathrm{FCS}}, P_{\mathrm{el}}) = \frac{R_{\mathrm{int}}}{V_{\mathrm{OC}}^2\, \bar{\eta}_{\mathrm{FCS}}\, H_\mathrm{i}}(P_{\mathrm{el}} - P_{\mathrm{FCS}})^2 \tag{25}$$

where $\bar{\eta}_{\mathrm{FCS}}$ denotes the mean FCS efficiency and H_i the lower heating value of hydrogen.

To consider the FCS model in the linear MPC, the degree of the polynomial fuel consumption model, i.e., $\dot{m}_{\mathrm{FCS}}(P_{\mathrm{FCS}})$, must be limited to two. Then, it can be directly considered in the quadratic objective function. With that, the overall fuel consumption model that is used in the objective function of the linear MPC in Eq. (22) is

$$\hat{\dot{m}}_{\mathrm{FCS}}(P_{\mathrm{FCS}}, P_{\mathrm{el}}) = \dot{m}_{\mathrm{FCS}}(P_{\mathrm{FCS}}) + \dot{m}_\Omega(P_{\mathrm{FCS}}, P_{\mathrm{el}}) \tag{26}$$

where the virtual fuel consumption representing the ohmic battery losses is included.

Local cost-to-go modeling

To consider the variation of the optimal cost-to-go depending on ξ_{k+N_p} in the quadratic objective function, the optimal cost-to-go is locally approximated with a polynomial model. Analyzing the optimum of the objective function of the MPC as a function of ξ_{k+N_p} reveals that not the absolute value of the cost-to-go but its partial derivative with respect to the SoC is relevant for the optimization (see lower plot in Fig. 7). Therefore, the partial derivative of the cost-to-go, and not the cost-to-go itself, is modeled with a local linear model around the current SoC ξ_k with

$$\left.\frac{\partial \hat{J}^*_{k+N_\mathrm{p}}}{\partial \xi}\right|_{\xi_k} = \gamma_0 + \gamma_1(\xi_{k+N_\mathrm{p}} - \xi_k) \tag{27}$$

where $\partial \hat{J}^*_{k+N_\mathrm{p}}/\partial \xi$ denotes the estimate of the partial derivative of the cost-to-go and γ_0 and γ_1 the model parameters. In this way, identifying irrelevant parameters is avoided. Typical profiles of the cost-to-go and its partial derivative and a local linear model are illustrated in Fig. 8. The partial derivative of the cost-to-go equals the equivalence factor of the ECMS. Consequently, the necessary data for this identification is available through

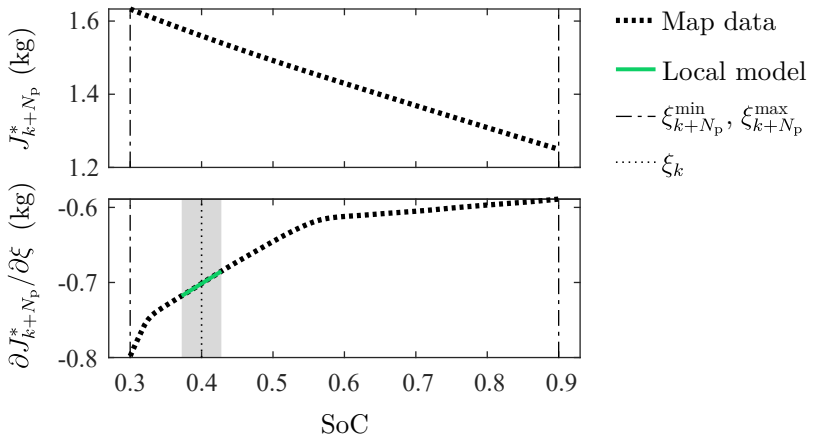

Figure 8: Typical profiles of the optimal cost-to-go (upper plot) and its partial derivative with respect to the SoC (lower plot) over the feasible SoC range. The lower plot includes a local linear model that is fitted within a predefined range (shaded area) around ξ_k. The figure is adapted from Publication C.

a position-based interpolation in the map $\lambda(s, \xi)$, which is the output of the offline optimization (see Section 1.5.2). Based on this model, the local quadratic approximation of the cost-to-go that is used in the objective function can be expressed with

$$\hat{J}^*_{k+N_p}(\xi_{k+N_p}) = (\gamma_0 - 2\gamma_1\xi_k)\,\xi_{k+N_p} + \gamma_1\xi^2_{k+N_p} \tag{28}$$

where constant terms, which are irrelevant to the optimization, are intentionally omitted.

Relation to the cost-to-go-based predictive ECMS

If the short-term prediction horizon approaches zero, the cost-to-go-based MPC corresponds to the cost-to-go-based predictive ECMS presented in Section 1.5.2. This relation can be shown with a single-step MPC

$$J_k = \dot{m}_{FCS}(P_{FCS,k})T_s + \hat{J}^*_{k+1}(\xi_{k+1}) \tag{29}$$

where the original powertrain model is considered, as in the predictive ECMS. The battery SoC model is discretized assuming a zero-order hold, which gives $\xi_{k+1} = \xi_k + T_s f(P_b)$. If now the prediction horizon approaches zero $T_s \to 0$, $\xi_{k+1} \to \xi_k$. Consequently, the local model of the derivative of the cost-to-go defined in Eq. (27) can be approximated with a constant $\lambda = \gamma_0$, and the linear term can be omitted. Plugging Eq. (28) with $\gamma_1 = 0$ and the discretized battery model into Eq. (29), the objective function of the MPC can be rewritten as:

$$J_k = \dot{m}_{FCS}(P_{FCS,k})T_s + \lambda\xi_k + \lambda T_s f(P_{el,k} - P_{FCS,k}). \tag{30}$$

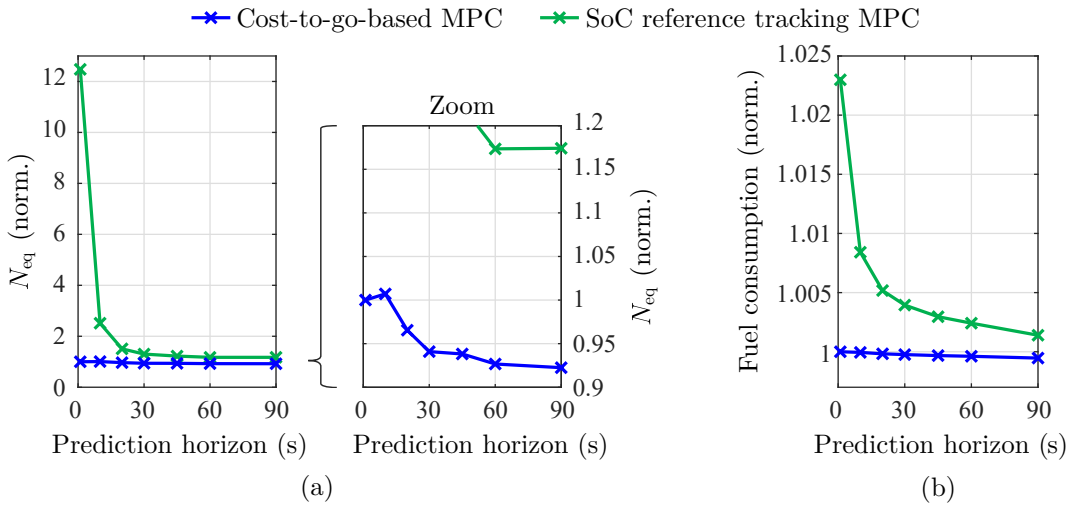

Figure 9: Comparison of (a) the equivalent number of FCS load cycles and (b) the fuel consumption (both normalized) as a function of the short-term prediction horizon length. The figure is adapted from Publication C.

Because the second term and T_s are constants, the arguments of $\min J_k$ and $\min H$, where H is the equivalent fuel consumption rate of the predictive ECMS according to Eq. (11), are identical.

Selected results

The cost-to-go-based energy management and its advantages were already analyzed in the results of the cost-to-go-based ECMS in Section 1.5.2. The focus here is the analysis of additional benefits from the inclusion of short-term predictions, which are assumed to coincide with the actual power demand. For this purpose, the effect of the length of the short-term prediction on two performance indices is analyzed based on the simulation results of a real driving mission. The first performance index is the equivalent number of FCS load cycles N_{eq}, which quantifies the dynamic load on the FCS. Dynamic load causes harsh operating conditions that affect the fuel cell lifetime [33]. Therefore, N_{eq} can be interpreted as a degradation measure. The second performance index is the fuel consumption for the driving mission. The results are shown in Fig. 9.

The equivalent number of FCS load cycles of the cost-to-go-based MPC significantly decreases with a growing short-term prediction horizon. For example, a 30 s short-term prediction horizon reduces N_{eq} by 6 % compared with the performance with a 1 s short-term prediction. The fuel consumption also decreases with longer short-term predictions but only to an insignificant extent (< 0.1 %). The results indicate that the main benefit of the integration of short-term predictions into the cost-to-go-based energy management is a reduction of the dynamic load on the FCS, which favors its durability.

Additionally, the cost-to-go-based MPC is benchmarked against an MPC that

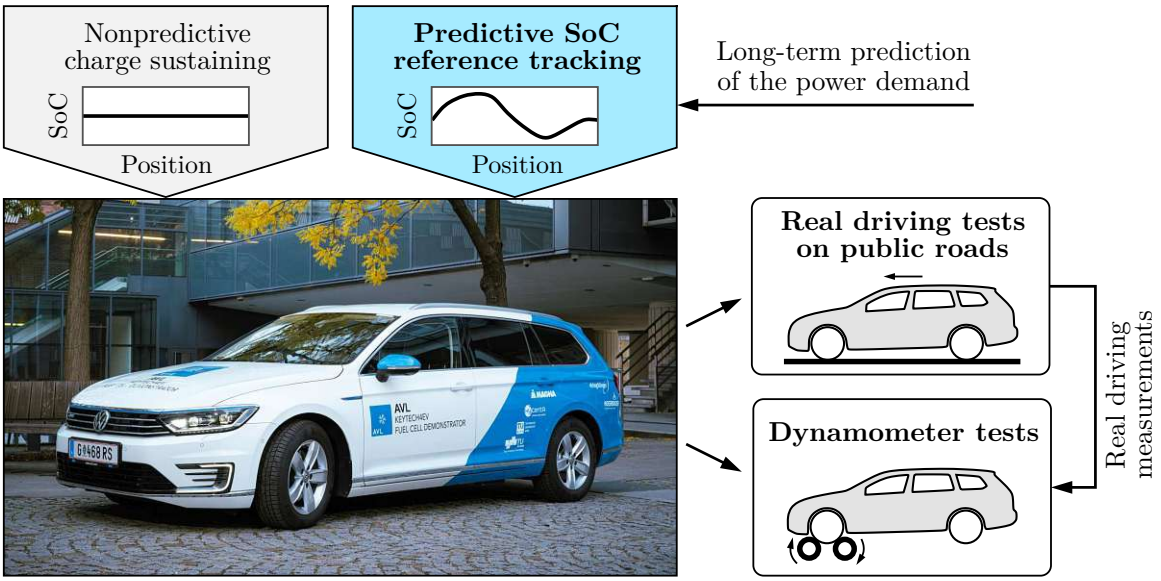

Figure 10: Experimental validation of the predictive SoC reference tracking with a fuel cell demonstrator vehicle of AVL List GmbH. The figure is adapted from Publication D.

tracks an optimized SoC reference trajectory, which is a state-of-the-art approach for combining short-term and long-term predictions [26]. The cost-to-go-based MPC performs considerably better regarding the fuel consumption and the equivalent number of load cycles, particularly with short prediction horizons where the assumed high accuracy is realistic. Most notably, the SoC reference tracking MPC stresses the FCS with significantly more dynamic load, which drastically increases if the short-term prediction horizon approaches zero. With a 1 s prediction horizon, the SoC reference tracking MPC causes an equivalent number of load cycles that is 12 times higher than the number of the cost-to-go MPC, and the fuel consumption is increased by more than 2 %. It can therefore be concluded that the cost-to-go-based energy management also brings significant advantages for the exploitation of short-term predictions.

1.5.5 Experimental validation with a real vehicle

So far, the investigated two-stage EMSs that are informed with a route-derived long-term prediction have shown remarkable performances in simulation. Even though the simulation studies in this work put a strong emphasis on real-world driving and include the most relevant disturbances with respect to the long-term prediction, such as traffic-induced variations in speed and vehicle standstills, simulations always deviate from reality because of modeling errors, unconsidered system behavior, and neglected environmental influences.

The objective of the contribution presented in this section is the experimental

validation of the effectiveness of route-derived long-term predictions for improving fuel efficiency. For this purpose, a two-stage EMS that considers long-term predictions of the power demand is benchmarked against a nonpredictive strategy in real driving tests with a fuel cell passenger vehicle (see Fig. 10). The power demand prediction is derived from the speed limits and the altitude profile along the route using the model of the longitudinal vehicle dynamics, as explained in Section 1.5.1. Both pieces of information are readily accessible if the route is planned before departure. The characteristics of the experimental validation are summarized below:

- Investigated EMS: The investigated two-stage EMS is a **predictive SoC reference tracking strategy**. The SoC reference trajectory is optimized based on the long-term prediction before departure and then tracked with a basic control law while driving (see also Fig. 1). This simpler realization of two-stage energy management is chosen here to assess the improvement by considering long-term predictions in more general. Further improvements are expected with the advanced cost-to-go-based methods presented in the previous sections.

- Nonpredictive benchmark: The benchmark for validating performance improvements is a nonpredictive **charge sustaining strategy**. To ensure a fair comparison, the charge sustaining strategy is based on the tracking controller of the predictive SoC reference tracking but uses a constant SoC reference instead of an optimized one.

- Performance criterion: The performance is quantified in the form of an **equivalent fuel consumption**. It considers the measured hydrogen consumption and additionally corrects variations in the traction energy and the energy contribution of the battery. The correction of these variations is crucial for the comparison of the individual real driving tests.

- **Real driving tests**: The first part of the validation consists of real driving tests that were repeatedly conducted for both EMSs on predefined routes on public roads. The real driving tests were strongly influenced by unpredicted disturbances, such as dense traffic, traffic control, and varying environmental conditions, and represent the actual application. The tests confirmed the robustness of the predictive SoC reference tracking and gave first impressions of the expected performance improvement.

- **Dynamometer tests**: In the second part of the validation, tests were performed on a chassis dynamometer testbed. Here, driving cycles can be reproduced, which allows for a direct performance comparison of the two EMSs and results with high significance. The dynamometer tests are based on real driving measurements and thus preserve the focus on the real-world application.

In the following, the main results of the dynamometer tests are presented. For the other results of the validation, the reader is referred to Publication D.

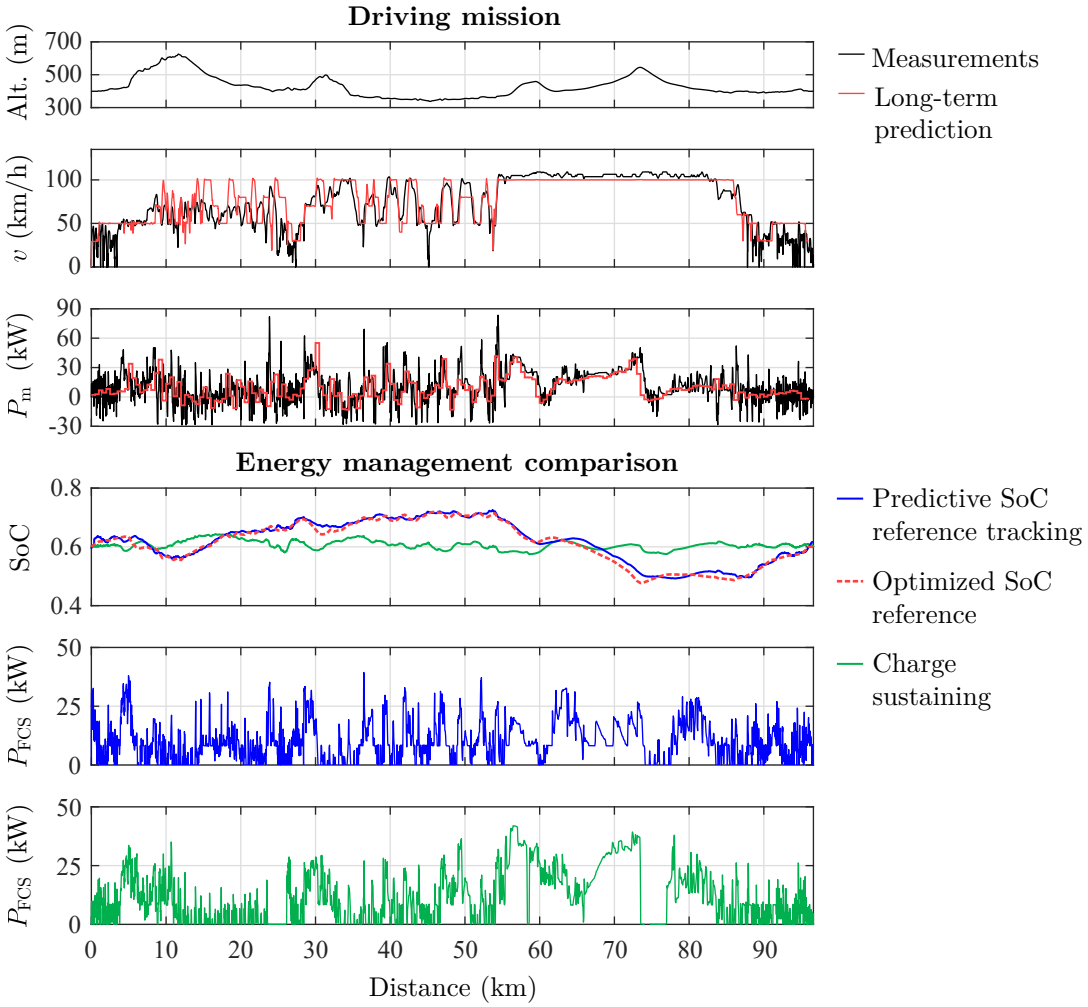

Figure 11: Results of the experimental validation on the dynamometer testbed. The figure is adapted from Publication D.

Selected dynamometer test results

The investigated real driving mission that was reproduced on the dynamometer testbed is shown in the three upper plots of Fig. 11. The route-derived long-term prediction gives good estimates of the actual velocity and the traction power demand but inevitably deviates due to real-world influences, particularly in the urban sections at the beginning and the end of the trip. The driving mission includes substantial changes in altitude, which have a strong impact on the traction power demand profile.

The three lower plots of Fig. 11 compare the predictive SoC reference tracking with the nonpredictive charge sustaining qualitatively. It is worth mentioning that both EMSs are implemented with a stopmode that allows the FCS to drop the power to 0 W while the FCS-related auxiliaries including the compressor remain active. Therefore, frequent

switching between active operation and the stopmode is possible, and the FCS is never completely shut down. Tracking a constant SoC reference of 0.6, the charge sustaining strategy shows a clear power following behavior, i.e., the FCS power strongly varies with the power demand. Under low power demand, the FCS enters the stopmode frequently. In contrast, the predictive SoC reference tracking strategy actively uses the battery as an energy buffer by following the optimized reference. In this way, inefficient FCS operation at high power is avoided, and FCS operation at low power, where the FCS efficiency peaks, is extended. The predictive SoC reference tracking also reduces the time spent in the stopmode. Consequently, the mean FCS efficiency is considerably increased from 50.1 % for the charge sustaining to 54.2 % for the predictive SoC reference tracking. The result is a significant reduction of 6.4 % in the equivalent fuel consumption compared with the charge sustaining strategy. This remarkable performance improvement validates the effectiveness of route-derived long-term predictions in combination with a two-stage EMS.

1.6 Scientific contributions

This dissertation presents several scientific contributions in the field of predictive energy management of fuel cell vehicles. The contributions successfully provide solutions to the research problems defined in Section 1.3, as summarized below.

RP.1 Robust exploitation of long-term predictions

- A two-stage energy management concept that robustly exploits long-term predictions with limited accuracy is proposed.
- The concept is based on the optimal cost-to-go, which provides predictive control information within the entire distance-SoC space.
- The proposed cost-to-go-based ECMS continuously adapts to the actual conditions, which ensures robustness against unpredicted disturbances and enables close-to-optimal fuel efficiency.
- Simplified, control-oriented modeling ensures low computational requirements and real-time capability.
- The concept is applicable to different vehicle categories, such as passenger vehicles, heavy-duty trucks, buses, and railway vehicles.

RP.2 Minimization of the number of fuel cell stack starts/stops

- Predictive fuel cell stack start/stop control is integrated into the cost-to-go-based energy management concept.

- The start/stop strategy is based on a map that indicates the optimal FCS states depending on the position and the SoC. The map is optimized based on the long-term prediction.
- A start/stop condition considering actual system measurements prevents inefficient start/stop actions and ensures smooth operation.
- The method robustly minimizes the number of harmful start/stop actions while preserving high fuel efficiency.
- A generic formulation makes the method applicable to single-stack and multi-stack FCSs.

RP.3 Consideration of short-term predictions

- A real-time EMS based on MPC is proposed to include short-term predictions that are updated in real time in the cost-to-go-based energy management concept.
- The additional consideration of short-term predictions allows for a reduction of dynamic load on the FCS, which mitigates the associated degradation.
- A linear MPC formulation ensures convergence and real-time capability.
- The equivalence between the cost-to-go-based ECMS and the cost-to-go-based MPC with a short-term prediction horizon approaching zero is shown.

RP.4 Experimental validation

- The effectiveness of route-derived long-term predictions in combination with two-stage energy management was experimentally validated with a real fuel cell passenger vehicle.
- The application-oriented validation was conducted based on real driving missions on public roads, where random influences such as traffic cause considerable disturbances with respect to the long-term prediction.
- A selected real driving mission was reproduced on a dynamometer testbed to directly compare the investigated predictive EMS with a nonpredictive benchmark.
- The dynamometer test revealed a considerable 6.4 % reduction in fuel consumption.

To conclude, this dissertation proposed an energy management concept for fuel cell vehicles that robustly exploits long-term predictions available from static route information. Continuously adapting to the actual conditions, the EMSs based on this concept achieve close-to-optimal fuel efficiency. Additionally, the number of fuel cell

stack start/stop events can be minimized, or transient operation of the FCS can be reduced by including real-time short-term predictions. Both are measures to mitigate FCS degradation. The proposed energy management concept therefore contributes to increasing the efficiency, durability, and competitiveness of fuel cell vehicles. Thanks to the model-based approach, the concept is applicable to different vehicle categories, such as passenger vehicles, heavy-duty trucks, and rail vehicles. Moreover, real-world experiments with a fuel cell vehicle validated the significant benefit of exploiting route-derived long-term predictions for increasing fuel efficiency.

Bibliography

[1] IEA. Global EV outlook 2023: Catching up with climate ambitions. *OECD Publishing*, 2023.

[2] Simone Lombardi, Laura Tribioli, Giulio Guandalini, and Paolo Iora. Energy performance and well-to-wheel analysis of different powertrain solutions for freight transportation. *International Journal of Hydrogen Energy*, 45(22):12535–12554, 2020.

[3] Genevieve Giuliano, Maged Dessouky, Sue Dexter, Jiawen Fang, Shichun Hu, and Marshall Miller. Heavy-duty trucks: The challenge of getting to zero. *Transportation Research Part D: Transport and Environment*, 93:102742, 2021.

[4] Emir Çabukoglu, Gil Georges, Lukas Küng, Giacomo Pareschi, and Konstantinos Boulouchos. Battery electric propulsion: An option for heavy-duty vehicles? Results from a Swiss case-study. *Transportation Research Part C: Emerging Technologies*, 88:107–123, 2018.

[5] Kelly L. Fleming, Austin L. Brown, Lew Fulton, and Marshall Miller. Electrification of Medium- and Heavy-Duty Ground Transportation: Status Report. *Current Sustainable/Renewable Energy Reports*, 8(3):180–188, September 2021.

[6] David A. Cullen, K. C. Neyerlin, Rajesh K. Ahluwalia, Rangachary Mukundan, Karren L. More, Rodney L. Borup, Adam Z. Weber, Deborah J. Myers, and Ahmet Kusoglu. New roads and challenges for fuel cells in heavy-duty transportation. *Nature Energy*, 6(5):462–474, May 2021. Publisher: Nature Publishing Group.

[7] Kate Forrest, Michael Mac Kinnon, Brian Tarroja, and Scott Samuelsen. Estimating the technical feasibility of fuel cell and battery electric vehicles for the medium and heavy duty sectors in California. *Applied Energy*, 276:115439, 2020.

[8] Emir Çabukoglu, Gil Georges, Lukas Küng, Giacomo Pareschi, and Konstantinos Boulouchos. Fuel cell electric vehicles: An option to decarbonize heavy-duty trans-

port? Results from a Swiss case-study. *Transportation Research Part D: Transport and Environment*, 70:35–48, 2019.

[9] Jasem Alazemi and John Andrews. Automotive hydrogen fuelling stations: An international review. *Renewable and Sustainable Energy Reviews*, 48:483–499, 2015.

[10] Zachary P. Cano, Dustin Banham, Siyu Ye, Andreas Hintennach, Jun Lu, Michael Fowler, and Zhongwei Chen. Batteries and fuel cells for emerging electric vehicle markets. *Nature Energy*, 3(4):279–289, April 2018. Publisher: Nature Publishing Group.

[11] Xinyou Lin, Yutian Xia, Wei Huang, and Hailin Li. Trip distance adaptive power prediction control strategy optimization for a plug-in fuel cell electric vehicle. *Energy*, 224:120232, 2021.

[12] Yonggang Liu, Jie Li, Zheng Chen, Datong Qin, and Yi Zhang. Research on a multi-objective hierarchical prediction energy management strategy for range extended fuel cell vehicles. *Journal of Power Sources*, 429:55–66, 2019.

[13] Yang Zhou, Alexandre Ravey, and Marie-Cécile Péra. A survey on driving prediction techniques for predictive energy management of plug-in hybrid electric vehicles. *Journal of Power Sources*, 412:480–495, 2019.

[14] Saeid Zendegan, Alessandro Ferrara, Stefan Jakubek, and Christoph Hametner. Predictive battery state of charge reference generation using basic route information for optimal energy management of heavy-duty fuel cell vehicles. *IEEE Transactions on Vehicular Technology*, 70(12):12517–12528, 2021.

[15] Bo Geng, James K. Mills, and Dong Sun. Two-stage energy management control of fuel cell plug-in hybrid electric vehicles considering fuel cell longevity. *IEEE Transactions on Vehicular Technology*, 61(2):498–508, 2012.

[16] He Tian, Xu Wang, Ziwang Lu, Yong Huang, and Guangyu Tian. Adaptive fuzzy logic energy management strategy based on reasonable SOC reference curve for online control of plug-in hybrid electric city bus. *IEEE Transactions on Intelligent Transportation Systems*, 19(5):1607–1617, 2018.

[17] Sichen Gao, Yuhua Zong, Fei Ju, Qun Wang, Weiwei Huo, Liangmo Wang, and Tao Wang. Scenario-oriented adaptive ECMS using speed prediction for fuel cell vehicles in real-world driving. *Energy*, 304:132028, 2024.

[18] Huizhong Gao, Zhijie Wang, Shaoping Yin, Jun Lu, Zhaoyuan Guo, and Weifeng

Ma. Adaptive real-time optimal energy management strategy based on equivalent factors optimization for hybrid fuel cell system. *International Journal of Hydrogen Energy*, 46(5):4329–4338, 2021.

[19] Dominik Moser, Harald Waschl, Roman Schmied, Hajrudin Efendic, and Luigi Del Re. Short term prediction of a vehicle's velocity trajectory using ITS. *SAE International Journal of Passenger Cars-Electronic and Electrical Systems*, 8(2015-01-0295):364–370, 2015.

[20] Fengqi Zhang, Junqiang Xi, and Reza Langari. Real-time energy management strategy based on velocity forecasts using V2V and V2I communications. *IEEE Transactions on Intelligent Transportation Systems*, 18(2):416–430, 2017.

[21] Eunjeong Hyeon, Daliang Shen, Dominik Karbowski, and Aymeric Rousseau. Forecasting short to mid-length speed trajectories of preceding vehicle using V2X connectivity for eco-driving of electric vehicles. *SAE International Journal of Advances and Current Practices in Mobility*, 3(2021-01-0431):1801–1809, 2021.

[22] Eunjeong Hyeon, Youngki Kim, Niket Prakash, and Anna G. Stefanopoulou. Short-term speed forecasting using vehicle wireless communications. In *2019 American Control Conference (ACC)*, pages 736–741, 2019.

[23] M. Piras, V. De Bellis, E. Malfi, R. Novella, and M. Lopez-Juarez. Adaptive ECMS based on speed forecasting for the control of a heavy-duty fuel cell vehicle for real-world driving. *Energy Conversion and Management*, 289:117178, 2023.

[24] Tao Zeng, Caizhi Zhang, Yanyi Zhang, Chenghao Deng, Dong Hao, Zhongwen Zhu, Hongxu Ran, and Dongpu Cao. Optimization-oriented adaptive equivalent consumption minimization strategy based on short-term demand power prediction for fuel cell hybrid vehicle. *Energy*, 227:120305, 2021.

[25] Xiyun Li, Yujie Wang, Duo Yang, and Zonghai Chen. Adaptive energy management strategy for fuel cell/battery hybrid vehicles using Pontryagin's minimal principle. *Journal of Power Sources*, 440:227105, 2019.

[26] Xinyou Lin, Xinhao Xu, and Haibo Lin. Predictive-ECMS based degradation protective control strategy for a fuel cell hybrid electric vehicle considering uphill condition. *eTransportation*, 12:100168, 2022.

[27] Xudong Zhang, Lingxiong Guo, Ningyuan Guo, Yuan Zou, and Guodong Du. Bi-level energy management of plug-in hybrid electric vehicles for fuel economy and

battery lifetime with intelligent state-of-charge reference. *Journal of Power Sources*, 481:228798, 2021.

[28] Yang Zhou, Alexandre Ravey, and Marie-Cécile Péra. Multi-objective energy management for fuel cell electric vehicles using online-learning enhanced Markov speed predictor. *Energy Conversion and Management*, 213:112821, 2020.

[29] Qiuhao Hu, Mohammad Reza Amini, Ilya Kolmanovsky, Jing Sun, Ashley Wiese, and Julia Buckland Seeds. Multihorizon model predictive control: An application to integrated power and thermal management of connected hybrid electric vehicles. *IEEE Transactions on Control Systems Technology*, 30(3):1052–1064, 2022.

[30] Lars Johannesson and Bo Egardt. A novel algorithm for predictive control of parallel hybrid powertrains based on dynamic programming. *IFAC Proceedings Volumes*, 40(10):343–350, 2007. 5th IFAC Symposium on Advances in Automotive Control.

[31] Chen Zhang and Ardalan Vahidi. Route preview in energy management of plug-in hybrid vehicles. *IEEE Transactions on Control Systems Technology*, 20(2):546–553, 2012.

[32] Viktor Larsson, Lars Johannesson Mårdh, Bo Egardt, and Sten Karlsson. Commuter route optimized energy management of hybrid electric vehicles. *IEEE Transactions on Intelligent Transportation Systems*, 15(3):1145–1154, 2014.

[33] Peng Ren, Pucheng Pei, Yuehua Li, Ziyao Wu, Dongfang Chen, and Shangwei Huang. Degradation mechanisms of proton exchange membrane fuel cell under typical automotive operating conditions. *Progress in Energy and Combustion Science*, 80:100859, 2020.

[34] Tong Zhang, Peiqi Wang, Huicui Chen, and Pucheng Pei. A review of automotive proton exchange membrane fuel cell degradation under start-stop operating condition. *Applied Energy*, 223:249–262, 2018.

[35] Yi Yu, Hui Li, Haijiang Wang, Xiao-Zi Yuan, Guangjin Wang, and Mu Pan. A review on performance degradation of proton exchange membrane fuel cells during startup and shutdown processes: Causes, consequences, and mitigation strategies. *Journal of Power Sources*, 205:10–23, 2012.

[36] Mohammadreza Moghadari, Mohsen Kandidayeni, Loïc Boulon, and Hicham Chaoui. Operating cost comparison of a single-stack and a multi-stack hybrid fuel cell vehicle through an online hierarchical strategy. *IEEE Transactions on Vehicular Technology*, 72(1):267–279, 2023.

[37] Xu Han, Feiqiang Li, Tao Zhang, Tong Zhang, and Ke Song. Economic energy management strategy design and simulation for a dual-stack fuel cell electric vehicle. *International Journal of Hydrogen Energy*, 42(16):11584–11595, 2017.

[38] Arivoli Anbarasu, Truong Quang Dinh, and Somnath Sengupta. Novel enhancement of energy management in fuel cell hybrid electric vehicle by an advanced dynamic model predictive control. *Energy Conversion and Management*, 267:115883, 2022.

[39] Caizhi Zhang, Tao Zeng, Qi Wu, Chenghao Deng, Siew Hwa Chan, and Zhixiang Liu. Improved efficiency maximization strategy for vehicular dual-stack fuel cell system considering load state of sub-stacks through predictive soft-loading. *Renewable Energy*, 179:929–944, 2021.

[40] Khalid Ettihir, Loïc Boulon, and Kodjo Agbossou. Energy management strategy for a fuel cell hybrid vehicle based on maximum efficiency and maximum power identification. *IET Electrical Systems in Transportation*, 6(4):261–268, 2016.

[41] Hongtao Zhang, Xianguo Li, Xinzhi Liu, and Jinyue Yan. Enhancing fuel cell durability for fuel cell plug-in hybrid electric vehicles through strategic power management. *Applied Energy*, 241:483–490, 2019.

[42] Alessandro Ferrara and Christoph Hametner. Predictive activation strategy for health-conscious energy management of multi-module fuel cell systems in heavy-duty long-haul electric trucks. In *16th International Conference on Engines & Vehicles*. SAE International, Aug. 2023.

[43] Mehdi Ansarey, Masoud Shariat Panahi, Hussein Ziarati, and Mohammad Mahjoob. Optimal energy management in a dual-storage fuel-cell hybrid vehicle using multi-dimensional dynamic programming. *Journal of Power Sources*, 250:359–371, 2014.

[44] Cong Geng, Shujian Mei, Li Liu, Wenhui Ma, and Qicheng Xue. Simulation and experimental research on energy management control strategy for fuel cell heavy-duty truck. *International Journal of Hydrogen Energy*, 69:1305–1318, 2024.

[45] Yuxiang Zhang, Rui Ma, Dongdong Zhao, Yigeng Huangfu, and Weiguo Liu. A novel energy management strategy based on dual reward function Q-learning for fuel cell hybrid electric vehicle. *IEEE Transactions on Industrial Electronics*, 69(2):1537–1547, 2022.

[46] Liangfei Xu, Jianqiu Li, and Minggao Ouyang. Energy flow modeling and real-time control design basing on mean values for maximizing driving mileage of a fuel cell bus. *International Journal of Hydrogen Energy*, 40(43):15052–15066, 2015.

[47] Xiangjun Li, Liangfei Xu, Jianfeng Hua, Xinfan Lin, Jianqiu Li, and Minggao Ouyang. Power management strategy for vehicular-applied hybrid fuel cell/battery power system. *Journal of Power Sources*, 191(2):542–549, 2009.

[48] Mehdi Sellali, Alexandre Ravey, Achour Betka, Abdellah Kouzou, Mohamed Benbouzid, Abdesslem Djerdir, Ralph Kennel, and Mohamed Abdelrahem. Multi-objective optimization-based health-conscious predictive energy management strategy for fuel cell hybrid electric vehicles. *Energies*, 15(4), 2022.

[49] Lino Guzzella and Antonio Sciarretta. *Vehicle Propulsion Systems: Introduction to Modeling and Optimization*. Springer Berlin Heidelberg, Berlin, Heidelberg, 2013.

[50] Olle Sundström and Lino Guzzella. A generic dynamic programming Matlab function. In *Proceedings of the IEEE International Conference on Control Applications*, pages 1625–1630, 2009.

[51] Lorenzo Serrao, Simona Onori, and Giorgio Rizzoni. ECMS as a realization of Pontryagin's minimum principle for HEV control. In *2009 American Control Conference*, pages 3964–3969, 2009.

Chapter 2

Publications

This chapter comprises the four research articles that describe the solutions to the stated research problems in detail. The research articles are first listed below and then included in full length.

Publication A

Sandro Kofler, Stefan Jakubek, and Christoph Hametner.
Cost-to-go-based predictive equivalent consumption minimization strategy for fuel cell vehicles considering route information.
2024 IEEE Intelligent Vehicles Symposium (IV), Pages 2910–2916, 2024.
DOI: 10.1109/IV55156.2024.10588715.

Publication B

Sandro Kofler, Stefan Jakubek, and Christoph Hametner.
Predictive energy management strategy with optimal stack start/stop control for fuel cell vehicles.
Applied Energy, Volume 377, Part B, Number 124513, 2025.
DOI: 10.1016/j.apenergy.2024.124513.

Publication C

Sandro Kofler, Zhang Peng Du, Stefan Jakubek, and Christoph Hametner.
Predictive energy management strategy for fuel cell vehicles combining long-term and short-term forecasts.
IEEE Transactions on Vehicular Technology, Volume 73, Issue 11, Pages 16364–16374, 2024.
DOI: 10.1109/TVT.2024.3424422.

Publication D

Sandro Kofler, Georg Rammer, Alexander Schnabel, David Weingrill, Peter Bardosch, Stefan Jakubek, and Christoph Hametner.
Real-vehicle experimental validation of a predictive energy management strategy for fuel cell vehicles.
Journal of Power Sources, Volume 629, Number 235901, 2025.
DOI: 10.1016/j.jpowsour.2024.235901.

2.1 Publication A

Sandro Kofler, Stefan Jakubek, and Christoph Hametner.
Cost-to-go-based predictive equivalent consumption minimization strategy for fuel cell vehicles considering route information.
2024 IEEE Intelligent Vehicles Symposium (IV), Pages 2910–2916, 2024.
DOI: 10.1109/IV55156.2024.10588715.

Contributions by the author of the dissertation[†]

- Conceptualization
- Methodology
- Software
- Validation
- Formal analysis
- Investigation
- Data curation
- Writing – original draft
- Visualization

[†]According to the Contributor Roles Taxonomy (CRediT), DOI: 10.3789/ansi.niso.z39.104-2022

Cost-To-Go-Based Predictive Equivalent Consumption Minimization Strategy for Fuel Cell Vehicles Considering Route Information

Sandro Kofler[1], Stefan Jakubek[1], and Christoph Hametner[2]

***Abstract*— The equivalent consumption minimization strategy (ECMS) is a well-established energy management strategy for hybrid vehicles, which is easily real-time implementable and can provide optimal energy management. However, optimality requires knowledge of the optimal equivalence factor, which highly depends on the driving cycle and is therefore unknown in advance. This work proposes a predictive ECMS for fuel cell hybrid vehicles, which derives a map describing the optimal equivalence factor for any vehicle position and battery state of charge from the optimal cost-to-go provided from an offline optimization. The offline optimization is conducted with dynamic programming before departure and considers a long-term driving cycle prediction derived from static route information such as speed limits and altitude. Based on the optimal equivalence factor map, the ECMS implicitly considers the long-term prediction in each instant allowing for continuous adaption to the current situation while driving. The performance of the predictive ECMS is demonstrated in a numerical study based on real-world driving cycles highlighting its robustness against unpredicted changes in traffic conditions.**

***Index Terms*— Dynamic programming, equivalent consumption minimization strategy, fuel cell vehicles, optimal energy management, predictive energy management.**

I. INTRODUCTION

Fuel cell electric vehicles are commonly equipped with a battery as secondary power source besides the fuel cell system (FCS). The battery can be used for recuperating energy, avoiding inefficient operation ranges of the FCS, and covering dynamic loads that are harmful for the FCS's lifetime. Thus, the hybridization allows for improving the fuel economy. However, the actual improvement in the fuel efficiency strongly depends on the energy management strategy (EMS), which determines the power split between the FCS and the battery. Besides fuel efficiency, battery state of charge (SoC) control is another important objective for an EMS to prevent overcharging or completely draining the battery. The optimal energy management depends on the power demand profile of the driving mission, which is a priori unknown, and, therefore, serves only as a theoretical benchmark.

A variety of EMSs aiming for approaching the optimal power split in a real-time implementation have been developed, including rule-based, optimization-based, and learning-based methods [1]. A well-established optimization-based method is the equivalent consumption minimization strategy (ECMS), which associates the battery usage with a virtual fuel consumption by means of an equivalence factor. The ECMS is particularly interesting because it is easily real-time implementable and, under certain assumptions, it can be analytically proven to be optimal [2]. However, optimality requires to use the optimal equivalence factor, which again depends on the driving mission and is unknown in advance.

Various works have been focusing on developing algorithms to obtain a performant equivalence factor [3]. A fundamental approach adapts the equivalence factor using a proportional-integral (PI) controller in combination with a constant SoC reference [4]. The SoC reference can also be optimized if a prediction of the driving mission, e.g., from route data, is available, which is known as a high-performing method [5], [6]. However, the performance strongly depends on the tuning of the PI controller [7]. An effective alternative to optimized SoC references for considering predictive information of the upcoming trip is the optimal cost-to-go, which describes the minimum amount of fuel to reach the destination depending on the vehicle position and the SoC. The optimal cost-to-go can be computed with dynamic programming (DP) and allows for deriving the optimal equivalence factor according to the prediction for any SoC and position [8], [9]. However, existing literature on the latter approach focuses mainly on hybrid vehicles with internal combustion engines. Other DP-based approaches derive the equivalence factor in alternative ways [10], [11].

The main contribution of this work is a cost-to-go-based predictive ECMS (P-ECMS) for fuel cell vehicles considering a long-term prediction derived from static route data, i.e., speed limits and elevation. Although the accuracy of such a prediction is limited, it is effective because it is available for the entire driving mission in advance, allowing for an offline optimization before departure. The optimization is conducted with DP based on a simplified powertrain model and yields the optimal cost-to-go. The execution of the DP algorithm is fast because the model includes only one state and a rough discretization is sufficient due to the limited accuracy of the prediction. The optimal cost-to-go implicitly provides the optimal equivalence factor according to the prediction for any situation, even if the actual SoC completely deviates from the originally optimal path due to unpredicted changes in traffic conditions. Consequently, a single offline optimization before departure is sufficient, and no recurrent optimization of the equivalence factor is required while driving. The approach takes into account SoC constraints in the offline optimization

This project is supported with funds from the Climate and Energy Fund and implemented in line with the "Zero Emission Mobility" program.

[1]Institute of Mechanics and Mechatronics, TU Wien, Vienna, Austria. E-mails: sandro.kofler@tuwien.ac.at, stefan.jakubek@tuwien.ac.at.

[2]Christian Doppler Laboratory for Innovative Control and Monitoring of Automative Powertrain Systems, TU Wien, Vienna, Austria. E-mail: christoph.hametner@tuwien.ac.at.

Corresponding author: Sandro Kofler.

and the real-time ECMS.

The remainder of this article is structured as follows. First, the simplified, control-oriented vehicle model is given in Section II before the energy management problem is stated and treated analytically in Section III to motivate the predictive EMS. Then, the proposed cost-to-go-based P-ECMS is described in Section IV. In Section V, an adaptive ECMS (A-ECMS) that adjusts the equivalence factor based on an optimized SoC reference is introduced as a high-performing benchmark for the subsequent numerical study. Finally, the numerical study demonstrates the performance of the P-ECMS using data of real-world driving cycles including considerable changes in traffic conditions in Section VI. The study underlines the robustness of the P-ECMS and shows its ability to satisfy SoC constraints.

II. System Modeling

Optimizing the energy management for a given driving mission requires a power demand prediction for the entire mission and a powertrain model. A simple power demand prediction can be derived from static route information, such as the elevation profile and speed limits, if the driving mission is planned in advance. This section first introduces a model of the longitudinal vehicle dynamics used to derive the power demand prediction from route information and, then, describes the hybrid powertrain model for optimizing the energy management.

A. Vehicle Dynamics for Power Demand Prediction

The dynamics of the vehicle velocity v considers the traction force of the electric motor, aerodynamic drag, rolling friction, and gravitational forces and can be written as

$$m\frac{\mathrm{d}v}{\mathrm{d}t} = \eta_{\mathrm{m}}^{\mathrm{sgn}\,P_{\mathrm{m}}}\frac{P_{\mathrm{m}}}{v} - \frac{\rho A_{\mathrm{f}} c_{\mathrm{d}}}{2}v^2 - c_{\mathrm{r}} m g\cos\theta - mg\sin\theta \tag{1}$$

where m denotes the vehicle mass, t the time, P_{m} the power of the electric motor, ρ the air density, A_{f} the frontal area of the vehicle, c_{d} the aerodynamic drag coefficient, c_{r} the rolling friction coefficient, g the acceleration due to gravity, and θ the road inclination angle [12]. The traction term takes into account the motor efficiency η_{m}. The overall electric power demand P_{el} considers the motor power and the power demand of the auxiliaries P_{aux}:

$$P_{\mathrm{el}} = P_{\mathrm{m}} + P_{\mathrm{aux}}. \tag{2}$$

With (1), the required motor power along the driving mission can be computed if the road inclination and the vehicle velocity are known. The elevation profile and, thus, the road inclination are determined by the topography of the planned route and directly available from terrain maps. In contrast, estimating the vehicle velocity is more challenging due to numerous stochastic influences, such as driver behavior, traffic, or weather conditions. A simple estimate for the velocity can be derived from speed limits, which are available along the planned route. Even though the accuracy of such a prediction is limited, it is effective for the given task because it is a priori available for the entire driving mission. Having the estimated motor power, a prediction of the overall electric power demand can be computed by adding an estimate of the auxiliary power demand.

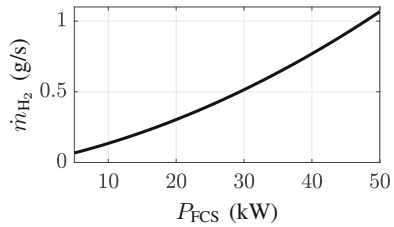

Fig. 1. The FCS model describes the fuel consumption rate as a function of the FCS power.

B. Hybrid Powertrain

The powertrain consists of two power sources: the FCS and the battery. The sum of the FCS power P_{FCS} and the battery power P_{b} satisfies the overall electric power demand:

$$P_{\mathrm{el}} = P_{\mathrm{FCS}} + P_{\mathrm{b}}. \tag{3}$$

The powertrain therefore has one degree of freedom, i.e., the power split between the FCS and the battery, which is determined by the EMS. Whereas the FCS can only provide a positive power output, the battery can also store energy coming from recuperative braking or the FCS.

The two powertrain components are modeled in a simplified, control-oriented way, building the basis for the ECMS formulation and a computationally efficient offline optimization by DP, the computational complexity of which grows exponentially with the number of states [13]. The goal is to optimize the fuel economy. Therefore, the fundamental quantity regarding the FCS is the fuel consumption rate $\dot{m}_{\mathrm{H_2}}$, which is modeled as a function of the FCS power (see Fig. 1). This fuel consumption curve can either be fitted to stationary measurement data or derived analytically [12]. The FCS model implicitly considers the power demand of FCS-related auxiliaries such as the compressor.

The battery is considered as an equivalent circuit model taking into account ohmic losses [12]. With that, the dynamics of the battery SoC ξ is expressed as a nonlinear function of the battery power

$$\dot{\xi} = f(P_{\mathrm{b}}) = -\frac{V_{\mathrm{OC}} - \sqrt{V_{\mathrm{OC}}^2 - 4P_{\mathrm{b}}R_{\mathrm{int}}}}{2Q_0 R_{\mathrm{int}}} \tag{4}$$

depending on the battery parameters V_{OC}, R_{int}, and Q_0 denoting the open-circuit voltage, internal ohmic resistance, and nominal capacity, respectively.

Based on that, the overall powertrain model includes only one state, which is the battery SoC, and one control input defining the power split, which is chosen to be the FCS power. The battery power is determined by the residual of the electric load according to (3) subject to the corresponding constraints.

III. ENERGY MANAGEMENT PROBLEM

The objective is to determine the optimal power split for the driving mission such that the fuel consumption is minimized:

$$\begin{aligned} \min_{P_{\text{FCS}}} J = &\int_{t_0}^{t_1} \dot{m}_{\text{H}_2}(P_{\text{FCS}}(t))\mathrm{d}t \\ \text{s.t.} \quad & P_{\text{FCS}}(t) \in \mathcal{U} \\ & P_{\text{b}}(t) \in \mathcal{B} \\ & \xi(t) \in \mathcal{X} \\ & \xi(t_0) = \xi_0 \\ & \xi(t_1) \in \mathcal{X}_1. \end{aligned} \tag{5}$$

Here, the sets $\mathcal{U}$, $\mathcal{B}$, $\mathcal{X}$, and $\mathcal{X}_1$ describe the feasible ranges of the FCS power, the battery power, the battery SoC, and the battery SoC at the end of the driving mission, respectively. The initial SoC is denoted by ξ_0.

This optimal control problem can be treated analytically with Pontryagin's minimum principle (PMP) [14]. Based on the Hamiltonian

$$H(P_{\text{FCS}}, \lambda, t) = \dot{m}_{\text{H}_2}(P_{\text{FCS}}) + \lambda f(P_{\text{el}}(t) - P_{\text{FCS}}) \tag{6}$$

a set of necessary conditions for the optimality of a solution can be formulated. If the control input P^*_{FCS} is optimal, then a costate λ^* exists such that

$$\dot{\xi}^*(t) = \frac{\partial H(P^*_{\text{FCS}}, \lambda^*, t)}{\partial \lambda} \tag{7a}$$

$$\dot{\lambda}^*(t) = -\frac{\partial H(P^*_{\text{FCS}}, \lambda^*, t)}{\partial \xi} \tag{7b}$$

$$\xi^*(t_0) = \xi_0 \tag{7c}$$

$$\xi^*(t_1) \in \mathcal{X}_1 \tag{7d}$$

and the Hamiltonian is minimized with respect to the control input within its feasible range at each point in time:

$$H(P^*_{\text{FCS}}, \lambda^*, t) \leq H(P_{\text{FCS}}, \lambda^*, t). \tag{7d}$$

Note that the right-hand side of (7b) equals zero because the specified battery SoC dynamics do not depend on the SoC itself and, therefore, λ^* is constant along the optimal path.

Based on these conditions, candidates for the optimal power split can be determined in each instant by solving a simple static minimization problem. This motivates the formulation of the ECMS, a real-time EMS determining the power split by minimizing an equivalent fuel consumption rate linking battery usage to the actual fuel consumption of the FCS via an equivalence factor. Indeed, this equivalent fuel consumption rate can be related to PMP's Hamiltonian with the equivalence factor corresponding to λ [2].

However, the optimal equivalence factor minimizing the overall fuel consumption and satisfying the terminal SoC constraint is a priori unknown and strongly depends on the initial SoC and the driving cycle. Here, the power demand prediction comes into play, allowing to determine prediction-based estimates of the equivalence factor for the planned driving mission. Even though this optimization could be conducted with PMP-based approaches, e.g., the variation of extremals [15], it is avoided here for two reasons: (i) The costate loses its optimality as soon as the SoC deviates from the originally optimal path. This deviation is inevitable since an ideal power demand prediction is impossible, and a recurrent optimization of the equivalence factor would be necessary throughout the driving mission. (ii) The PMP-based solution of the problem does not allow for considering state constraints directly. Instead, this work proposes to determine prediction-based estimates of the optimal equivalence factor based on DP, which is elaborated in the following.

IV. PREDICTIVE ENERGY MANAGEMENT

The proposed predictive EMS consists of two stages. Before departure, the energy management for the planned driving mission is optimized based on the long-term power demand prediction, which is derived from static route information considering the vehicle dynamics (see Section II-A). This offline optimization is conducted with DP, which allows to consider constraints on states and inputs, and yields the optimal cost-to-go, i.e., the amount of fuel required to reach the intended destination along the optimal path, for any position and SoC. Therefore, the optimal cost-to-go provides optimal feedforward information for any situation.

While driving, the real-time energy management is based on an ECMS, whereby the equivalence factor is derived from the optimal cost-to-go from the DP. Consequently, the equivalence factor adapts independently of what happened in the past to the current position along the route and the current SoC and takes the optimal value according to the long-term prediction for the trip remainder.

The major benefit of this cost-to-go-based P-ECMS is that a reoptimization of the equivalence factor during the driving mission is not required. Even if the long-term prediction has deviated completely from the actual power demand in the past, the optimal cost-to-go provides the optimal equivalence factor according to the prediction for the remainder of the driving mission. In the following, the prediction-based offline optimization with DP and the cost-to-go-based real-time P-ECMS are described.

A. Offline Optimization With Dynamic Programming

To solve the optimal control problem (5) with DP, the power demand prediction is segmented with a relatively rough step size to reduce the computational complexity. This segmentation does not necessarily affect the overall performance because of the limited accuracy of the long-term prediction. Here, a distance-based segmentation is chosen, which neglects vehicle standstills and directly yields a distance-based cost-to-go [16]. In contrast to its time-based counterpart, the distance-based formulation is beneficial for the real-time energy management because it is not affected by a deviating velocity prediction. The segmentation can be equidistant or adaptive depending on the power demand signal, which can further reduce the computational complexity [13].

Moreover, the battery model (4) is discretized assuming a zero-order hold for the battery power

$$\xi_{l+1} = \xi_l - \frac{V_{\mathrm{OC}} - \sqrt{V_{\mathrm{OC}}^2 - 4(P_{\mathrm{el},l} - P_{\mathrm{FCS},l})R_{\mathrm{int}}}}{2Q_0 R_{\mathrm{int}}}\Delta t_l \quad (8)$$

where $P_{\mathrm{el},l}$ and $P_{\mathrm{FCS},l}$ denote the mean power demand and the mean FCS power of the l-th segment, respectively. The time to cover the l-th segment Δt_l varies depending on the velocity due to the distance-based segmentation. Furthermore, the state (ξ) and the control input (P_{FCS}) are quantized within their feasible ranges yielding the finite sets $\mathcal{X}^{\mathrm{q}}$ and $\mathcal{U}^{\mathrm{q}}$.

The DP algorithm operates backwards starting at the final position of the driving mission and proceeding segment by segment until the initial position is reached. At the l-th position s_l, the minimum amount of fuel required to reach the destination, i.e., the optimal cost-to-go, is determined for all states in $\mathcal{X}^{\mathrm{q}}$ by minimizing the sum of the transition cost and the cost-to-go at the $(l+1)$-th position, which was computed previously:

$$\begin{aligned} J_l^{\mathrm{o}}(\xi_l) = &\min_{P_{\mathrm{FCS},l}} \left(\dot{m}_{\mathrm{H_2}}(P_{\mathrm{FCS},l})\Delta t_l + J_{l+1}^{\mathrm{o}}(\xi_{l+1})\right) \\ &\text{s.t. } P_{\mathrm{FCS},l} \in \mathcal{U}^{\mathrm{q}} \\ &\quad P_{\mathrm{b},l} \in \mathcal{B} \\ &\quad \xi_{l+1} \in \mathcal{X}_{l+1} \\ &\forall \xi_l \in \mathcal{X}^{\mathrm{q}}. \end{aligned} \quad (9)$$

The set $\mathcal{X}_{l+1} \subseteq \mathcal{X}$ denotes the feasible SoC range at the $(l+1)$-th position, and $(N-1)$ is the number of segments. The algorithm yields the optimal cost-to-go $J^{\mathrm{o}}(s,\xi)$ for all nodes in the discrete distance-SoC grid, i.e., the cost-to-go results in the form of a 2-D map depending on the position and the SoC. Note that the superscript $^{\mathrm{o}}$ denotes optimality regarding the power demand prediction, whereas the superscript * used above denotes optimality regarding the actual power demand.

Comparing the necessary conditions of PMP on the one side and the Hamilton-Jacobi-Bellman equation, interpretable as the continuous-time counterpart of DP, on the other side reveals that the optimal costate corresponds to the partial derivative of the optimal cost-to-go with respect to the state [15]. Consequently, estimates of the optimal equivalence factor can be determined by numerically differentiating the cost-to-go:

$$\bar{\lambda}^{\mathrm{o}}(s,\xi) = \frac{\partial J^{\mathrm{o}}(s,\xi)}{\partial \xi}. \quad (10)$$

Based on linear interpolation, the resulting 2-D map provides estimates of the optimal equivalence factor for any feasible SoC and position along the driving mission, allowing for continuously adapting the energy management to the actual situation.

B. Real-Time Predictive ECMS

Provided with the estimate of the optimal equivalence factor for the current position and SoC, the ECMS determines the optimal FCS power depending on the current power demand with

$$P_{\mathrm{FCS}}^{\mathrm{o}} = \arg\min_{P_{\mathrm{FCS}}} H(P_{\mathrm{FCS}}, \lambda^{\mathrm{o}}, t) \quad (11)$$

subject to the specified FCS and battery power constraints. Since the ECMS does not consider SoC constraints directly, the equivalence factor is adapted in the neighborhood of the constraints favoring charging the battery close to ξ_{min} and discharging close to ξ_{max} [17]. Here, a quadratic adaption is formulated involving two parameters:

$$\lambda^{\mathrm{o}} = \begin{cases} \bar{\lambda}^{\mathrm{o}} + \lambda_{\mathrm{ad}} \left(\frac{\xi - \xi_{\mathrm{max}} + \xi_{\mathrm{th}}}{\xi_{\mathrm{th}}}\right)^2, & \xi > \xi_{\mathrm{max}} - \xi_{\mathrm{th}} \\ \bar{\lambda}^{\mathrm{o}} - \lambda_{\mathrm{ad}} \left(\frac{-\xi + \xi_{\mathrm{min}} + \xi_{\mathrm{th}}}{\xi_{\mathrm{th}}}\right)^2, & \xi < \xi_{\mathrm{min}} + \xi_{\mathrm{th}} \\ \bar{\lambda}^{\mathrm{o}}, & \text{otherwise.} \end{cases} \quad (12)$$

The adaption gets active within a certain threshold ξ_{th} to the constraints and increases quadratically with decreasing gap to the constraints. At the constraints, the adaption takes $\pm\lambda_{\mathrm{ad}}$. In this work, $\xi_{\mathrm{th}} = 0.05$ and $\lambda_{\mathrm{ad}} = 0.3$ are chosen.

V. Adaptive ECMS

In the following numerical study, the proposed P-ECMS is compared to an A-ECMS that adjusts the equivalence factor based on the deviation from a distance-based SoC reference trajectory ξ^{ref} with a PI controller [4]:

$$\bar{\lambda}^{\mathrm{a}} = \lambda_0 + k_{\mathrm{P}}(\xi^{\mathrm{ref}} - \xi) + k_{\mathrm{I}} \int_0^t (\xi^{\mathrm{ref}} - \xi)\mathrm{d}\tau. \quad (13)$$

Here, λ_0 denotes the initial equivalence factor, and k_{P} and k_{I} are the PI controller gains. For a fair comparison with the P-EMCS, the SoC reference trajectory is optimized with the DP algorithm (9). For this purpose, the optimal control inputs $P_{\mathrm{FCS}}^{\mathrm{o}}$ are stored during the backward procedure for all nodes in the distance-SoC grid. The optimal trajectory is then computed in forward direction starting at ξ_0 and interpolating in the optimal control inputs. With that, the A-ECMS is based on exactly the same prediction and offline optimization as the P-ECMS.

The A-ECMS combined with an optimized SoC reference is a powerful method, but its performance strongly depends on the tuning of the PI controller and the choice of λ_0 [7]. For the study, the PI controller was tuned based on several real-world driving cycles resulting in $k_{\mathrm{P}} = -0.7\,\mathrm{kg}$ and $k_{\mathrm{I}} = -6 \cdot 10^{-5}\,\mathrm{kg\,s^{-1}}$. The value of k_{P} increases in the last 5 % of the driving cycle to ensure a comparable SoC at the end. The optimal choice of λ_0 depends on the driving mission and is unknown in advance. As for the P-ECMS, the equivalence factor is adjusted according to (12) in the neighborhood of the SoC constraints giving λ^{a}, and the real-time power split is determined with (11).

VI. Numerical Study

The proposed P-ECMS is analyzed and compared to the A-ECMS, which represents a high-performing benchmark, in simulation. The numerical study is based on two independent real-world driving cycles including substantial changes in

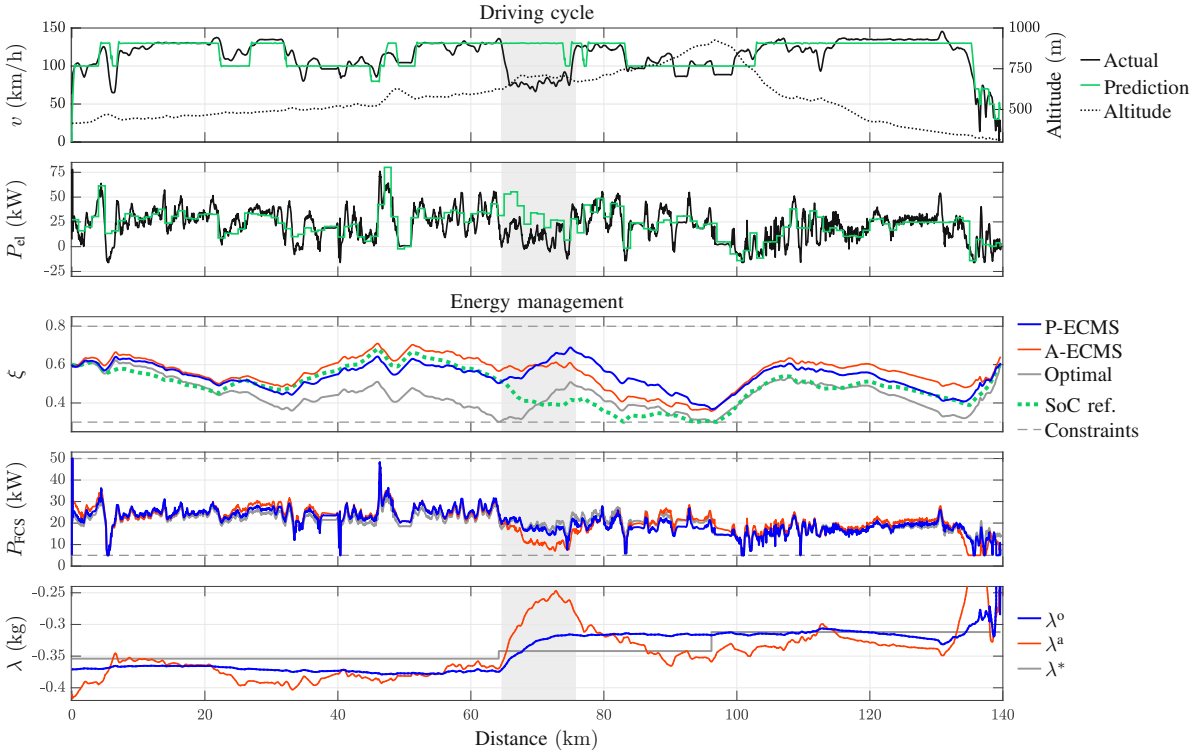

Fig. 2. **Driving cycle A**: Upper plots: Actual data and predictions of the velocity and the power demand. Lower plots: Trajectories of the SoC, the FCS power, and the equivalence factor resulting from the P-ECMS, the A-ECMS ($\lambda_0 = -0.41$) and the optimal power split. The shaded areas mark a roadworks section.

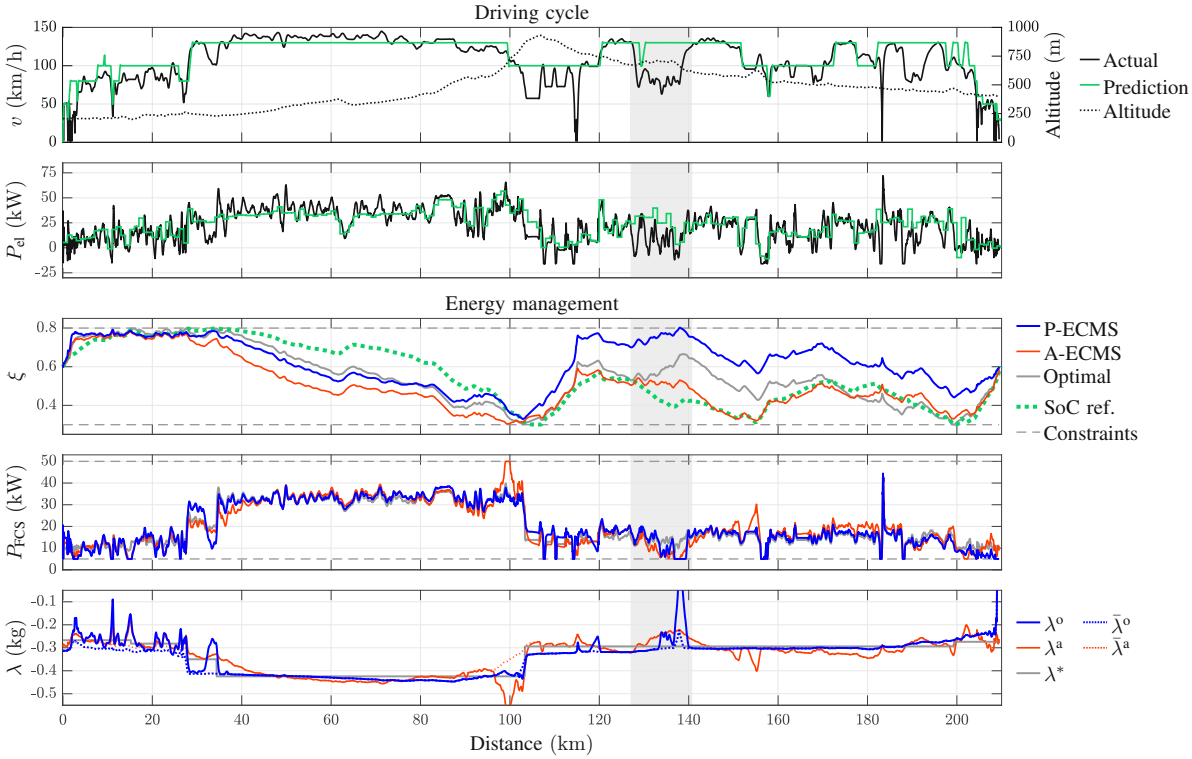

Fig. 3. **Driving cycle B**: Upper plots: Actual data and predictions of the velocity and the power demand. Lower plots: Trajectories of the SoC, the FCS power, and the equivalence factor resulting from the P-ECMS, the A-ECMS ($\lambda_0 = -0.29$) and the optimal power split. The shaded areas mark a roadworks section.

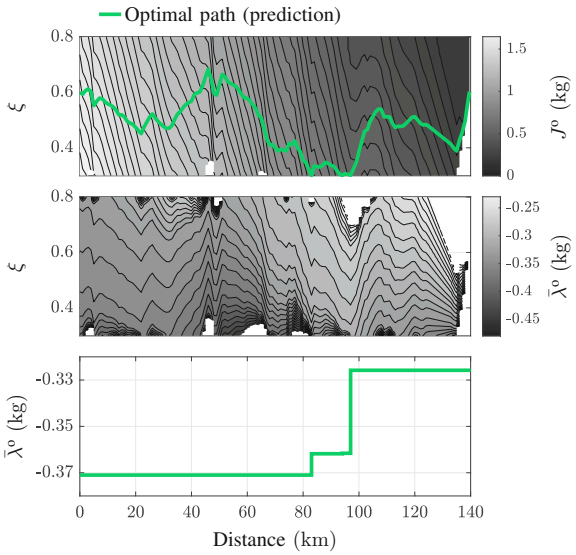

Fig. 4. Results of the offline optimization based on the power demand prediction for driving cycle A: optimal cost-to-go (first plot), optimal equivalence factor (second plot), and trajectory of the optimal equivalence factor along the optimal path (idealized, third plot).

altitude, which are called "A" and "B" in the following. The actual velocity signals were measured during test drives and show considerable deviations with respect to the long-term prediction based on speed limits due to the influences of traffic and temporary roadworks. In this study, the legal speed limits and the elevation along the route, on which the offline optimization is based, were extracted from map data with *AVL Route Studio*, which is a test cycle preparation tool. The velocity prediction takes into account vehicle dynamics at points where the speed limits change. With the velocity prediction and the altitude data, the power demand was predicted based on the longitudinal vehicle model. The velocity, altitude, and power demand profiles of the driving cycles A and B are presented in the upper parts of Figs. 2 and 3, respectively.

The study considers a passenger vehicle with a mass of $1950\,\mathrm{kg}$, which is equipped with a FCS with a maximum power of $50\,\mathrm{kW}$ and a battery with a nominal capacity of $4.95\,\mathrm{kW\,h}$. The polynomial fuel consumption model of the FCS was fitted to measurement data and is shown in Fig. 1. The battery was also modeled based on measurement data resulting in the following parameters: $V_{\mathrm{OC}} = 175\,\mathrm{V}$, $R_{\mathrm{int}} = 0.075\,\Omega$, and $Q_0 = 28.28\,\mathrm{A\,h}$. The efficiency of the motor is approximated with $\eta_{\mathrm{m}} = 0.87$. The control-relevant constraints are specified with $5\,\mathrm{kW} \leq P_{\mathrm{FCS}} \leq 50\,\mathrm{kW}$, $-20\,\mathrm{kW} \leq P_{\mathrm{b}} \leq 30\,\mathrm{kW}$, $0.3 \leq \xi \leq 0.8$, and $\xi(t_1) \geq 0.6$. The initial SoC is 0.6.

A. Offline Optimization

For the offline optimization based on the route-based power demand prediction, the feasible ranges of the SoC and the FCS power are quantized with 150 and 60 grid points, respectively, and an equidistant distance grid with a step size of $1\,\mathrm{km}$ is chosen. The DP algorithm yields optimized information for both compared methods, i.e., the optimal cost-to-go depending on the position and the SoC for the P-ECMS and the optimal path minimizing the amount of fuel for the A-ECMS. The resulting optimal cost-to-go map and the optimal SoC trajectory of driving cycle A are illustrated in the first plot of Fig. 4.

Intuitively, the cost-to-go decreases as the position along the driving mission progresses and equals zero at the destination. The relationship between the cost-to-go and the SoC is also negative; increasing the SoC means that more energy is stored in the battery and, thus, less fuel is required to reach the destination. White areas in the cost-to-go plot mark infeasibility with respect to the predicted power demand.

The map defining the optimal equivalence factor for the P-ECMS is derived from the optimal cost-to-go with (10) and is shown in second plot of Fig. 4. Due to the aforementioned inverse relationship between the cost-to-go and the SoC, the equivalence factor is always negative. An increase in the SoC entails a decrease in the absolute value of the optimal equivalence factor, which can be interpreted as a reduction in the "cost" for battery usage. Since the optimal equivalence factor does not change over time as long as the state constraints are not relevant (see Section III), the contour lines of the equivalence factor map describe optimal paths for any point within the feasible distance-SoC space. At points where state constraints become active, in particular, shortly before kilometer 100, a subset of the optimal paths unite making it evident that the optimal equivalence factor changes at these points. The third plot of Fig. 4 illustrates these changes along the overall optimal path for the prediction.

B. Qualitative Evaluation

The trajectories of the SoC, the FCS power, and the equivalence factor resulting from the P-ECMS and the A-ECMS are illustrated in the lower parts of Figs. 2 and 3. Also, the optimal solution regarding the actual power demand is shown as a benchmark. In the following, the general behavior of the ECMSs is compared based on driving cycle A. Then, the SoC constraint satisfaction is studied based on driving cycle B.

As shown in Fig. 2, the A-ECMS adapts the equivalence factor depending on the deviation from the optimized SoC reference. The FCS power remains relatively close to the optimum as long as the power demand prediction is accurate. However, within the highlighted roadworks section, the prediction overestimates the power demand significantly, affecting the quality of the SoC reference. Consequently, the equivalence factor increases rapidly due to the SoC feedback and the power split deviates from the optimum.

In contrast to the A-ECMS, the P-ECMS is provided with optimized information, i.e., the optimized equivalence factor, within the entire feasible SoC range. Therefore, the strategy has more freedom to move away from the optimal path according to the prediction in case of unpredicted events, which can be seen in the roadworks section. Similar to the optimal power split, the P-ECMS takes advantage of the lower power demand to charge the battery. The FCS

TABLE I
COMPARISON OF FUEL CONSUMPTION

Driving cycle A			
EMS	**λ_0 (kg)**	**m_{H_2} (kg)**	**Rel. difference**
P-ECMS	-	1.465	0 %
Optimal	-	1.454	−0.8 %
A-ECMS	−0.25	1.484	1.3 %
A-ECMS	−0.29	1.476	0.8 %
A-ECMS	−0.33	1.474	0.6 %
A-ECMS	−0.37	1.474	0.6 %
A-ECMS	−0.41	1.478	0.9 %
A-ECMS	−0.45	1.483	1.2 %
Driving cycle B			
EMS	**λ_0 (kg)**	**m_{H_2} (kg)**	**Rel. difference**
P-ECMS	-	2.273	0 %
Optimal	-	2.248	−1.1 %
A-ECMS	−0.25	2.288	0.7 %
A-ECMS	−0.29	2.278	0.2 %
A-ECMS	−0.33	2.276	0.1 %
A-ECMS	−0.37	2.280	0.3 %
A-ECMS	−0.41	2.286	0.6 %
A-ECMS	−0.45	2.297	1.1 %

power initially remains almost unchanged and decreases only gradually as the SoC increases and, consequently, the equivalence factor adapts. Compared to the A-ECMS, the behavior of the equivalence factor is much smoother and, therefore, closer to the optimum.

Unlike in driving cycle A, SoC constraint handling is vital in driving cycle B (see Fig. 3). Because of the comparably low power demand at the beginning of the driving mission, both methods approach the upper SoC constraint triggering the adaption of the equivalence factor (12). Consequently, the FCS power is decreased and constraint violation is avoided. Driving cycle B also includes a roadworks section with considerable deviation from the velocity prediction. Again, the P-ECMS charges the battery similarly to the optimal solution until the upper SoC constraint is approached. In contrast, the A-ECMS keeps discharging the battery and, therefore, behaves less optimally.

C. Quantitative Evaluation

Tab. I compares the hydrogen consumption m_{H_2} of the P-ECMS, the optimal energy management, and the A-ECMS with different initial equivalence factors for both driving cycles. The comparison of the A-ECMS results indicates the effect of λ_0 on the fuel economy; an excellent performance can be achieved but requires an appropriate choice of λ_0, which is unknown in advance. Moreover, the A-ECMS performance depends on the choice of the PI controller gains, which is not further discussed here for the sake of brevity. In contrast, a particular advantage of the P-ECMS is that its performance does not rely on any tuning. The P-ECMS performs consistently better than the A-ECMS regarding the investigated driving cycles, where improvements of up to 1.3 % could be achieved in the fuel economy. This is remarkable considering that the optimal energy management is only approximately 1 % better than the P-ECMS. Note that marginal differences in the final SoC are taken into account in m_{H_2}.

REFERENCES

[1] M. İnci, M. Büyük, M. H. Demir, and G. İlbey, "A review and research on fuel cell electric vehicles: Topologies, power electronic converters, energy management methods, technical challenges, marketing and future aspects," *Renewable and Sustainable Energy Reviews*, vol. 137, p. 110648, 2021. [Online]. Available: https://doi.org/10.1016/j.rser.2020.110648

[2] L. Serrao, S. Onori, and G. Rizzoni, "ECMS as a realization of Pontryagin's minimum principle for HEV control," in *2009 American Control Conference*, 2009, pp. 3964–3969. [Online]. Available: https://doi.org/10.1109/ACC.2009.5160628

[3] F. Zhang, K. Xu, C. Zhou, S. Han, H. Pang, and Y. Cui, "Predictive equivalent consumption minimization strategy for hybrid electric vehicles," in *2019 IEEE Vehicle Power and Propulsion Conference (VPPC)*, 2019, pp. 1–5. [Online]. Available: https://doi.org/10.1109/VPPC46532.2019.8952549

[4] S. Onori and L. Serrao, "On adaptive-ECMS strategies for hybrid electric vehicles," *Int. Sci. Conf. Hybrid Electr. Veh.*, pp. 1–7, 01 2011.

[5] M. Piras, V. De Bellis, E. Malfi, J. M. Desantes, R. Novella, and M. Lopez-Juarez, "Incorporating speed forecasting and soc planning into predictive ecms for heavy-duty fuel cell vehicles," *International Journal of Hydrogen Energy*, vol. 55, pp. 1405–1421, 2024. [Online]. Available: https://doi.org/10.1016/j.ijhydene.2023.11.250

[6] F. Tianheng, Y. Lin, G. Qing, H. Yanqing, Y. Ting, and Y. Bin, "A supervisory control strategy for plug-in hybrid electric vehicles based on energy demand prediction and route preview," *IEEE Trans. Veh. Technol.*, vol. 64, no. 5, pp. 1691–1700, 2015. [Online]. Available: https://doi.org/10.1109/TVT.2014.2336378

[7] D. Chen, Y. Kim, and A. G. Stefanopoulou, "Predictive equivalent consumption minimization strategy with segmented traffic information," *IEEE Trans. Veh. Technol.*, vol. 69, no. 12, pp. 14 377–14 390, 2020. [Online]. Available: https://doi.org/10.1109/TVT.2020.3034552

[8] C. Zhang and A. Vahidi, "Route preview in energy management of plug-in hybrid vehicles," *IEEE Trans. Contr. Syst. Technol.*, vol. 20, no. 2, pp. 546–553, 2012. [Online]. Available: https://doi.org/10.1109/TCST.2011.2115242

[9] V. Larsson, L. Johannesson Mårdh, B. Egardt, and S. Karlsson, "Commuter route optimized energy management of hybrid electric vehicles," *IEEE Trans. Intell. Transport. Syst.*, vol. 15, no. 3, pp. 1145–1154, 2014. [Online]. Available: https://doi.org/10.1109/TITS.2013.2294723

[10] J. Han, D. Kum, and Y. Park, "Synthesis of predictive equivalent consumption minimization strategy for hybrid electric vehicles based on closed-form solution of optimal equivalence factor," *IEEE Trans. Veh. Technol.*, vol. 66, no. 7, pp. 5604–5616, 2017. [Online]. Available: http://doi.org/10.1109/TVT.2017.2660764

[11] D. Pei and M. J. Leamy, "Dynamic Programming-Informed Equivalent Cost Minimization Control Strategies for Hybrid-Electric Vehicles," *Journal of Dynamic Systems, Measurement, and Control*, vol. 135, no. 5, p. 051013, 06 2013. [Online]. Available: https://doi.org/10.1115/1.4024788

[12] L. Guzzella and A. Sciarretta, *Vehicle Propulsion Systems: Introduction to Modeling and Optimization*. Berlin, Heidelberg: Springer Berlin Heidelberg, 2013. [Online]. Available: https://doi.org/10.1007/978-3-642-35913-2_2

[13] S. Kofler, Z. P. Du, S. Jakubek, and C. Hametner, "Adaptive step size dynamic programming for optimal energy management of fuel cell vehicles," in *2023 IEEE Vehicle Power and Propulsion Conference (VPPC)*, 2023, pp. 1–6. [Online]. Available: https://doi.org/10.1109/VPPC60535.2023.10403120

[14] H. P. Geering, *Optimal Control with Engineering Applications*. Berlin, Heidelberg: Springer Berlin Heidelberg, 2007. [Online]. Available: https://doi.org/10.1007/978-3-540-69438-0

[15] D. E. Kirk, *Optimal Control Theory: An Introduction*. Dover Publications, 2004.

[16] S. Kofler, Z. P. Du, S. Jakubek, and C. Hametner, "Predictive energy management strategy for fuel cell vehicles combining long-term and short-term forecasts," *Submitted for publication*, 2024.

[17] J. Han, Y. Park, and D. Kum, "Optimal adaptation of equivalent factor of equivalent consumption minimization strategy for fuel cell hybrid electric vehicles under active state inequality constraints," *Journal of Power Sources*, vol. 267, pp. 491–502, 2014. [Online]. Available: https://doi.org/10.1016/j.jpowsour.2014.05.067

2.2 Publication B

Sandro Kofler, Stefan Jakubek, and Christoph Hametner.
Predictive energy management strategy with optimal stack start/stop control for fuel cell vehicles.
Applied Energy, Volume 377, Part B, Number 124513, 2025.
DOI: 10.1016/j.apenergy.2024.124513.

Contributions by the author of the dissertation[†]

- Conceptualization
- Methodology
- Software
- Formal analysis
- Investigation
- Data curation
- Writing – original draft
- Visualization

[†]According to the Contributor Roles Taxonomy (CRediT), DOI: 10.3789/ansi.niso.z39.104-2022

Applied Energy 377 (2025) 124513

Contents lists available at ScienceDirect

Applied Energy

journal homepage: www.elsevier.com/locate/apenergy

Predictive energy management strategy with optimal stack start/stop control for fuel cell vehicles

Sandro Kofler [a,*], Stefan Jakubek [a], Christoph Hametner [b]

[a] Institute of Mechanics and Mechatronics, TU Wien, Getreidemarkt 9, Vienna, 1060, Austria
[b] Christian Doppler Laboratory for Innovative Control and Monitoring of Automotive Powertrain Systems, TU Wien, Getreidemarkt 9, Vienna, 1060, Austria

ARTICLE INFO

Keywords:
Optimal energy management
Predictive start/stop
Health-aware control
Multi-stack fuel cell system
Dynamic programming
Equivalent consumption minimization strategy

ABSTRACT

Energy management strategies (EMSs) for fuel cell vehicles aim at high fuel efficiency but must also consider the lifetimes of the fuel cell system (FCS) and the battery. Regarding both objectives, fuel cell stack shutdowns play a decisive role in real-world driving situations with low or negative power demand. However, each stack start/stop event is associated with degradation, which is why it is important to keep the number of starts/stops low. This work proposes a predictive EMS with optimal stack start/stop control that takes advantage of a route-based prediction of the entire driving mission to minimize both the fuel consumption and the number of start/stop events. Before departure, the prediction of the entire driving mission is processed in a single offline optimization with dynamic programming. This optimization yields maps providing the real-time EMS with optimal control information that continuously adapts depending on the position along the driving mission and the battery state of charge. Considering this predictive information, the real-time EMS optimizes start/stop actions and the stack power such that the cost-to-go, i.e., the fuel consumption for the trip remainder including start/stop penalties, is implicitly minimized in each instant. In this way, the EMS continuously adapts to the actual conditions, making it robust against unpredicted disturbances, e.g., due to traffic. The superior performance of the proposed strategy compared to state-of-the-art start/stop methods is demonstrated in numerical studies based on real-world driving missions for different vehicle classes with single and multi-stack FCSs.

1. Introduction

The energy management strategy (EMS) of a fuel cell vehicle is responsible for the power allocation between the fuel cell system (FCS), which can consist of multiple fuel cell stacks in parallel [1], and the battery. The primary objective of an EMS is to maximize fuel efficiency. However, the energy management also has a strong impact on the lifetimes of the two powertrain components, which can be increased by avoiding harmful operating conditions [2–5]. For fuel cell stacks, these conditions include low idle power operation, high power operation, dynamic power requests, and, in particular, frequent start/stop events [6–10]. Regarding the battery, high charging and discharging currents as well as extreme states of charge (SoC) favor degradation [11]. This work proposes an optimization-based predictive EMS with stack start/stop control that

- minimizes the fuel consumption while keeping the number of stack starts/stops low,
- prevents other harmful operating conditions with constraints,
- considers a long-term prediction of the driving mission,
- optimally adapts to the actual conditions,
- and is computationally fast and easily implementable.

The proposed concept is based on the equivalent consumption minimization strategy (ECMS), a well-established optimization-based EMS that is easily real-time implementable and yet offers strong energy management performances if the so-called equivalence factor, which expresses a virtual fuel consumption for the use of battery energy, is chosen appropriately. Numerous methods have been proposed for determining performant equivalence factors [12]. Because the optimal equivalence factor strongly depends on the driving mission, predictive ECMS approaches are particularly interesting if a suitable prediction of the planned trip is available. Commonly, an SoC reference trajectory is optimized based on the prediction before departure, and the equivalence factor is then adapted by tracking the SoC reference while driving [13–16]. An effective alternative to optimized SoC reference trajectories are maps expressing the optimal equivalence factor depending on the position along the route and the SoC [17,18], which enables performance improvements as demonstrated in [19]. However, these

* Corresponding author.
E-mail addresses: sandro.kofler@tuwien.ac.at (S. Kofler), stefan.jakubek@tuwien.ac.at (S. Jakubek), christoph.hametner@tuwien.ac.at (C. Hametner).

https://doi.org/10.1016/j.apenergy.2024.124513
Received 10 June 2024; Received in revised form 23 August 2024; Accepted 13 September 2024
Available online 26 September 2024

Nomenclature

Acronyms

DP	Dynamic programming
ECMS	Equivalent consumption minimization strategy
EMS	Energy management strategy
FCS	Fuel cell system
PMP	Pontryagin's minimum principle
SoC	State of charge

Subscripts

curr	Current
final	Final
idle	Idle limit
ind	Indication of map
init	Initial
max	Maximum
min	Minimum

Greek letters

Δt	DP sampling interval (s)
δ	Correction coefficient of rotating mass
η_m	Traction motor efficiency
θ	Road inclination angle (rad)
$\bar{\lambda}^*_{n_\mathrm{st}}$	Adapted equivalence factor for n_st (kg)
λ	Equivalence factor (kg)
λ_ad	Adaption parameter (kg)
λ_SoC	Equivalence factor adaption close to SoC constraints (kg)
$\lambda^*_{n_\mathrm{st}}$	Optimal equivalence factor for n_st (kg)
ξ	Battery SoC
ξ_th	SoC constraint threshold
ρ	Air density (kg/m^3)

Latin letters

A_f	Vehicle frontal area (m^2)
c_d	Aerodynamic drag coefficient
c_r	Rolling friction coefficient
f	Battery SoC dynamics (1/s)
g	Gravitational acceleration (m/s^2)
H	Equivalent fuel consumption rate (kg/s)
$H^*_{n_\mathrm{st}}$	Optimal equivalent fuel consumption rate for n_st (kg/s)
J	Objective function of offline optimization (kg)
J^*	Optimal cost-to-go (kg)
L	Number of grid points in time
l	Step index
$\dot{m}_\mathrm{FCS}$	FCS fuel consumption rate (kg/s)
$\dot{m}_\mathrm{st}$	Stack fuel consumption rate (kg/s)
m	Vehicle mass (kg)
$\mathcal{N}$	Set of possible FCS states
$\mathcal{N}^*$	Set of optimal FCS states
N_st	Number of stacks
n_st	FCS state (number of active stacks)
$\mathcal{P}$	Feasible stack power range (W)
p	Start/stop penalty (kg)
P_b	Battery power (W)
P_el	Electric power demand (W)
P_FCS	FCS power (W)
P_st	Stack power (W)
P^*_st	Optimal stack power (W)
P_aux	Auxiliary power demand (W)
P_m	Traction motor power (W)
Q_0	Battery capacity (A s)
R_int	Internal ohmic resistance (Ω)
s	Position (m)
t	Time (s)
u_st	FCS state in next instant
u^*_st	Optimal FCS state
v	Vehicle velocity (m/s)
v_lim	Speed limits considering cornering speeds (m/s)
V_OC	Open-circuit voltage (V)
v_pred	Predicted vehicle velocity (m/s)
x_st	Current FCS state

predictive ECMS approaches do not include fuel cell stack start/stop control.

Stack start/stop control is particularly relevant in real-world driving situations with low electric power demand, such as in urban areas, or negative power demand, for example, when descending on roads with steep gradients. Shutting down the FCS or individual stacks in these situations can be advantageous in several ways: First, the overall operation time of the FCS is reduced, and harmful low-power operation is avoided. Next, the stack fuel consumption is zero, and the related auxiliary load can be reduced. Last, overcharging the battery, i.e., exceeding a specified upper boundary on the SoC, can be prevented, and the battery charging current is decreased when the power demand is negative, mitigating the strain on the battery. However, unnecessary start/stop actions must be avoided to limit the corresponding impact on the stack lifetime.

In the literature, a common approach for making fuel cell stack start/stop decisions are instantaneous rule-based strategies, which perform start/stop actions depending on the battery SoC [20], the power demand [21,22], the SoC and the power demand [23–28], the requested stack power [29,30], or specified constraints, e.g., on the stack voltage and temperature [31]. More sophisticated methods determine the optimal stack state, i.e., on or off, for the present power demand based on an instantaneous optimization of an equivalent fuel consumption [32]. All strategies mentioned so far are instantaneous, meaning that certain conditions might provoke infeasibly frequent start/stop events. To tackle this issue, instantaneous strategies often include a minimum hold time for the stack state [24,30,33] or a hysteresis [20,25]. Alternatively, optimization-based methods considering short-term predictions [33,34] or neural network-based concepts [35] have been proposed to keep the number of starts/stops low. However, even though these measures are able to reduce the number of start/stop actions, unnecessary and inefficient starts/stops cannot be fully avoided. For example, the FCS might be shut down due to low power demand just before entering a high-power section. Here, taking advantage of a long-term driving mission prediction can be interesting. In [36], such a prediction was considered to optimally plan positions for starts/stops along the route before departure, which allows for a considerable reduction of starts/stops. However, unpredicted disturbances might lead to considerable performance deterioration because the method does not adapt to the actual conditions.

To sum up, the state of the art of fuel cell stack start/stop control can be divided into two main approaches: The more common one is

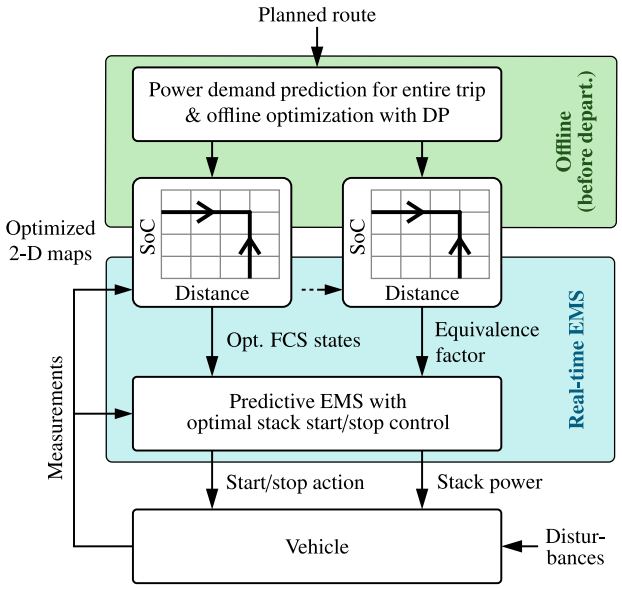

Fig. 1. Proposed energy management concept: The offline optimization based on a route-informed long-term prediction of the power demand yields optimized maps, which are considered in the real-time control. The map outputs and the real-time EMS continuously adapt depending on the actual measurements.

based on instantaneous decisions that cannot fully prevent inefficient start/stop actions. Addressing this problem, the other approach considers a long-term prediction to optimally plan start/stop positions before departure. However, if the actual conditions considerably deviate from the prediction, which must be expected due to hardly predictable influences such as traffic, the performance of this position-based predictive approach might suffer severely. The current literature lacks methods that exploit the long-term prediction more robustly.

Addressing the research gap, this work proposes a predictive EMS with fuel cell stack start/stop control that maximizes fuel efficiency while minimizing start/stop events. The key contributions are summarized as follows:

1. The proposed concept coherently integrates optimal stack start/stop control into an optimization-based predictive EMS based on the ECMS.
2. A long-term prediction for the entire driving mission is considered to optimize 2-D maps before departure. These maps provide optimal control information that continuously adapts to actual system measurements.
3. Considering the predictive information from the maps, the EMS optimally adapts to the actual conditions, i.e., power demand and system states, in each instant. This continuous adaption ensures robustness against unpredicted disturbances.
4. Thanks to the map-based design, computationally complex optimizations over receding horizons are avoided. Therefore, the EMS has low computational requirements and is easily real-time implementable.
5. The predictive concept is benchmarked against the two state-of-the-art start/stop approaches in numerical studies based on real-world driving missions.

The concept extends the predictive ECMS proposed in [19], which uses a similar, map-based approach for robustness against disturbances but does not include start/stop control. This means the FCS remains active during the entire driving mission, which is inefficient or even infeasible in many situations as discussed above. The proposed energy management concept is illustrated in Fig. 1. Before departure, a power demand prediction for the entire driving mission is derived from easily accessible static route information, i.e., the elevation profile and speed limits, based on the vehicle longitudinal dynamics. The prediction enables the optimization of the energy management before departure, where the fuel consumption including penalties on start/stop actions is minimized. This offline optimization is conducted with dynamic programming (DP) [37]. DP breaks the optimization problem into a series of subproblems, where the so-called cost-to-go, i.e., the fuel consumption including start/stop penalties, is minimized for each point in the discrete state space. Consequently, maps providing optimal control information within the entire distance–SoC space and not just along the globally optimal path can be extracted. These 2-D maps are the output of the offline optimization and highly valuable for the real-time control, where deviations from the globally optimal path are expected due to unpredicted disturbances. While driving, the real-time control continuously reads out the optimal control information, i.e., an FCS state indication and the equivalence factor, for the current vehicle position and SoC from the 2-D maps. Considering this predictive information and current state measurements, the real-time control then optimizes the FCS state, i.e., the number of active stacks, and the stack power such that the cost-to-go for the trip remainder is implicitly minimized in each instant. In this way, the real-time EMS continuously adapts to the actual conditions, which makes it inherently robust against disturbances where the actual power demand deviates from the prediction. The predictive EMS achieves an excellent fuel efficiency, keeps the number of start/stop events low, and provides reliable SoC control. Moreover, the proposed concept has low computational requirements. The offline DP is fast and the resulting 2-D maps have a compact size because the offline optimization can be performed with a rough discretization due to the limited accuracy of the long-term prediction. Therefore, departure is possible shortly after the route was planned. Because the prediction is already processed in the offline optimization, the real-time control can be based on a simple, one-dimensional optimization. Thus, it is computationally fast and easily implementable because explicit optimizations over receding prediction horizons are unnecessary.

The remainder of this article is structured as follows. First, the control-oriented vehicle modeling for the predictive EMS is introduced in Section 2. Then, the proposed predictive EMS with optimal stack start/stop control is elaborated in Section 3. In Section 4, two alternative start/stop strategies from the literature, i.e., an instantaneous strategy and a position-based predictive strategy, are described as benchmarks for the subsequent numerical studies. The results of the numerical studies based on real-world driving missions are presented in Section 5, demonstrating the performance and robustness of the method. Finally, Section 6 concludes this article. In the Appendix, the analytically optimal power allocation for a multi-stack FCS is derived, and the convexity of the equivalent fuel consumption function used in the real-time control is shown.

2. Vehicle modeling

To optimize the energy management for a planned driving mission before departure, suitable models of the vehicle are required. First, a model of the vehicle dynamics is used to derive a prediction of the power demand for the entire driving mission from static route information, i.e., speed limits and the elevation profile along the planned route. Subsequently, a model of the hybrid powertrain is used to optimize the energy management based on the prediction. This powertrain model is also relevant for the ECMS-based real-time energy management. The two models are described in the following.

2.1. Vehicle dynamics

To derive the power demand from the speed limits and altitude profile along the route, a model of the longitudinal vehicle dynamics

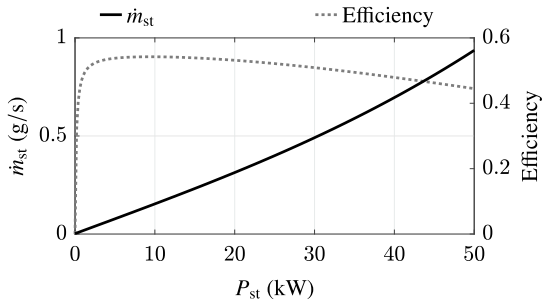

Fig. 2. Fuel consumption curve and corresponding efficiency curve of a fuel cell stack.

is used. The model considers the traction force of the electric motor, aerodynamic drag, rolling friction, and gravitational force [37]:

$$\delta m \frac{\mathrm{d}v}{\mathrm{d}t} = \eta_{\mathrm{m}}^{\operatorname{sgn} P_{\mathrm{m}}} \frac{P_{\mathrm{m}}}{v} - \frac{\rho A_{\mathrm{f}} c_{\mathrm{d}}}{2} v^2 - c_{\mathrm{r}} m g \cos\theta - m g \sin\theta. \tag{1}$$

Here, δ denotes the correction coefficient of rotating mass, m the vehicle mass, v the vehicle velocity, t the time, η_{m} the efficiency of the traction motor, P_{m} the power of the traction motor, ρ the air density, A_{f} the frontal area of the vehicle, c_{d} the aerodynamic drag coefficient, c_{r} the rolling friction coefficient, g the gravitational acceleration, and θ the road inclination angle. The inclination angle can be derived from the altitude profile.

2.2. Hybrid powertrain

The hybrid powertrain consists of the FCS and the battery. The overall system power, i.e., the sum of the FCS power P_{FCS} and the battery power P_{b}, satisfies the electric power demand of the vehicle:

$$P_{\mathrm{el}} = P_{\mathrm{FCS}} + P_{\mathrm{b}}. \tag{2}$$

The objective of the EMS is to determine the power split between the FCS and the battery such that the fuel efficiency is maximized while avoiding harmful operation of the two components. The two powertrain components are described with simplified, control-oriented models, which build the basis for the ECMS and allow for a computationally efficient offline optimization with DP. Regarding the latter, an excessive number of states might even impede the optimization in reasonable time [38].

The FCS consists of a single stack or N_{st} equal stacks in a parallel configuration. The fuel consumption rate $\dot{m}_{\mathrm{st}}$ of an individual stack is modeled as a function of the corresponding stack net power P_{st} (see Fig. 2). This fuel consumption curve is assumed to be strictly convex within the operational stack power range and implicitly considers the power demand of stack-related auxiliaries, such as the compressor. It can either be fitted to measurement data or derived analytically, see [37]. The stacks can be started and stopped individually, which is described by the number of active stacks $n_{\mathrm{st}} \in \mathcal{N}$, where the set of integers $\mathcal{N} = \{0, \dots, N_{\mathrm{st}}\}$ covers the possible numbers of active stacks. When shut down, the stacks are assumed to consume no fuel. When operating, all active stacks provide the same power output, which represents the optimal power allocation regarding fuel efficiency assuming that the fuel consumption curves of all stacks are identical and convex (see Appendix A). With this predefined power allocation between the stacks, the FCS net power P_{FCS} and the overall fuel consumption rate $\dot{m}_{\mathrm{FCS}}$ are determined by only two control inputs (n_{st} and P_{st}), which considerably simplifies the optimization problem of the EMS:

$$P_{\mathrm{FCS}} = n_{\mathrm{st}} P_{\mathrm{st}} \tag{3}$$

$$\dot{m}_{\mathrm{FCS}} = n_{\mathrm{st}} \dot{m}_{\mathrm{st}}(P_{\mathrm{st}}). \tag{4}$$

To avoid harmful power requests from the stacks, constraints on the absolute stack power and the stack power rate are specified.

The battery is modeled with an equivalent circuit model considering ohmic losses, see [37]. With that, the dynamics of the battery SoC ξ is a nonlinear function of the battery power

$$\dot{\xi} = f(P_{\mathrm{b}}) = -\frac{V_{\mathrm{OC}} - \sqrt{V_{\mathrm{OC}}^2 - 4 P_{\mathrm{b}} R_{\mathrm{int}}}}{2 Q_0 R_{\mathrm{int}}} \tag{5}$$

where the battery parameters V_{OC}, R_{int}, and Q_0 denote the open-circuit voltage, internal ohmic resistance, and battery capacity, respectively. For the offline optimization with DP, the battery model is discretized assuming a zero-order hold for the battery power and a constant sampling interval $\Delta t = t_{l+1} - t_l$ yielding

$$\xi_{l+1} = \xi_l - \frac{V_{\mathrm{OC}} - \sqrt{V_{\mathrm{OC}}^2 - 4 P_{\mathrm{b},l} R_{\mathrm{int}}}}{2 Q_0 R_{\mathrm{int}}} \Delta t. \tag{6}$$

Health-aware constraints for the battery are specified for the battery power and the SoC.

To sum up, the overall powertrain model has only one state (ξ) and two inputs (n_{st} and P_{st}), which define the FCS power. The battery takes the residual of the power demand subject to the corresponding constraints. This simple model is highly beneficial for keeping the computational complexity of the offline optimization low. Note that the term "FCS state" is used synonymously for the number of active stacks in this article.

3. Predictive energy management

The predictive EMS comprises two stages:

1. The offline optimization of the energy management before departure (see Section 3.1).
2. The real-time energy management with optimal stack start/stop control (see Section 3.2).

The offline optimization determines the optimal energy management for the planned driving mission such that the fuel consumption and the number of stack start/stop actions are minimized. It is based on a long-term power demand prediction covering the entire driving mission and conducted with DP, which facilitates the consideration of constraints on states and inputs. The outcome of the offline optimization are two maps providing optimal control information depending on the position along the route, the SoC, and the current FCS state: One map indicates the optimal FCS state and the other one describes the optimal cost-to-go, i.e., the minimum cost for reaching the destination. In the subsequent postprocessing step, the information of these maps is brought into a memory-saving 2-D representation that depends on the position and SoC only and can directly be handled by the real-time control.

The real-time part of the EMS is based on the ECMS, which determines the FCS power such that the equivalent fuel consumption rate H is minimized in each instant. The equivalent fuel consumption rate does not only include the actual fuel consumption rate of the FCS but also considers the use of battery energy through the equivalence factor λ:

$$H(P_{\mathrm{st}}, n_{\mathrm{st}}, \lambda, P_{\mathrm{el}}) = n_{\mathrm{st}} \dot{m}_{\mathrm{st}}(P_{\mathrm{st}}) + \lambda f(P_{\mathrm{el}} - n_{\mathrm{st}} P_{\mathrm{st}}). \tag{7}$$

As shown in [39], the equivalent fuel consumption rate can be related to the Hamiltonian of Pontryagin's minimum principle (PMP). Because of this analogy, the ECMS could theoretically provide candidates for the overall optimal solution if the optimal equivalence factor, which strongly depends on the driving mission, was known. Based on these findings, the idea of the presented concept is to determine estimates of the optimal equivalence factor based on the driving mission prediction. More precisely, prediction-based estimates of the optimal equivalence

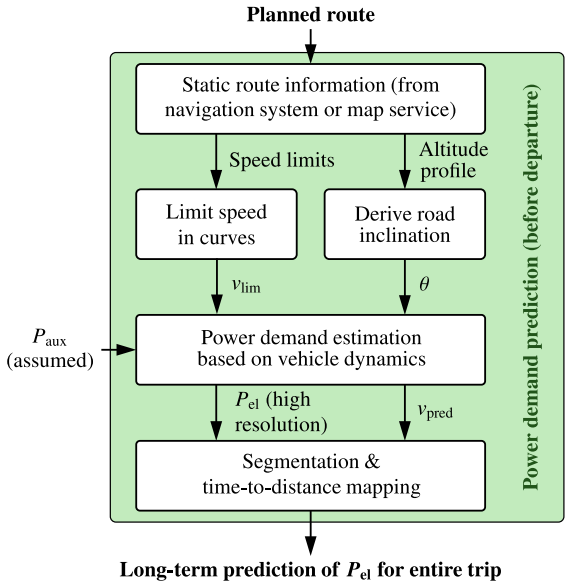

Fig. 3. Schematic illustration of the procedure for obtaining the long-term power demand prediction.

factor are derived from the optimal cost-to-go map of the offline optimization, which is part of the postprocessing step. The map implicitly considers the prediction for the trip remainder for any position and SoC, allowing for continuous adaption of the equivalence factor to the actual conditions. The resulting predictive ECMS implicitly optimizes the predicted cost-to-go in each instant in real time and provides a close-to-optimal energy management performance, which was demonstrated without start/stop control for higher-power driving missions in [19].

Building on this concept, this works extends the predictive ECMS with an optimal fuel cell stack start/stop control. For this purpose, the map indicating the optimal FCS states, i.e., the optimal numbers of active stacks according to the offline optimization, is used as a "suggestion", which also adapts depending on the position and SoC. However, the FCS state indication from the map is not followed directly; additionally a real-time start/stop condition is evaluated. Similarly to the ECMS, this start/stop condition considers the actual power demand and system states and, therefore, avoids inefficient and unnecessary start/stop actions when the actual power demand deviates from the prediction. Besides the resulting robustness against unpredicted disturbances, one of the key benefits of the map-based concept is that the real-time control implicitly considers the long-term prediction in each instant without requiring computationally expensive optimizations over receding prediction horizons, which strongly facilitates its implementation. In the remainder of this section, the offline optimization and the real-time energy management are described in detail first. Then, the computational complexity of the method and its limitation are addressed.

3.1. Offline optimization before departure

The offline optimization of the energy management is conducted before departure and includes three steps: long-term power demand prediction for the entire driving mission, optimization with DP, and postprocessing of the optimized maps. The three steps are described in the following.

3.1.1. Long-term power demand prediction

To effectively avoid unnecessary start/stop actions and minimize the fuel consumption through active involvement of the battery, a long-term prediction of the power demand is necessary. The long-term prediction is derived based on the vehicle dynamics model and covers the entire trip. For this purpose, suitable predictions of the vehicle velocity and road inclination angle along the planned route are required. Both can be derived from static route information that is easily accessible through navigation systems or map services, i.e., speed limits and the altitude profile, as illustrated in Fig. 3. To avoid infeasible predictions in curves, the speed is limited depending on the road curvature, which is particularly relevant in urban and mountainous areas, yielding v_{lim}. This speed prediction intentionally excludes vehicle standstills, e.g., at intersections, because the position and the duration of these standstills are assumed to be almost unpredictable. Having the speed prediction and inclination angle, the traction motor power prediction can be derived with a simple forward simulation based on the model of the longitudinal vehicle dynamics of Eq. (1). In this simulation, the traction motor power is determined by tracking v_{lim} considering system and motor power constraints. This approach prevents the prediction of infeasible motor power during velocity transients and uphill driving. The simulation also yields the corresponding feasible speed prediction v_{pred}. The prediction of the overall power demand for the planned trip is then obtained after adding an estimate of the power demand of the auxiliary systems P_{aux}:

$$P_{\mathrm{el}} = P_{\mathrm{m}} + P_{\mathrm{aux}}. \tag{8}$$

To keep the computational complexity of the subsequent optimization of the energy management with DP low, it is performed with a relatively rough discretization, which is defined by Δt. Therefore, the power demand prediction is segmented with

$$P_{\mathrm{el},l} = \frac{\int_{t_l}^{t_{l+1}} P_{\mathrm{el}}\,\mathrm{d}t}{\Delta t} \tag{9}$$

for all $l = 1 \ldots (L-1)$, where $t_1 = 0$ and t_L denotes the elapsed time at the destination. The segmented power demand prediction is the input for the offline optimization. Finally, a time-to-distance mapping based on the speed prediction is performed, which defines the positions s_l for all $l = 1 \ldots (L-1)$:

$$s_l = \int_0^{t_l} v_{\mathrm{pred}}(t)\,\mathrm{d}t. \tag{10}$$

The description in the distance domain is used for defining the 2-D maps resulting from the offline optimization because, unlike the time-based description, it is not affected if the actual velocity deviates from the prediction. Therefore, it is advantageous for the real-time control, where deviations are expected. Note that the time-to-distance mapping is bijective because the velocity prediction excludes vehicle standstills.

The quality of the power demand prediction is dominated by the accuracy of the speed limit-based velocity prediction. Unlike the road inclination angle, which is determined by the topography of the route, the vehicle velocity is influenced by a number of stochastic factors, e.g., traffic, vehicle standstills, and driver behavior, which are almost unpredictable within long prediction horizons. Due to the limited accuracy of the long-term prediction, the rough discretization for the DP does not necessarily affect the prediction quality further. However, despite its limited accuracy, the long-term prediction is highly effective for the predictive energy management. It enables the offline optimization of the energy management before departure and provides the long prediction horizon necessary to effectively avoid unnecessary start/stop actions and actively involve the battery in the energy management. Moreover, the proposed EMS is designed to handle unpredicted disturbances as it continuously adapts to the actual conditions.

3.1.2. Offline optimization with dynamic programming

The offline optimization of the energy management is based on the long-term power demand prediction for the entire driving mission (see Fig. 4). The objective is to determine the optimal energy management such that the fuel consumption and the number of start/stop actions are

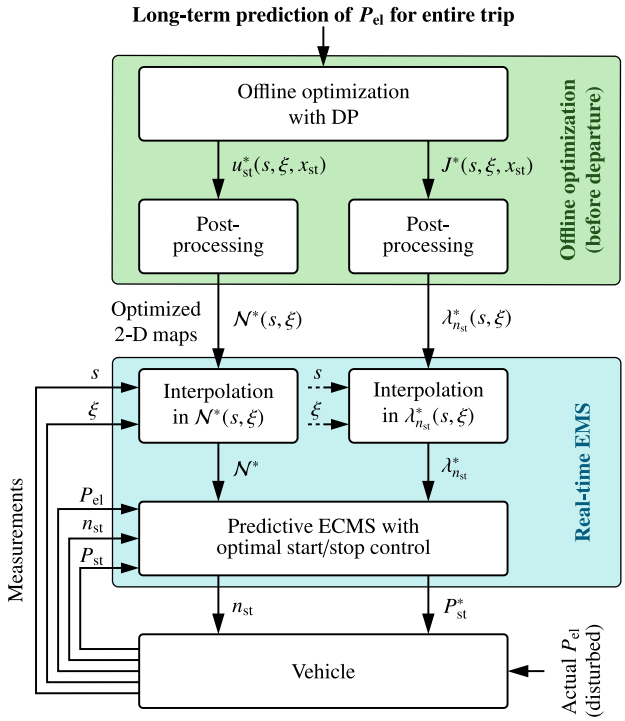

Fig. 4. Schematic illustration of the predictive EMS with optimal stack start/stop control.

minimized. The optimal control problem is formulated in discrete-time

$$\begin{aligned}\min J = \sum_{l=1}^{L-1} & \dot{m}_{FCS}(n_{st,l}, P_{st,l})\Delta t + p|n_{st,l+1} - n_{st,l}| \\ \text{s.t.} \quad & n_{st,l} \in \mathcal{N}, \\ & P_{st,idle} \le P_{st,l} \le P_{st,max}, \\ & P_{b,min} \le P_{b,l} \le P_{b,max}, \\ & \xi_{min} \le \xi_l \le \xi_{max}, \quad \forall l \in \{1,\dots,L-1\}, \\ & \xi_1 = \xi_{init}, \quad n_{st,1} = 0, \\ & \xi_L \ge \xi_{final}, \quad n_{st,L} = 0\end{aligned} \tag{11}$$

where p denotes a penalty on start/stop actions, $P_{st,idle}$ the minimum stack power when switched on, and $P_{st,max}$ the maximum stack power. The minimum and maximum constraint for the battery power are denoted by $P_{b,min}$ and $P_{b,max}$, respectively, and the minimum and maximum constraint for the battery SoC by ξ_{min} and ξ_{max}, respectively. The initial SoC is denoted by ξ_{init} and the minimum final SoC by ξ_{final}. To keep the computational complexity of the optimization low, a relatively rough sampling interval is chosen. Therefore, the constraints on the FCS power rate can be neglected here because the corresponding dynamics are much faster.

To obtain the two maps indicating the optimal FCS states and describing the optimal cost-to-go, i.e., the cost to reach the destination along the optimal path, the optimal control problem is solved with DP, which operates with discretized states and inputs. Note that the consideration of the start/stop penalty in the objective function introduces a second, discrete state to the problem besides the SoC, which is the *current* number of active stacks, i.e., the current FCS state. In the following, the current FCS state is denoted by x_{st} to have a clear distinction from the decision variable u_{st}, which defines the number of active stacks in the *next instant*, i.e., $x_{st,l+1} = u_{st,l}$. The DP algorithm proceeds backward in time, minimizing the cost-to-go J_l for all ξ_l and $x_{st,l}$ in the discrete state space at each time step $l = (L-1)\dots 1$

$$\begin{aligned}J^*_l(\xi_l, x_{st,l}) = \min_{u_{st,l}, P_{st,l}} \big(& \dot{m}_{FCS}(u_{st,l}, P_{st,l})\Delta t + p|u_{st,l} - x_{st,l}| \\ & + J^*_{l+1}(\xi_{l+1}, u_{st,l}) \big)\end{aligned} \tag{12}$$

subject to the specified constraints. More details regarding the DP implementation can be found in the literature, e.g., [40].

The outcome of the DP algorithm are discrete 3-D maps describing the optimal number of active stacks $u^*_{st}(s,\xi,x_{st})$ and the optimal cost-to-go $J^*(s,\xi,x_{st})$ depending on the position, SoC, and current number of active stacks. Note that the description in the distance domain is based on the time-to-distance mapping specified in Eq. (10) and is advantageous for the real-time control.

3.1.3. Postprocessing of the optimal control information

The maps resulting from the DP represent the optimal energy management regarding the prediction within the entire 3-D distance-state space. To use this optimized information efficiently in the real-time control, a postprocessing step is necessary, which yields 2-D maps depending only on the position and SoC (see Fig. 4). This section first elaborates how the map indicating the optimal number of active stacks can be transformed into the 2-D representation. Then, it describes how 2-D maps providing estimates of the optimal equivalence factor for the ECMS are derived from the optimal cost-to-go map.

The map $u^*_{st}(s,\xi,x_{st})$ provides the optimal number of active stacks depending on the current number of active stacks for each evaluated position and SoC. For example, $x_{st} = 0 \rightarrow u^*_{st} = 0$ and $x_{st} = 1 \rightarrow u^*_{st} = 1$ indicates that remaining in the current FCS state is optimal according to the prediction. Because of the start/stop penalty, changing the number of active stacks is avoided unless an alternative is so much more fuel-efficient that the penalty is overcompensated. Considering this behavior, the explicit dependency of the optimal number of active stacks (u^*_{st}) from the current number (x_{st}) becomes irrelevant, and the information of $u^*_{st}(s,\xi,x_{st})$ can be condensed in a memory-efficient 2-D map $\mathcal{N}^*(s,\xi)$ indicating the set of the optimal FCS states depending on the position and SoC only:

$$\mathcal{N}^*(s,\xi) = \{n \in \mathcal{N} : \exists m \in \mathcal{N}\ u^*_{st}(s,\xi,m) = n\}. \tag{13}$$

An example of this FCS state indication map for a single-stack FCS on a driving mission with strongly varying power demand is illustrated in Fig. 5. The black areas indicate situations where activating the stack is beneficial, whereas the gray areas indicate situations where shutting down the stack is better. For the hatched areas, the optimal FCS state is not unique because the improvement through a potential start/stop action does not compensate for the penalty. The indication for these areas can be interpreted as "remain in the current FCS state", i.e., maintaining the current number of active stacks. The optimal FCS states clearly depend on both the position and the SoC.

The FCS state indication map only provides information for the start/stop control. To determine the stack power based on the ECMS, an appropriate estimate of the optimal equivalence factor is necessary. Such an estimate can be derived by partially differentiating the optimal cost-to-go with respect to the SoC

$$\lambda^*_{n_{st}}(s,\xi) = \frac{\partial J^*(s,\xi,n_{st})}{\partial \xi} \tag{14}$$

which is performed numerically. This link between the optimal equivalence factor, which corresponds to the optimal costate of PMP, and the optimal cost-to-go can be derived by comparing the necessary conditions of PMP and the Hamilton–Jacobi-Bellman equation, which can be interpreted as continuous-time counterpart of DP, see [41]. The resulting equivalence factor estimates are stored in N_{st} 2-D maps $\lambda^*_{n_{st}}(s,\xi)$, one for each possible FCS state apart from 0, where all stacks are shut down. The maps allow for continuous adaption of the equivalence factor to the current position and SoC in the real-time control, which is a strong benefit over alternative approaches.

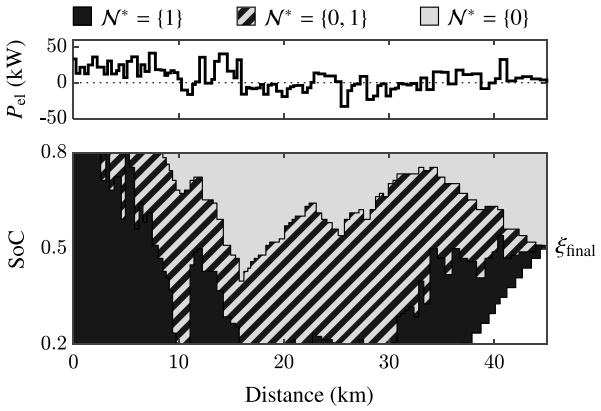

Fig. 5. Map indicating the optimal FCS states depending on the position and SoC (lower plot) for a single-stack FCS on a driving mission with varying power demand (upper plot).

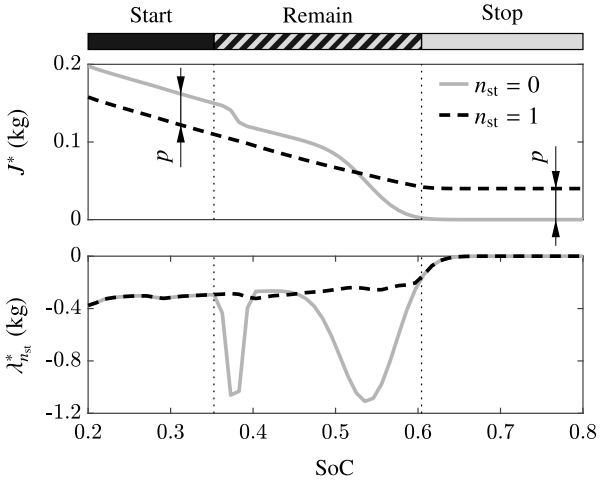

Fig. 6. Profiles of the optimal cost-to-go and optimal equivalence factor over the SoC corresponding to the position 13.5 km of the driving mission shown in Fig. 5. The bar at the top indicates the optimal FCS state indications of $\mathcal{N}^*$ for the single-stack FCS.

Fig. 6 illustrates the behavior of the optimal cost-to-go and equivalence factor over the SoC. It shows that the difference in the cost-to-go between the two FCS states is saturated in the value of the start/stop penalty in SoC ranges with a clear optimum regarding the FCS state, i.e., "start" and "stop". The reason for this behavior is that accepting the penalty to immediately switch from the FCS state with the higher cost-to-go to the one with the lower cost-to-go is optimal. Consequently, the optimal equivalence factors are identical for these two FCS state indications. In the SoC range where "remain" is indicated, the absolute difference in the cost-to-go between the two FCS states is smaller than the start/stop penalty and varies. Therefore, the corresponding optimal equivalence factors are also different. The fluctuations of the equivalence factors in this range are caused by the discrete nature of the FCS state. Note that $\lambda^*_{n_{st}} \leq 0$ because an increase in the SoC means that more energy is stored in the battery, and thus, the cost-to-go decreases since less fuel is required to reach the destination. Only if the energy stored in the battery exceeds the energy demand of the trip remainder, the fuel amount required to reach the destination is zero and $\lambda^*_{n_{st}} = 0$ (see Fig. 6).

3.2. Real-time energy management with optimal stack start/stop control

To optimize the number of active stacks and the stack power, the real-time EMS considers the actual power demand and system states and reads out the optimal control information, i.e., the optimal FCS state indication and the equivalence factor, from the maps $\mathcal{N}^*(s, \xi)$ and $\lambda^*_{n_{st}}(s, \xi)$ (see Fig. 4). The optimal control information from the maps continuously adapts to the current position and SoC and implicitly considers SoC constraints. However, situations where the actual power demand considerably deviates from the prediction might still provoke SoC constraint violations in the real-time control because these situations are not covered in the offline optimization. Therefore, a mechanism for avoiding SoC constraint violation is included in the real-time strategy, which adapts the equivalence factor in the neighborhood of the SoC constraints, similar as in [42]. The equivalence factor must be decreased close to ξ_{min} to favor charging the battery and increased close to ξ_{max} to favor discharging. Here, the adaption λ_{SoC} is based on a quadratically formulated offset

$$\lambda_{SoC} = \begin{cases} \lambda_{ad} \left(\frac{\xi - \xi_{max} + \xi_{th}}{\xi_{th}} \right)^2, & \xi > \xi_{max} - \xi_{th} \\ -\lambda_{ad} \left(\frac{-\xi + \xi_{min} + \xi_{th}}{\xi_{th}} \right)^2, & \xi < \xi_{min} + \xi_{th} \\ 0, & \text{otherwise} \end{cases} \tag{15}$$

where ξ_{th} and λ_{ad} are tuning parameters. The offset gets active at the threshold ξ_{th} to the constraints and takes the value $\pm\lambda_{ad}$ at the constraints. The adaption is added to the estimate of the optimal equivalence factor for the current position and SoC considering a saturation at zero:

$$\bar{\lambda}^*_{n_{st}} = \min\left(\lambda^*_{n_{st}} + \lambda_{SoC}, 0\right). \tag{16}$$

In the following, the two steps of the real-time strategy are elaborated: first, the decision on the number of active stacks and then the optimization of the stack power based on the ECMS.

3.2.1. Predictive stack start/stop control

A nearest neighbor interpolation in $\mathcal{N}^*(s, \xi)$ yields the set of optimal FCS states for the current position and SoC. If the current FCS state $n_{st,curr}$ is included in the set, no start/stop action is required. Otherwise, the FCS state of the set that is closest to the current one is considered as the indicated FCS state $n_{st,ind}$ according to $\mathcal{N}^*$. To further prevent SoC constraint violation if the power demand considerably deviates from the prediction, this FCS state indication is overruled if the specified SoC boundaries are reached: If $\xi \leq \xi_{min}$, then $n_{st,ind} \geq 1$. If $\xi \geq \xi_{max}$, then $n_{st,ind} = \min \mathcal{N}^*$, i.e., the lowest number in the set of optimal FCS states is chosen. This means the FCS might keep operating if a high power demand was predicted ahead.

The optimal FCS state indication is not followed directly because it does not take into account the actual power demand, which might considerably deviate from the prediction. Additionally, the optimal equivalent fuel consumption rates of the current and the indicated FCS state are compared, which consider the actual power demand. The indicated start/stop action is only realized if the following condition is satisfied:

$$H^*_{n_{st,ind}} < H^*_{n_{st,curr}} \tag{17}$$

with

$$H^*_{n_{st,ind}} = \min_{P_{st} \in \mathcal{P}} H(P_{st}, n_{st,ind}, \bar{\lambda}^*_{n_{st,ind}}, P_{el}) \quad \text{and} \tag{18}$$

$$H^*_{n_{st,curr}} = \min_{P_{st} \in \mathcal{P}} H(P_{st}, n_{st,curr}, \bar{\lambda}^*_{n_{st,curr}}, P_{el}). \tag{19}$$

Here, the set $\mathcal{P}$ denotes the feasible stack power range, which is defined in more detail in Section 3.2.2. The equivalence factors are extracted from the corresponding maps by linear interpolation based on the current position and SoC, and the SoC constraint offset according to Eq. (16) is considered. This real-time start/stop condition suppresses the map-indicated start/stop action as long as the current FCS state is more efficient under the current power demand. For example, shutting down a stack is avoided when an unpredicted acceleration occurs. Note that considering the start/stop penalty in the real-time start/stop

condition is physically infeasible because the penalty expresses an absolute fuel amount while the condition is based on fuel consumption rates.

To compute the equivalent fuel consumption rate for $n_{\mathrm{st,ind}} = 0$ or $n_{\mathrm{st,curr}} = 0$, the equivalence factor λ_1^* is taken without discrepancy because $\lambda_0^* = \lambda_1^*$ whenever a start/stop action is indicated by the optimal FCS state map (see Section 3.1.3). Note that no minimization is required in this case.

3.2.2. Predictive ECMS

A linear interpolation in $\lambda_{n_{\mathrm{st}}}^*(s,\xi)$ for the chosen FCS state gives the estimate of the optimal equivalence factor for the current position and SoC, which implicitly considers the prediction of the trip remainder. To ensure SoC constraint satisfaction, the offset is added to the equivalence factor according to Eq. (16). With that, the ECMS determines the individual stack power such that the equivalent fuel consumption rate of the FCS according to Eq. (7) is minimized for the current power demand, i.e.,

$$P_{\mathrm{st}}^* = \arg\min_{P_{\mathrm{st}} \in \mathcal{P}} H(P_{\mathrm{st}}, n_{\mathrm{st}}, \bar{\lambda}_{n_{\mathrm{st}}}^*, P_{\mathrm{el}}). \tag{20}$$

Here, the feasible stack power range described by $\mathcal{P}$ reflects the specified stack power constraints and stack power rate constraints, which are approximated by maximum power increments per sample. If relevant and feasible, $\mathcal{P}$ is restricted to additionally consider the battery power constraints.

The optimization in Eq. (20) is one-dimensional. Moreover, the function to be minimized, i.e., H, has a unique minimum because it is strictly convex (see Appendix B), which ensures convergence. Therefore, the optimization can be solved with simple methods, e.g., the golden-section search [43], and low computational requirements.

3.3. Computational complexity and limitation

One of the key benefits of the proposed concept is the low computational complexity of both stages, i.e., offline optimization and real-time control. The complexity of the DP algorithm used for the offline optimization depends on the discretization intervals of time, states, and control inputs, see [37]. Due to the limited accuracy of the long-term prediction, rough discretization intervals can be chosen in the DP without affecting the real-time performance because certain deviations from the prediction are expected. Consequently, the DP computation time is kept low, and the optimized maps can be provided shortly after the route was planned. Exemplary numbers regarding discretization intervals and computation time are given in the numerical results in Section 5.1.

In the real-time control, computationally expensive optimizations over receding prediction horizons are unnecessary because the maps resulting from the offline optimization provide the predictive information in a form that can be directly used in the real-time EMS. Therefore, the real-time control is based on a simple, one-dimensional optimization, which can be solved with low computational complexity. This strongly facilitates the real-time implementation of the method.

The most important limitation regarding control performance is the quality of the long-term prediction. However, a sufficient prediction quality to benefit from the predictive concept is easily achievable based on static route information. Even though the accuracy of the route-derived prediction is limited because of random influences, such as traffic, it allows for significant performance improvements over nonpredictive approaches. Moreover, the method's design ensures continuous adaption to the actual power demand and system measurements, which considerably reduces the sensitivity with respect to the prediction quality compared to nonadaptive predictive approaches. The advantages over the mentioned alternatives are demonstrated in the numerical studies in Section 5.

4. Alternative start/stop strategies for benchmarking

In the numerical studies in Section 5, the proposed predictive EMS with map-based start/stop control is compared with two alternative start/stop strategies from the literature. Both benchmark strategies determine the individual stack power with the predictive ECMS according to Eq. (20) using exactly the same optimal equivalence factor map as the proposed map-based strategy, which ensures a fair comparison that focuses on the start/stop control. The first strategy is a nonpredictive strategy that instantaneously decides on start/stop actions considering the current power demand. The second one is an advanced strategy that considers the long-term prediction to plan optimal start/stop positions before departure. The two benchmark strategies are outlined in the following.

4.1. Instantaneous start/stop strategy

The instantaneous start/stop strategy is optimization-based. It continuously evaluates the equivalent fuel consumption rates of the possible FCS states considering the current power demand and equivalence factor and selects the most efficient FCS state analogously to Eq. (17), see also [44–46]. However, without further restrictions, the instantaneous decision would entail infeasibly frequent start/stop actions, which is why a minimum hold time of 60 s is specified after each change in the FCS state, see [24,30,33].

4.2. Position-based predictive start/stop strategy

The position-based predictive strategy uses the offline optimization of the energy management (see Section 3.1.2) to plan optimal positions for starts/stops based on the long-term prediction before departure. In the real-time control, start/stop actions are performed according to the position-based plan, as proposed in [36].

5. Numerical results

The proposed predictive EMS with map-based stack start/stop control is evaluated for two vehicle classes in simulation. First, a qualitative and quantitative evaluation where the map-based strategy is benchmarked against two start/stop strategies from the literature (see Section 4) is presented for a passenger vehicle equipped with a single-stack FCS. Then, the performance of the proposed method is demonstrated for a heavy-duty truck with a dual-stack FCS. To ensure a realistic performance validation, both numerical studies are based on real-world driving missions that were recorded on public roads. Therefore, the numerical studies cover random influences on the power demand that are relevant in real-world driving, such as dense traffic, standstills with varying standstill times, other vehicles, and driver behavior. These real driving influences cause significant deviations from the long-term prediction as in the real application and guarantee an application-oriented evaluation.

The vehicle and powertrain parameters of the two vehicles and the chosen EMS preferences are summarized in Table 1. The stack idle power, i.e., the minimum stack power during active operation, is chosen relatively high to prevent harmful operation caused by low idle powers. The fuel cell stack of the passenger vehicle is modeled with a polynomial fuel consumption curve fitted to stationary measurements, which is shown together with the corresponding efficiency curve in Fig. 2. For the truck stacks, this fuel consumption curve was scaled linearly such that the fuel efficiency behavior within the stack power range is preserved.

The remainder of this section is structured into four parts:

1. Description of the driving mission prediction and the offline optimization (see Section 5.1).

Table 1
Parameters of the passenger vehicle and the heavy-duty truck.

Model parameters	Passenger vehicle	Truck
Total vehicle mass, m (kg)	1950	33 000
Auxiliary power, P_{aux} (kW)	1	10
Number of stacks, N_{st}	1	2
Stack idle power, $P_{\text{st,idle}}$ (kW)	8	9.5
Max. stack power, $P_{\text{st,max}}$ (kW)	50	155
Max. stack power rate (kW s^{-1})	±25	±50
Battery energy capacity (kW h)	4.95	84.8
Battery capacity, Q_0 (A h)	28.28	121.5
Open-circuit voltage, V_{OC} (V)	175	698
Internal ohmic resistance, R_{int} (Ω)	0.075	0.112
Min. battery power, $P_{\text{b,min}}$ (kW)	−15	−210
Max. battery power, $P_{\text{b,max}}$ (kW)	50	420
Energy management parameters	**Passenger vehicle**	**Truck**
Min. SoC, ξ_{min}	0.3	0.3
Max. SoC, ξ_{max}	0.7	0.7
Initial SoC, ξ_{init}	0.5	0.5
Final SoC, ξ_{final}	0.5	0.5
SoC constraint threshold, ξ_{th}	0.05	0.05
Adaption parameter, λ_{ad} (kg)	0.3	1
DP sampling interval, Δt (s)	35	51
No. of state (ξ) grid points in DP	100	80
No. of input (P_{st}) grid points in DP	80	60
Start/stop penalty, p (kg)	0.01	0.01

2. Qualitative and quantitative comparison of the predictive EMS with map-based start/stop control with the two benchmark strategies based on the passenger vehicle (see Section 5.2).
3. Analysis of the real-time start/stop condition (see Section 5.3).
4. Demonstration of the predictive EMS with map-based start/stop control for the heavy-duty truck with dual-stack FCS (see Section 5.4).

5.1. Driving mission prediction and offline optimization

The power demand prediction for the entire driving mission is based on the altitude profile and the speed limits along the planned route, which are easily accessible. For the numerical studies, both route information was obtained from *AVL Route Studio*, which is a tool for generating and simulating driving cycles. The tool takes into account vehicle dynamics during velocity transients and limits the maximum velocity depending on the road curvature. In this way, a decent long-term velocity prediction can conveniently be obtained for testing purposes.

The discretization intervals for the DP were selected by analyzing the trade-off between the overall EMS performance and computation time and are shown in Table 1. 120 time segments were chosen for the investigated 60 km driving mission of the passenger vehicle and 360 time segments for the 360 km driving mission of the truck study. The latter was segmented more roughly because it is a highway mission where fewer transients are expected. In either case, the rough discretization ensures a fast computation of the offline DP and compact sizes of the optimized maps used in the real-time energy management, i.e., $\mathcal{N}^*(s,\xi)$ and $\lambda^*_{n_{\text{st}}}(s,\xi)$. To give an idea, the computation time of the DP algorithm was in the magnitude of 10^{-1} s using MATLAB on a computer equipped with an AMD Ryzen 7 PRO 5850U.

5.2. Comparative study based on passenger vehicle

The map-based predictive start/stop strategy is compared with the two alternatives based on measurements of a real-world driving mission covering 60 km, which is depicted in Fig. 7(a). The driving mission has a high urban share characterized by a fluctuating but on average low electric power demand and random standstills. The second half of the

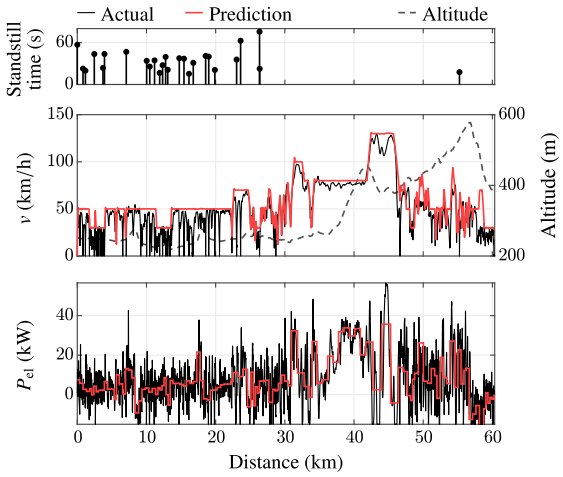

(a) Investigated real-world driving mission.

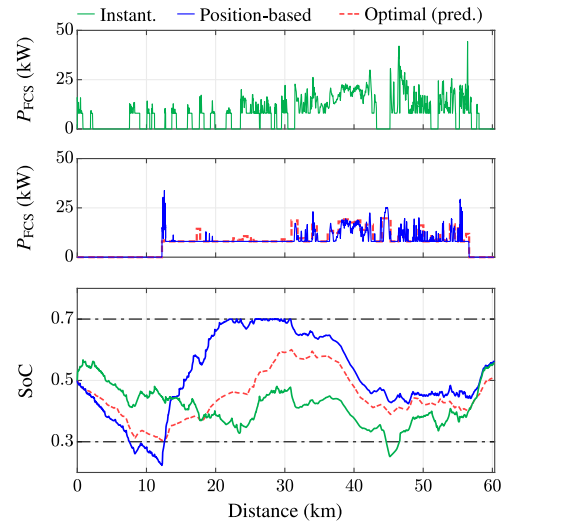

(b) Predictive ECMS with benchmark start/stop strategies (instantaneous and position-based predictive) and the optimal solution regarding the prediction.

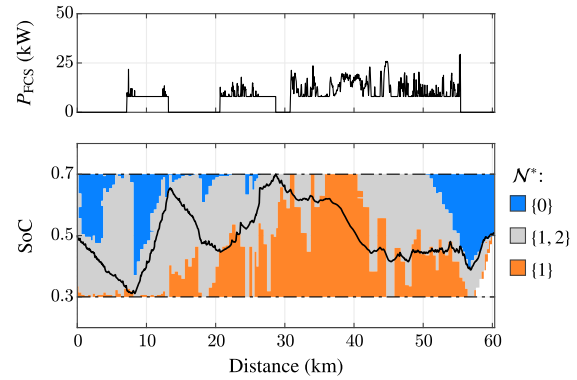

(c) Predictive ECMS with proposed map-based start/stop strategy. The colors in the SoC plot indicate the optimal FCS states according to $\mathcal{N}^*$.

Fig. 7. Comparison of the map-based start/stop strategy with the two benchmark strategies based on a real-world driving mission.

driving mission shows rural and highway sections including changes in altitude and, therefore, higher power demands. Nevertheless, the mean power demand of the driving mission is significantly lower than the stack idle power, making stack shutdowns highly relevant in order to save fuel and satisfy the SoC constraints. The route-based prediction of the driving mission, which is also shown in Fig. 7(a), gives a good

estimate of the velocity and power demand, particularly outside urban areas, but inevitably lacks the random fluctuations and standstills due to traffic.

The trajectories representing the energy management of the benchmark strategies are depicted in Fig. 7(b). Not considering predictive information, the instantaneous start/stop strategy determines the FCS state only depending on the current power demand and equivalence factor. The result is a high number of start/stop actions affecting the FCS lifetime. The number of starts/stops would be even higher without the specified 60 s hold time, during which the FCS state cannot be changed. However, the hold time also brings drawbacks: Around 43 km, the power demand is negative causing the nonpredictive strategy to shut down the stack. Within the subsequent 60 s time span, where the FCS cannot be started, an acceleration on an uphill section causes high power demand, which cannot be fully provided because it exceeds the maximum battery power. In addition to the unsatisfied power demand, the minimum SoC constraint is violated.

In contrast to the instantaneous strategy, the position-based predictive start/stop strategy optimizes positions for start/stop actions based on the power demand prediction considering the start/stop penalty (see second plot of Fig. 7(b)). As a result, the number of starts/stops is considerably reduced to 2, and the stack is active when high power demand is expected, including the aforementioned load spike after 43 km. However, the prediction does not reflect the influences due to traffic, particularly standstills, and thus underestimates the actual energy demand in the initial urban part of the driving mission. Consequently, the predicted optimal stack starting position is too late, and the minimum SoC constraint is severely violated around 10 km. Likewise, the charging of the battery by the idling FCS during standstills is not reflected by the prediction, causing a saturation of the SoC in its upper boundary. A violation of the upper SoC constraint is only prevented because the excess energy is wasted in a breaking resistor, considerably affecting the fuel efficiency.

The proposed map-based strategy makes start/stop decisions based on the optimal FCS state indication map, which is illustrated besides the resulting trajectories of the FCS power and SoC in Fig. 7(c). Having a single-stack FCS, the map includes three optimal FCS state indications, namely "stop" ($\mathcal{N}^* = \{0\}$), "start" ($\mathcal{N}^* = \{1\}$), and "remain" ($\mathcal{N}^* = \{0, 1\}$). Note that starting the stack is more relevant under higher power demands, whereas stopping is more relevant under lower power demands. The optimal FCS state indication map allows the proposed strategy to consider not only the position but also the actual SoC in the start/stop decision. The relevance of both position and SoC for optimal start/stop decisions is demonstrated in the start action shortly after 20 km. In contrast to further depleting the battery, the FCS is started right before a high-power section, which is beneficial for the overall fuel efficiency. However, if the actual battery SoC was sufficiently high at this position, the FCS start would have been delayed to the next high-power phase. Likewise, the last shutdown after 55 km is performed before the final decent with negative power demand so that energy can be recuperated efficiently. However, if the SoC was lower at this position, the FCS shutdown would have been delayed until the battery is sufficiently charged to satisfy the final SoC constraint. This illustrates that the map-based strategy benefits from the long-term prediction while optimally responding to the actual conditions. Also, the map-based strategy provides reliable SoC control and keeps the number of start/stop actions low.

The resulting performance benefits over the benchmark strategies are quantified in Table 2. Following the optimized start/stop positions, the position-based strategy starts and stops the stack only once, respectively. However, the low number of starts/stops comes at the expense of a SoC constraint violation and a fuel consumption, which is more than 11% higher than the one of the instantaneous strategy. The instantaneous method achieves a decent fuel efficiency but performs 40 start/stop events, which is clearly too high. In contrast, the proposed map-based strategy reduces the number of start/stop events to only 6 while even outperforming the instantaneous strategy regarding the fuel consumption, which is further decreased by 0.9%. Consequently, the map-based method also achieves the best result regarding the objective function of the offline optimization according to Eq. (11) with reductions of 58.7% and 4.4% with respect to the instantaneous and the position-based strategy, respectively. Note that the objective function was evaluated with the simulation sampling interval here to be more precise. To estimate the effects of the investigated strategies on the lifetimes of the powertrain components, Table 2 also includes the stack operation time of the FCS and the battery throughput. For the investigated driving mission, the map-based strategy reduces the stack operation time by 18.3% compared to the position-based strategy at the cost of a comparably small increase of 4% in the battery throughput. The instantaneous strategy shows a further decrease in the stack operation time, but the impact of the extensive number of starts/stops must be taken into account here.

Table 2
Quantitative comparison of the three start/stop strategies for the passenger vehicle driving mission.

	Map-based	Instant.	Position-based
Equivalent fuel consumption[a] (kg/100km)	**0.876**	**0.884**	**0.985**
Relative difference	**0**%	**+0.9**%	**+12.5**%
Number of starts/stops	**6**	**40**	**2**
J (kg)	0.588	0.932	0.613
Relative difference	0%	+58.7%	+4.4%
Stack operation time (h)	0.99	0.82	1.17
Relative difference	0%	−17.5%	+18.3%
Battery throughput (A h)	72.9	71.8	70
Relative difference	0%	−1.6%	−4%

[a] Takes into account deviations in the final SoC.

5.3. Analysis of the real-time start/stop condition

To adapt to the actual power demand, the map-based strategy does not follow the optimal FCS state indications of $\mathcal{N}^*$ directly but additionally considers the real-time start/stop condition of Eq. (17) before performing any start/stop action. The optimal FCS state according to this condition is a function of the power demand and the equivalence factor. This relation can be illustrated with a threshold for the power demand, which separates the area where active stack operation is optimal from the one where a shutdown is optimal depending on the equivalence factor (see Fig. 8).

The benefit of considering the real-time start/stop condition is demonstrated in Fig. 9, which zooms into the passenger vehicle driving mission. When the optimal FCS state indication according to $\mathcal{N}^*$ turns 1, the power demand is negative and keeps further decreasing. Activating the stack in this situation would strain the battery and lead to a loss of energy as the battery charging power limit is reached. The real-time start/stop condition ensures that the stack is not started until the power demand increases and, therefore, ensures that the strategy adapts to the actual driving conditions. Analogously, stack stops are prevented as long as the power demand is too high, ensuring efficient and smooth operation.

5.4. Demonstration for heavy-duty truck with dual-stack FCS

The capabilities of the predictive ECMS with the map-based start/stop strategy are demonstrated for a 33 t truck with dual-stack FCS based on measurements of a real-world driving mission. The investigated final part of the mission crosses the Brenner Pass, one of the most important corridors for road freight transport in Europe [47], and is particularly challenging due to substantial changes in altitude (see upper two plots of Fig. 10). The prediction matches the measured

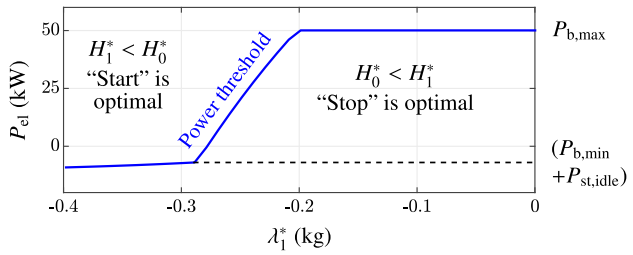

Fig. 8. Illustration of the real-time start/stop condition for the single-stack FCS: The optimal FCS state depends on the power demand and equivalence factor.

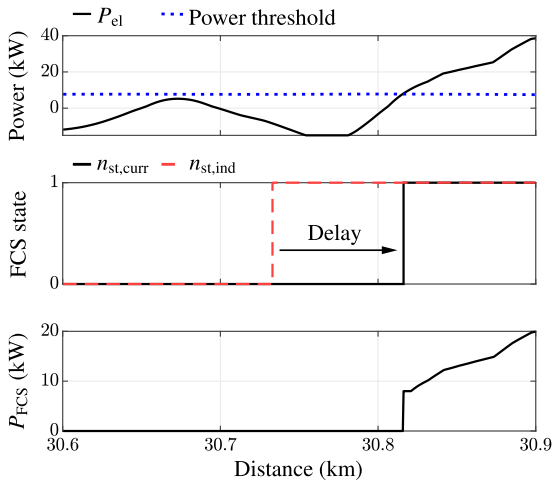

Fig. 9. Fuel-efficient delay of the stack start due to low power demand.

velocity well for most of the driving mission but considerably deviates in certain sections due to traffic.

The trajectories of the FCS power, FCS state, and SoC and the optimal FCS state indication map are shown in the lower three plots of Fig. 10. The map expresses six FCS state indications depending on the position and SoC corresponding to the three available FCS states of the dual-stack FCS. During the uphill section, the map indicates that both stacks should operate independently of the SoC, which is necessary as the power demand exceeds the individual maximum stack power of 155 kW. In the subsequent initial part of the descent, there is a clear indication that both stacks should be stopped as the power demand reaches the minimum battery power due to the steep slopes. Then, however, the optimal FCS state indications also depend on the SoC. For the investigated mission, starting only one stack is sufficient to satisfy the energy demand of the final part of the trip and reduces the number of start/stop actions. However, if any significant disturbances occurred, the strategy would adapt optimally according to the map, providing SoC control and high fuel efficiency while keeping the number of start/stop events low.

6. Conclusions

This article proposed a predictive EMS with optimal stack start/stop control for single and multi-stack FCSs that minimizes fuel consumption while keeping the number of harmful stack start/stop events low. Before departure, static route information is used to derive a power demand prediction for the entire driving mission. Based on this long-term prediction, the energy management for the planned trip is optimized, which yields 2-D maps storing optimal control information for the real-time control. While driving, the real-time EMS optimizes start/stop decisions and the stack power considering the predictive information from the maps. Thanks to the map-based design, the predictive EMS

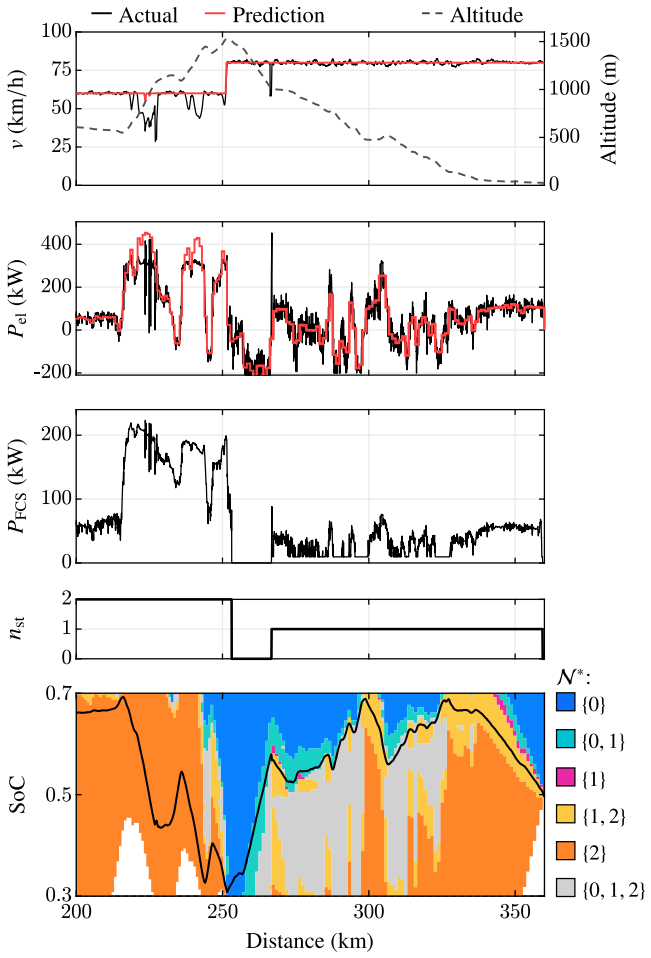

Fig. 10. Proposed predictive ECMS with the map-based start/stop strategy analyzed for a dual-stack FCS based on a real-world driving mission. The colors in the SoC plot indicate the optimal FCS states according to $\mathcal{N}^*$.

continuously adapts to the actual power demand and system states, ensuring robustness against unpredicted disturbances. Moreover, the design strongly facilitates the real-time implementation because of its low computational requirements. The predictive concept was benchmarked against two state-of-the-art start/stop methods in numerical studies of a single-stack passenger vehicle on a real-world driving mission. Compared to the first benchmark, an instantaneous strategy, the proposed strategy considerably reduced the number of start/stop events from 40 to 6 and, at the same time, decreased the fuel consumption by 0.9%. Whereas the second benchmark, an advanced predictive strategy optimizing start/stop positions before departure, performed only 2 start/stop events, it consumed considerable 12.5% more fuel than the proposed strategy. Both benchmark methods caused SoC constraint violations, whereas the proposed strategy provided reliable SoC control thanks to its adaptability. Finally, the capabilities of the predictive concept were also demonstrated for a truck with a dual-stack FCS.

CRediT authorship contribution statement

Sandro Kofler: Writing – original draft, Visualization, Software, Methodology, Investigation, Formal analysis, Data curation, Conceptualization. **Stefan Jakubek:** Writing – review & editing, Project administration, Funding acquisition. **Christoph Hametner:** Writing – review & editing, Validation, Supervision, Resources, Project administration, Funding acquisition.

Declaration of competing interest

The authors declare that they have no known competing financial interests or personal relationships that could have appeared to influence the work reported in this paper.

Data availability

Data will be made available on request.

Acknowledgments

This work was supported with funds from the Climate and Energy Fund and implemented in line with the "Zero Emission Mobility" Program [grant numbers 878123, 885044]. The authors acknowledge the TU Wien Bibliothek for financial support through its Open Access Funding Program.

Appendix A. Optimal power allocation with identical stacks

The sum of the individual stack powers P_i of the FCS consisting of N_{st} identical stacks must satisfy the requested FCS power

$$P_{FCS} = \sum_{i=1}^{N_{st}} P_i \tag{A.1}$$

and the total fuel consumption rate of the FCS is

$$\dot{m}_{FCS} = \sum_{i=1}^{N_{st}} \dot{m}_{st}(P_i) \tag{A.2}$$

where $\dot{m}_{st}(P_{st})$ is assumed to be a strictly convex function of P_{st} for $P_{st,idle} \leq P_{st} \leq P_{st,max}$. After plugging Eq. (A.1) into Eq. (A.2), the total fuel consumption rate can be expressed as a function of the first $(N_{st}-1)$ stack powers:

$$\dot{m}_{FCS} = \sum_{i=1}^{N_{st}-1} \dot{m}_{st}(P_i) + \dot{m}_{st}(P_{FCS} - \sum_{i=1}^{N_{st}-1} P_i). \tag{A.3}$$

Optimizing Eq. (A.3) analytically, i.e., setting the partial derivatives with respect to the stack powers zero, gives a set of $(N_{st}-1)$ equations

$$\frac{\partial \dot{m}_{FCS}}{\partial P_i} = \frac{d\dot{m}_{st}}{dP_{st}}(P_i) - \frac{d\dot{m}_{st}}{dP_{st}}(P_{N_{st}}) = 0 \tag{A.4}$$

which, under the assumption of identical and strictly convex stack fuel consumption curves, only holds true if all individual stack powers are identical:

$$P_i = P_j \quad \forall i, j \in \{1, \dots, N_{st}\}, j \neq i. \tag{A.5}$$

Appendix B. Convexity of equivalent fuel consumption function

The equivalent fuel consumption function H, which is defined in Eq. (7), consists of two terms. The first term $n_{st}\dot{m}_{st}(P_{st})$ is based on the fuel consumption curve, which is strictly convex in P_{st} by assumption. Considering that $V_{OC}^2/(4R_{int})$ is the theoretical maximum of P_b and $\lambda = -|\lambda| \leq 0$, the analysis of the second term $\lambda f(P_{el} - n_{st}P_{st})$ shows that it is convex in P_{st}:

$$\frac{\partial^2(\lambda f)}{\partial P_{st}^2} = \frac{2|\lambda| n_{st}^2 R_{int}}{Q_0} \left(V_{OC}^2 - 4R_{int}P_b\right)^{-\frac{3}{2}} \geq 0. \tag{B.1}$$

Consequently, H is strictly convex in P_{st}.

References

[1] Zhou S, Fan L, Zhang G, Gao J, Lu Y, Zhao P, Wen C, Shi L, Hu Z. A review on proton exchange membrane multi-stack fuel cell systems: architecture, performance, and power management. Appl Energy 2022;310:118555. http://dx.doi.org/10.1016/j.apenergy.2022.118555.

[2] Fletcher T, Thring R, Watkinson M. An energy management strategy to concurrently optimise fuel consumption & PEM fuel cell lifetime in a hybrid vehicle. Int J Hydrog Energy 2016;41(46):21503–15. http://dx.doi.org/10.1016/j.ijhydene.2016.08.157.

[3] Ferrara A, Jakubek S, Hametner C. Energy management of heavy-duty fuel cell vehicles in real-world driving scenarios: Robust design of strategies to maximize the hydrogen economy and system lifetime. Energy Convers Manage 2021;232:113795. http://dx.doi.org/10.1016/j.enconman.2020.113795.

[4] Zou W, Li J, Yang Q, Wan X, He Y, Lan H. A real-time energy management approach with fuel cell and battery competition-synergy control for the fuel cell vehicle. Appl Energy 2023;334:120667. http://dx.doi.org/10.1016/j.apenergy.2023.120667.

[5] López-Ibarra JA, Goitia-Zabaleta N, Herrera VI, Gazta ñaga H, Camblong H. Battery aging conscious intelligent energy management strategy and sensitivity analysis of the critical factors for plug-in hybrid electric buses. eTransportation 2020;5:100061. http://dx.doi.org/10.1016/j.etran.2020.100061.

[6] Chen H, Pei P, Song M. Lifetime prediction and the economic lifetime of proton exchange membrane fuel cells. Appl Energy 2015;142:154–63. http://dx.doi.org/10.1016/j.apenergy.2014.12.062.

[7] Ren P, Pei P, Li Y, Wu Z, Chen D, Huang S. Degradation mechanisms of proton exchange membrane fuel cell under typical automotive operating conditions. Prog Energy Combust Sci 2020;80:100859. http://dx.doi.org/10.1016/j.pecs.2020.100859.

[8] Yu Y, Li H, Wang H, Yuan X-Z, Wang G, Pan M. A review on performance degradation of proton exchange membrane fuel cells during startup and shutdown processes: Causes, consequences, and mitigation strategies. J Power Sources 2012;205:10–23. http://dx.doi.org/10.1016/j.jpowsour.2012.01.059.

[9] Bae SJ, Kim S-J, Park JI, Park CW, Lee J-H, Song I, Lee N, Kim K-B, Park J-Y. Lifetime prediction of a polymer electrolyte membrane fuel cell via an accelerated startup–shutdown cycle test. Int J Hydrog Energy 2012;37(12):9775–81. http://dx.doi.org/10.1016/j.ijhydene.2012.03.104.

[10] Leng Y, Yang D, Ming P, Zhang C. A comparative study of corrosion resistance evaluation of bipolar plate materials for proton exchange membrane fuel cell. eTransportation 2021;10:100139. http://dx.doi.org/10.1016/j.etran.2021.100139.

[11] Timilsina L, Badr PR, Hoang PH, Ozkan G, Papari B, Edrington CS. Battery degradation in electric and hybrid electric vehicles: A survey study. IEEE Access 2023;11:42431–62. http://dx.doi.org/10.1109/ACCESS.2023.3271287.

[12] Chen Z, Liu Y, Ye M, Zhang Y, Chen Z, Li G. A survey on key techniques and development perspectives of equivalent consumption minimisation strategy for hybrid electric vehicles. Renew Sustain Energy Rev 2021;151:111607. http://dx.doi.org/10.1016/j.rser.2021.111607.

[13] Piras M, De Bellis V, Malfi E, Desantes JM, Novella R, Lopez-Juarez M. Incorporating speed forecasting and SOC planning into predictive ECMS for heavy-duty fuel cell vehicles. Int J Hydrog Energy 2024;55:1405–21. http://dx.doi.org/10.1016/j.ijhydene.2023.11.250.

[14] Zhang H, Lei N, Liu S, Fan Q, Wang Z. Data-driven predictive energy consumption minimization strategy for connected plug-in hybrid electric vehicles. Energy 2023;283:128514. http://dx.doi.org/10.1016/j.energy.2023.128514.

[15] Chen D, Kim Y, Stefanopoulou AG. Predictive equivalent consumption minimization strategy with segmented traffic information. IEEE Trans Veh Technol 2020;69(12):14377–90. http://dx.doi.org/10.1109/TVT.2020.3034552.

[16] Tianheng F, Lin Y, Qing G, Yanqing H, Ting Y, Bin Y. A supervisory control strategy for plug-in hybrid electric vehicles based on energy demand prediction and route preview. IEEE Trans Veh Technol 2015;64(5):1691–700, URL https://doi.org/10.1109/TVT.2014.2336378.

[17] Zhang C, Vahidi A. Route preview in energy management of plug-in hybrid vehicles. IEEE Trans Control Syst Technol 2012;20(2):546–53. http://dx.doi.org/10.1109/TCST.2011.2115242.

[18] Larsson V, Johannesson Mårdh L, Egardt B, Karlsson S. Commuter route optimized energy management of hybrid electric vehicles. IEEE Trans Intell Transp Syst 2014;15(3):1145–54. http://dx.doi.org/10.1109/TITS.2013.2294723.

[19] Kofler S, Jakubek S, Hametner C. Cost-to-go-based predictive equivalent consumption minimization strategy for fuel cell vehicles considering route information. In: 2024 IEEE intelligent vehicles symposium. IV, 2024, p. 2910–6. http://dx.doi.org/10.1109/IV55156.2024.10588715.

[20] Ettihir K, Boulon L, Agbossou K. Energy management strategy for a fuel cell hybrid vehicle based on maximum efficiency and maximum power identification. IET Electr Syst Transp 2016;6(4):261–8. http://dx.doi.org/10.1049/iet-est.2015.0023.

[21] Macias Fernandez A, Kandidayeni M, Boulon Lc, Chaoui H. An adaptive state machine based energy management strategy for a multi-stack fuel cell hybrid electric vehicle. IEEE Trans Veh Technol 2020;69(1):220–34. http://dx.doi.org/10.1109/TVT.2019.2950558.

[22] Cardozo J, Marx N, Boulon L, Hissel D. Comparison of multi-stack fuel cell system architectures for residential power generation applications including electrical vehicle charging. In: 2015 IEEE vehicle power and propulsion conference. VPPC, 2015, p. 1–6. http://dx.doi.org/10.1109/VPPC.2015.7352912.

[23] Kandidayeni M, Macias A, Boulon L, Kelouwani S. Investigating the impact of ageing and thermal management of a fuel cell system on energy management strategies. Appl Energy 2020;274:115293, doi:j.apenergy.2020.115293. URL https://doi.org/10.1016/j.apenergy.2020.115293.

[24] Feroldi D, Serra M, Riera J. Energy management strategies based on efficiency map for fuel cell hybrid vehicles. J Power Sources 2009;190(2):387–401. http://dx.doi.org/10.1016/j.jpowsour.2009.01.040.

[25] Zhang H, Li X, Liu X, Yan J. Enhancing fuel cell durability for fuel cell plug-in hybrid electric vehicles through strategic power management. Appl Energy 2019;241:483–90. http://dx.doi.org/10.1016/j.apenergy.2019.02.040.

[26] Geng C, Jin X, Zhang X. Simulation research on a novel control strategy for fuel cell extended-range vehicles. Int J Hydrog Energy 2019;44(1):408–20. http://dx.doi.org/10.1016/j.ijhydene.2018.04.038, State of the Art Materials for Hydrogen Energy.

[27] Marx N, Hissel D, Gustin F, Boulon L, Agbossou K. On the sizing and energy management of an hybrid multistack fuel cell – battery system for automotive applications. Int J Hydrog Energy 2017;42(2):1518–26. http://dx.doi.org/10.1016/j.ijhydene.2016.06.111.

[28] Moghadari M, Kandidayeni M, Boulon L, Chaoui H. Operating cost comparison of a single-stack and a multi-stack hybrid fuel cell vehicle through an online hierarchical strategy. IEEE Trans Veh Technol 2023;72(1):267–79. http://dx.doi.org/10.1109/TVT.2022.3205879.

[29] Li H, Ravey A, N'Diaye A, Djerdir A. Online adaptive equivalent consumption minimization strategy for fuel cell hybrid electric vehicle considering power sources degradation. Energy Convers Manage 2019;192:133–49. http://dx.doi.org/10.1016/j.enconman.2019.03.090.

[30] Geng B, Mills JK, Sun D. Two-stage energy management control of fuel cell plug-in hybrid electric vehicles considering fuel cell longevity. IEEE Trans Veh Technol 2012;61(2):498–508. http://dx.doi.org/10.1109/TVT.2011.2177483.

[31] Wang T, Li Q, Yin L, Chen W, Breaz E, Gao F. Hierarchical power allocation method based on online extremum seeking algorithm for dual-PEMFC/Battery hybrid locomotive. IEEE Trans Veh Technol 2021;70(6):5679–92. http://dx.doi.org/10.1109/TVT.2021.3078752.

[32] Han X, Li F, Zhang T, Zhang T, Song K. Economic energy management strategy design and simulation for a dual-stack fuel cell electric vehicle. Int J Hydrog Energy 2017;42(16):11584–95. http://dx.doi.org/10.1016/j.ijhydene.2017.01.085.

[33] Anbarasu A, Dinh TQ, Sengupta S. Novel enhancement of energy management in fuel cell hybrid electric vehicle by an advanced dynamic model predictive control. Energy Convers Manage 2022;267:115883. http://dx.doi.org/10.1016/j.enconman.2022.115883.

[34] Zhang C, Zeng T, Wu Q, Deng C, Chan SH, Liu Z. Improved efficiency maximization strategy for vehicular dual-stack fuel cell system considering load state of sub-stacks through predictive soft-loading. Renew Energy 2021;179:929–44. http://dx.doi.org/10.1016/j.renene.2021.07.090.

[35] Min D, Song Z, Chen H, Wang T, Zhang T. Genetic algorithm optimized neural network based fuel cell hybrid electric vehicle energy management strategy under start-stop condition. Appl Energy 2022;306:118036. http://dx.doi.org/10.1016/j.apenergy.2021.118036.

[36] Ferrara A, Hametner C. Predictive activation strategy for health-conscious energy management of multi-module fuel cell systems in heavy-duty long-haul electric trucks. In: 16th international conference on engines & vehicles. SAE International; 2023, http://dx.doi.org/10.4271/2023-24-0138.

[37] Guzzella L, Sciarretta A. Vehicle propulsion systems: introduction to modeling and optimization. Berlin, Heidelberg: Springer Berlin Heidelberg; 2013, http://dx.doi.org/10.1007/978-3-642-35913-2{_}2.

[38] Kofler S, Du ZP, Jakubek S, Hametner C. Adaptive step size dynamic programming for optimal energy management of fuel cell vehicles. In: 2023 IEEE vehicle power and propulsion conference. VPPC, 2023, p. 1–6. http://dx.doi.org/10.1109/VPPC60535.2023.10403120.

[39] Serrao L, Onori S, Rizzoni G. ECMS as a realization of Pontryagin's minimum principle for HEV control. In: 2009 American control conference. 2009, p. 3964–9. http://dx.doi.org/10.1109/ACC.2009.5160628.

[40] Sundström O, Guzzella L. A generic dynamic programming Matlab function. In: Proceedings of the IEEE international conference on control applications. 2009, p. 1625–30. http://dx.doi.org/10.1109/CCA.2009.5281131.

[41] Kirk DE. Optimal control theory: an introduction. Dover Publications; 2004.

[42] Han J, Park Y, Kum D. Optimal adaptation of equivalent factor of equivalent consumption minimization strategy for fuel cell hybrid electric vehicles under active state inequality constraints. J Power Sources 2014;267:491–502. http://dx.doi.org/10.1016/j.jpowsour.2014.05.067.

[43] Antoniou A, Lu W-S. Practical optimization: algorithms and engineering applications. New York, NY: Springer US; 2021, http://dx.doi.org/10.1007/978-1-0716-0843-2.

[44] Elbert P, Nüesch T, Ritter A, Murgovski N, Guzzella L. Engine On/Off control for the energy management of a serial hybrid electric bus via convex optimization. IEEE Trans Veh Technol 2014;63(8):3549–59. http://dx.doi.org/10.1109/TVT.2014.2304137.

[45] Guo N, Shen J, Xiao R, Yan W, Chen Z. Energy management for plug-in hybrid electric vehicles considering optimal engine ON/OFF control and fast state-of-charge trajectory planning. Energy 2018;163:457–74. http://dx.doi.org/10.1016/j.energy.2018.08.116.

[46] Liu T, Feng L, Zhu W. Fuel minimization of a hybrid electric racing car by quasi-pontryagin's minimum principle. IEEE Trans Veh Technol 2021;70(6):5551–64. http://dx.doi.org/10.1109/TVT.2021.3075729.

[47] Nocera S, Cavallaro F, Irranca Galati O. Options for reducing external costs from freight transport along the Brenner corridor. Eur Transp Res Rev 2018;10(2):53. http://dx.doi.org/10.1186/s12544-018-0323-7.

2.3 Publication C

Sandro Kofler, Zhang Peng Du, Stefan Jakubek, and Christoph Hametner.
Predictive energy management strategy for fuel cell vehicles combining long-term and short-term forecasts.
IEEE Transactions on Vehicular Technology, Volume 73, Issue 11, Pages 16364–16374, 2024.
DOI: 10.1109/TVT.2024.3424422.

Contributions by the author of the dissertation[†]

- Conceptualization
- Methodology
- Software
- Validation
- Formal analysis
- Investigation
- Data curation
- Writing – original draft
- Visualization

[†]According to the Contributor Roles Taxonomy (CRediT), DOI: 10.3789/ansi.niso.z39.104-2022

16364 IEEE TRANSACTIONS ON VEHICULAR TECHNOLOGY, VOL. 73, NO. 11, NOVEMBER 2024

Predictive Energy Management Strategy for Fuel Cell Vehicles Combining Long-Term and Short-Term Forecasts

Sandro Kofler, *Graduate Student Member, IEEE*, Zhang Peng Du, Stefan Jakubek, and Christoph Hametner

***Abstract*—Fuel cell electric vehicles are usually hybrid vehicles requiring an energy management strategy (EMS) to determine the power split between the fuel cell system and a battery. The performance of an EMS can be improved by taking into account forecasts of the vehicle velocity. Simple estimates derived from static route information, e.g., speed limits, can already provide a significant performance increase because they are available before departure and for the entire driving mission. However, such long-term predictions can deviate considerably from the actual velocity because of dynamic influences, such as traffic, roadworks, or weather. Here, short-term predictions from vehicular communication systems provide more accurate real-time information and allow the EMS to react better to the actual driving conditions. This article proposes a predictive EMS that optimally combines the information of long-term and short-term forecasts. Before departure, a dynamic programming algorithm optimizes the energy management based on static route information yielding a distance-based map describing the optimal cost-to-go. While driving, a model predictive controller (MPC) optimizes the energy management in real time considering the short-term prediction and including the optimal cost-to-go representing the long-term information as terminal cost. A computationally efficient linear MPC implementation is proposed, and the significant performance benefit over an MPC that tracks an optimized battery state of charge reference is demonstrated in a numerical study.**

***Index Terms*—Cost-to-go, dynamic programming, energy management, fuel cell vehicle, fuel optimal control, model predictive control, velocity prediction.**

I. INTRODUCTION

FUEL cell electric vehicles (FCEVs) are commonly designed as hybrid vehicles, i.e., their powertrain includes a battery as an auxiliary power source besides the fuel cell system (FCS). The battery allows for recuperating kinetic energy and avoiding low-efficient operation ranges of the FCS [1]. In this way, the hybrid configuration of the powertrain offers benefits in terms of fuel economy, which, however, strongly rely on the energy management, i.e., the power split between the FCS and the battery. Besides fuel economy, other important aspects are associated with the energy management, such as battery charge control and the lifetimes of the power sources: Extremely charging or discharging the battery provokes degradation and might even cause infeasible operation, particularly in the case of heavy-duty vehicles. Therefore, the battery's state of charge (SoC) should remain within a predefined range during operation. To mitigate the degradation of the FCS, dynamic transients and high peaks in the FCS power demand should be avoided [2], [3]. The globally optimal power split considering the aforementioned criteria could only be realized if the power demand of the entire driving mission would be known in advance, which is noncausal [4]. Here, predictive energy management strategies (EMSs) come into play. With an appropriate vehicle model, the future power demand can be estimated based on predictions of the altitude and velocity profiles of the upcoming driving mission. Whereas the altitude can directly be derived from topographical data if the route is planned in advance, estimating the velocity is more difficult.

Vehicle velocity prediction is a challenging task due to numerous stochastic influences such as driver behavior, traffic flow, traffic signals, and environmental influences [5], [6], [7]. The uncertainty grows with the length of the prediction horizon, which is why it is impossible to predict the velocity of a human-driven vehicle for an entire driving mission with a high accuracy. A simple *long-term* estimate of the velocity along a planned route can be based on static route information such as speed limits [8], [9], [10]. Even though such a long-term prediction is not very accurate, it can considerably improve the energy management performance because it is available for the entire driving mission in advance. In contrast, more accurate velocity predictions can be provided by onboard, *short-term* prediction methods based on intelligent transportation systems (ITSs). In addition to static route information, these methods are provided with real-time information regarding the actual driving conditions, such as traffic, roadworks, or weather, through vehicle-to-vehicle (V2V) and vehicle-to-infrastructure (V2I) communication [11], [12], [13].

In the literature, two-stage EMS approaches are often found to consider long-term predictions of the entire driving mission.

Manuscript received 7 March 2023; revised 22 November 2023; accepted 2 July 2024. Date of publication 8 July 2024; date of current version 7 November 2024. This work was supported in part by the Climate and Energy Fund and implemented in line with the "Zero Emission Mobility" Program, and in part by the TU Wien Bibliothek through its Open Access Funding Program. The review of this article was coordinated by Prof. Ayan Mallik. *(Corresponding author: Sandro Kofler.)*

Sandro Kofler, Zhang Peng Du, and Stefan Jakubek are with the Institute of Mechanics and Mechatronics, TU Wien, 1060 Vienna, Austria (e-mail: sandro.kofler@tuwien.ac.at; zhang.peng.du@tuwien.ac.at; stefan.jakubek@tuwien.ac.at).

Christoph Hametner is with the Christian Doppler Laboratory for Innovative Control and Monitoring of Automative Powertrain Systems, TU Wien, 1060 Vienna, Austria (e-mail: christoph.hametner@tuwien.ac.at).

Digital Object Identifier 10.1109/TVT.2024.3424422

Commonly, a reference trajectory for the battery SoC is optimized based on the long-term prediction in the first stage. This offline optimization is often performed with dynamic programming (DP) [14], [15], which is a numerical method for solving dynamic optimization problems. The strengths of DP are the capabilities to deal with nonlinear problems and consider constraints on inputs and states. In the second stage, an online strategy determines the power split between the primary power source and the battery while driving such that the SoC reference profile is tracked. To improve the performance and react to the actual driving conditions, online strategies can additionally take into account the more accurate short-term predictions, e.g., based on model predictive control (MPC), an optimal control framework allowing to consider constraints and predictions within a certain prediction horizon [14], [16], [17].

However, using SoC reference trajectories to consider feedforward information has a drawback. Optimized long-term information of the trip is only available along the SoC reference trajectory. If the actual power demand deviates from the underlying long-term prediction, which is likely because the prediction is only based on static route information, the actual SoC is expected to deviate from its reference. Tracking the SoC reference trajectory, i.e., forcing the SoC back to the reference, is a suboptimal behavior [18]. Of course, the reference trajectory could be re-optimized, but this requires additional computational resources.

An effective alternative for providing optimized long-term information is the optimal cost-to-go [19], which can be computed with DP [18], [20], [21]. The optimal cost-to-go describes the minimum amount of fuel needed to reach the intended destination as a function of the position along the trip and the SoC. This means that the long-term information is available within the entire SoC range in contrast to an SoC reference trajectory. Again, MPC is a suitable basis for additionally considering short-term predictions to react to the actual driving conditions. Here, the optimal cost-to-go can be included as terminal cost in the objective function [20], [22], [23]. Even though cost-to-go-based MPC methods are available in the literature, they focus on hybrid electric vehicles powered by internal combustion engines but not FCEVs. Moreover, the majority of the cost-to-go-based MPCs are based on nonlinear formulations, which might complicate their real-time onboard implementation [24].

The main contribution of this work is a predictive EMS for FCEVs using DP to compute the optimal cost-to-go based on static route information before departure and a linear, cost-to-go-based MPC taking into account short-term predictions to react to the actual driving conditions. The distinctive feature of the proposed EMS is that optimized long-term information is considered in the form of the optimal cost-to-go, which, unlike an SoC reference trajectory, provides information within the entire SoC range. Consequently, optimized information is available even if the actual SoC completely deviates from the originally optimal path. The DP algorithm used to conduct the offline optimization allows to consider state and input constraints and can handle nonlinearities. The computational complexity of the DP, which is often reported to be a limiting factor [21], [23], is kept low because only one state is involved and a rather rough discretization is sufficient for the optimization based on the long-term prediction derived from static route information. The offline DP yields the optimal cost-to-go in the form of a 2-D map depending on the position along the trip and the SoC. Here, a distance-based rather than a time-based description of the cost-to-go is chosen to be independent of the actual velocity, which is initially unknown. The online energy management is conducted with an MPC considering real-time, short-term predictions within the prediction horizon and an approximation of the optimal cost-to-go as terminal cost. In this way, the MPC optimally combines the short-term prediction with the optimized long-term information and minimizes the amount of fuel for the trip remainder in each instant. The proposed MPC is based on a computationally efficient, linear formulation, which is highly beneficial for the onboard implementation.

The remainder of this article is structured as follows. First, a control-oriented model of the FCEV is presented in Section II. Then, the proposed EMS is described in Section III, followed by the linear formulation of the MPC in Section IV. In Section V, the proposed MPC is compared to an MPC that tracks an optimized SoC reference trajectory. The comparison is based on the simulation of a real-world driving cycle. A conclusion in Section VI finalizes this article.

II. System Modeling

Optimizing the energy management of an upcoming driving mission requires knowledge of the future vehicle power demand and the powertrain characteristics. A prediction of the power demand is not directly available but can be derived from a prediction of the vehicle velocity considering the longitudinal vehicle dynamics. In the following, control-oriented models of the vehicle dynamics and the hybrid powertrain are described.

A. Vehicle Dynamics

The longitudinal model of the vehicle considers the traction force, aerodynamic drag, rolling resistance, and gravitational force and is expressed by

$$\delta m \frac{\mathrm{d}v}{\mathrm{d}t} = \frac{P_{\mathrm{tr}}}{v} - \frac{\rho A_{\mathrm{f}} c_{\mathrm{d}}}{2} v^2 - c_{\mathrm{r}} m g \cos\theta - m g \sin\theta \quad (1)$$

where v denotes the vehicle velocity, t the time, m the vehicle mass, δ the correction coefficient of rotating mass, ρ the air density, A_{f} the vehicle frontal area, c_{d} the drag coefficient, c_{r} the rolling resistance coefficient, g the gravitational acceleration, and θ the inclination angle of the road. The traction power P_{tr} is provided by an electric motor. The input power of the motor

$$P_{\mathrm{m}} = P_{\mathrm{tr}}\, \eta_{\mathrm{m}}^{-\mathrm{sgn}\, P_{\mathrm{tr}}} \quad (2)$$

considers power losses in the inverter and the motor approximated with the efficiency η_{m}. The overall electric power demand P_{el} of the vehicle is the sum of the motor input power and the power consumption of the auxiliary systems P_{aux}:

$$P_{\mathrm{el}} = P_{\mathrm{m}} + P_{\mathrm{aux}}. \quad (3)$$

16366 IEEE TRANSACTIONS ON VEHICULAR TECHNOLOGY, VOL. 73, NO. 11, NOVEMBER 2024

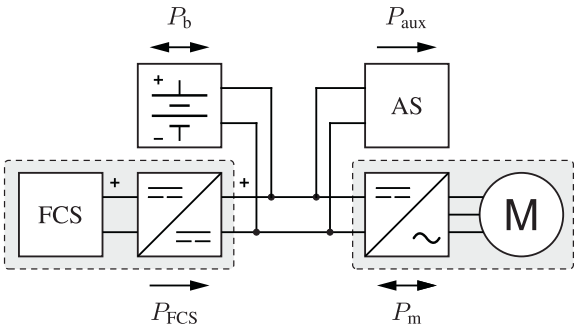

Fig. 1. Hybrid vehicle configuration consisting of the FCS, battery, traction motor, and auxiliary systems (AS). The arrows indicate the possible directions of the power flows.

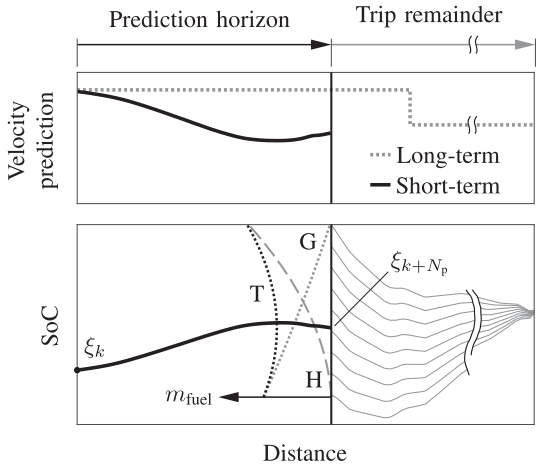

Fig. 2. The MPC optimizes the power split such that the total fuel amount (T), which is the sum of the fuel consumed within the prediction horizon (H) and the optimal cost-to-go (G), is minimized. The optimal cost-to-go represents the fuel amount of optimal paths for the trip remainder.

With that, a prediction of the electric power demand can be derived from predictions of the vehicle velocity and the inclination angle of the road, which can be derived from the elevation profile.

B. Hybrid Powertrain

The vehicle is equipped with a hybrid powertrain with two power sources: the FCS and a battery (see Fig. 1). Whereas the FCS can only provide power, the battery can also store energy coming from the FCS or the electric motor during regenerative braking. The sum of the FCS power P_FCS and the battery power P_b satisfies the overall electric load:

$$P_\mathrm{el} = P_\mathrm{FCS} + P_\mathrm{b}. \tag{4}$$

The hybrid configuration of the powertrain implies one degree of freedom, i.e., the power split between the FCS and the battery. The EMS determines the FCS power, which is assumed to be provided within reasonable time. The residual of the power demand is provided by the battery, subject to the corresponding constraints.

The FCS is considered in the form of a simplified, quasistatic model determined by measurements, where the fuel consumption rate $\dot{m}_{\mathrm{H}_2}$ of the FCS is a monotonically increasing function of the FCS power. The FCS model implicitly considers the losses in the converter and the power demand of the corresponding auxiliaries, such as the compressor.

The battery is modeled in the form of an equivalent circuit with three parameters: the open-circuit voltage V_OC, the internal battery resistance R_int, and the nominal battery capacity Q_0 [25]. The dynamics of the battery SoC ξ is described by a nonlinear function depending on the battery power:

$$\frac{\mathrm{d}\xi}{\mathrm{d}t} = f(P_\mathrm{b}) = -\frac{V_\mathrm{OC} - \sqrt{V_\mathrm{OC}^2 - 4P_\mathrm{b}R_\mathrm{int}}}{2Q_0R_\mathrm{int}}. \tag{5}$$

With this control-oriented description, the dynamic model of the powertrain has only one state, which is the battery SoC.

III. PREDICTIVE ENERGY MANAGEMENT

The proposed predictive EMS comprises two stages. Before departure, the energy management of the hybrid powertrain is optimized based on a long-term prediction of the power demand, which is available for the entire driving mission. This *offline optimization* is conducted with DP and yields a 2-D map describing the optimal cost-to-go, i.e., the minimum amount of fuel required to reach the intended destination, as a function of the position along the trip and the SoC.

While driving, the *online MPC* successively optimizes the power split considering a more accurate short-term prediction and the optimal cost-to-go at the end of the prediction horizon. Here, the cost-to-go provides optimized long-term information for the entire SoC range. As illustrated in Fig. 2, the cost-to-go decreases with an increasing SoC at the end of the prediction horizon since more energy is available from the battery for the remaining trip. However, a higher SoC at the end of the prediction horizon implies a higher fuel consumption within the horizon because the battery needs to be charged. The optimal power split minimizes the sum of the fuel consumed within the prediction horizon and the cost-to-go.

In the following, the two EMS stages and the corresponding predictions are described in detail.

A. Offline Optimization With Dynamic Programming

The offline optimization of the energy management requires a long-term prediction of the power demand. Planning the route before departure gives access to static route information such as the elevation profile and speed limits. Based on the speed limits, an estimate of the vehicle velocity can be derived considering simplified vehicle dynamics during transients and maximum cornering speeds. With the known elevation profile and the estimated velocity profile, an estimate of the vehicle power demand for the entire driving mission can be derived based on the model of the vehicle dynamics (see Section II-A).

The optimization aims at minimizing the fuel consumption for the planned trip under the consideration of the battery SoC

dynamics

$$\begin{aligned} \min J = & \int_{t_0}^{t_1} \dot{m}_{\mathrm{H_2}}(P_{\mathrm{FCS}}(t))\mathrm{d}t \\ \text{s.t.} \quad & P_{\mathrm{FCS}}(t) \in \mathcal{U} \\ & P_{\mathrm{b}}(t) \in \mathcal{B} \\ & \xi(t) \in \mathcal{X} \\ & \xi(t_0) = \xi_0 \\ & \xi(t_1) \in \mathcal{X}_1 \end{aligned} \tag{6}$$

where the sets $\mathcal{U}$, $\mathcal{B}$, $\mathcal{X}$, and $\mathcal{X}_1$ cover the feasible ranges according to the specified constraints on the FCS power, the battery power, the SoC, and the terminal SoC, respectively, and ξ_0 denotes the initial SoC. The set $\mathcal{X}_1$ is commonly specified by a minimum boundary for the final SoC. Based on Bellman's principle of optimality, the discrete counterpart of the dynamic optimization problem can be solved by a recursive backward algorithm known as dynamic programming [26]. For this purpose, the battery model (5) is discretized assuming a zero-order hold for the power demand and the FCS power giving

$$\xi_{l+1} = \xi_l - \frac{V_{\mathrm{OC}} - \sqrt{V_{\mathrm{OC}}^2 - 4(P_{\mathrm{el},l} - P_{\mathrm{FCS},l})R_{\mathrm{int}}}}{2Q_0 R_{\mathrm{int}}}\Delta t_l \tag{7}$$

where $\Delta t_l = t_{l+1} - t_l$. The problem is solved in the distance domain meaning that the trip is divided into $N-1$ distance segments. Consequently, Δt_l varies depending on the velocity and the length of the segment, and sections where the vehicle velocity is zero are ignored. The mean power demand of the l-th segment is derived from the prediction with

$$P_{\mathrm{el},l} = \frac{\int_{t_l}^{t_{l+1}} P_{\mathrm{el}}\,\mathrm{d}t}{\Delta t_l}. \tag{8}$$

The DP algorithm optimizes a sequence of subproblems starting at the position $N-1$ and successively stepping backwards until the beginning of the trip:

$$\begin{aligned} J_l^*(\xi_l) = \min_{P_{\mathrm{FCS},l}} & \left[\dot{m}_{\mathrm{H_2}}(P_{\mathrm{FCS},l})\Delta t_l + J_{l+1}^*(\xi_{l+1})\right] \\ \text{s.t.} \quad & P_{\mathrm{FCS},l} \in \mathcal{U}^{\mathrm{q}} \\ & P_{\mathrm{b},l} \in \mathcal{B} \\ & \xi_{l+1} \in \mathcal{X}_{l+1} \\ & \forall \xi_l \in \mathcal{X}^{\mathrm{q}}. \end{aligned} \tag{9}$$

The finite sets $\mathcal{U}^{\mathrm{q}}$ and $\mathcal{X}^{\mathrm{q}}$ result from the quantization of $\mathcal{U}$ and $\mathcal{X}$, respectively. The set $\mathcal{X}_{l+1} \subseteq \mathcal{X}$ covers the feasible states at the position $l+1$ subject to the constraints. The resulting optimal cost-to-go function $J_l^*(\xi_l)$ describes the minimum amount of fuel needed to reach the intended destination from the position l as a function of the SoC. The optimal cost-to-go is stored as a discrete map for each position of the distance grid. Moreover, the boundaries $\xi_l^{\min}$ and $\xi_l^{\max}$ of $\mathcal{X}_l$ are stored for all positions.

The computational complexity of the DP algorithm grows linearly with the number of segments and, thus, linearly with the length of the long-term prediction if an equidistant segmentation is chosen. However, the complexity can be kept low because a rather rough segmentation is sufficient for the offline optimization due to the limited accuracy of the long-term prediction. To save further computational time, the step size can also be determined adaptively depending on the power demand signal [27].

B. Online Model Predictive Control

Since the long-term prediction is only based on static route information, a deviation from the actual power demand because of dynamic influences, such as traffic, roadworks, or weather, is inevitable. To improve the performance and better react to the actual driving conditions, the online MPC additionally considers short-term predictions. Such predictions can be provided by forecasting systems considering V2V and V2I communication [11] and are expected to be more accurate than the long-term prediction because, in addition to static route data, they consider real-time information.

The objective function of the MPC consists of two terms representing the fuel consumption within the prediction horizon and a terminal cost

$$J_k = \sum_{j=k}^{k+N_{\mathrm{p}}-1} \dot{m}_{\mathrm{H_2}}(P_{\mathrm{FCS},j})T_{\mathrm{s}} + J_{k+N_{\mathrm{p}}}^*(\xi_{k+N_{\mathrm{p}}}(\boldsymbol{P}_{\mathrm{FCS},k})) \tag{10}$$

where T_{s} denotes the constant sampling time and $\boldsymbol{P}_{\mathrm{FCS},k} = [P_{\mathrm{FCS},k}, \ldots, P_{\mathrm{FCS},k+N_{\mathrm{p}}-1}]^{\mathrm{T}}$ denotes the sequence of the FCS power within the prediction horizon of N_{p} samples. The index k denotes quantities at the current instant. Note that the indexing based on k is independent of the indexing based on l used in the DP. The terminal cost represents the cost-to-go at the end of the prediction horizon, which is obtained by distance-based interpolation in the cost-to-go map resulting from the offline optimization. It is a function of the terminal SoC and, therefore, the sequence of control inputs.

The optimal sequence of control inputs at the instant k is determined by minimizing the objective function

$$\begin{aligned} \boldsymbol{P}_{\mathrm{FCS},k}^* = \arg\min_{\boldsymbol{P}_{\mathrm{FCS},k}} & J_k \\ \text{s.t.} \quad & P_{\mathrm{FCS},k+n} \in \mathcal{U} \\ & \Delta P_{\mathrm{FCS},k+n} \in \mathcal{R} \\ & P_{\mathrm{b},k+n} \in \mathcal{B} \\ & \xi_{k+n} \in \mathcal{X} \\ & \xi_{k+N_{\mathrm{p}}} \in \mathcal{X}_{k+N_{\mathrm{p}}} \end{aligned} \tag{11}$$

with

$$\Delta P_{\mathrm{FCS},k} = P_{\mathrm{FCS},k} - P_{\mathrm{FCS},k-1} \tag{12}$$

and $n = 0, 1, \ldots, N_{\mathrm{p}} - 1$, whereby the short-term power demand prediction is considered as disturbance. The set $\mathcal{R}$ describes constraints on the increments of the FCS power, which are necessary to avoid requesting infeasible transients from the FCS. The consideration of these constraints is only relevant in the MPC because the offline DP is based on a considerably rougher discretization, where the FCS dynamics are negligible. The boundaries $\xi_{k+N_{\mathrm{p}}}^{\min}$ and $\xi_{k+N_{\mathrm{p}}}^{\max}$ defining the set of feasible

states $\mathcal{X}_{k+N_\mathrm{p}}$ at the end of the prediction horizon are determined by distance-based linear interpolation. The constraints on the battery power, the SoC, and the SoC at the end of the prediction horizon are implemented as soft constraints to prevent infeasibility. According to the receding horizon principle, only the first step $P^*_{\mathrm{FCS},k}$ is actually applied to the system. In the next sampling instant, the measurements and the short-term prediction are updated, and the procedure is repeated [28].

The two terms of the objective function have counteracting effects on the optimization. The minimization of the fuel consumption within the prediction horizon is favored by a low FCS power. However, a lower FCS power implies a lower SoC at the end of the prediction horizon and, consequently, a higher cost-to-go because less energy is stored in the battery. The optimal power split is a trade-off and minimizes the amount of fuel needed to reach the intended destination based on the available information, which consists of the short-term prediction and the optimized long-term information.

IV. Linear MPC Formulation

The optimal control problem of the online MPC must be solved onboard and in real time. Therefore, reducing the computational complexity for solving the problem is highly beneficial for the implementation. In this section, a computationally efficient linear MPC formulation is derived. First, the battery SoC model is linearized. Then, a local quadratic approximation of the cost-to-go is formulated, and a physically motivated quadratic objective function taking into account ohmic battery losses is derived. The formulation allows to constrain increments of the FCS power to prevent the FCS from infeasible power rates.

A. Model Linearization

The battery SoC model (5) is linearized at the operating point $P_{\mathrm{b,op}} = 0\,\mathrm{W}$ yielding

$$\frac{\mathrm{d}\xi}{\mathrm{d}t} = -\frac{P_\mathrm{b}}{Q_0 V_\mathrm{OC}} + R(P_\mathrm{b}) \tag{13}$$

where R denotes the remainder. The linearized model is then discretized with T_s assuming a zero-order hold for the battery power. An incremental formulation of the control input, i.e., the FCS power, is chosen to allow constraining the control moves. Therefore, the state vector includes two states, which are the SoC and the FCS power: $\boldsymbol{x}_k = [\xi_k\,,\, P_{\mathrm{FCS},k-1}]^\mathrm{T}$. Considering $P_\mathrm{b} = P_\mathrm{el} - P_\mathrm{FCS}$, the linear discrete-time state-space model can be written as

$$\boldsymbol{x}_{k+1} = \begin{bmatrix} 1 & -c \\ 0 & 1 \end{bmatrix} \boldsymbol{x}_k + \begin{bmatrix} -c \\ 1 \end{bmatrix} \Delta u_k + \begin{bmatrix} c \\ 0 \end{bmatrix} w_k \tag{14a}$$

$$\boldsymbol{y}_k = \boldsymbol{x}_k \tag{14b}$$

where

$$\Delta u_k = \Delta P_{\mathrm{FCS},k}, \quad w_k = P_{\mathrm{el},k}, \quad c = -\frac{T_\mathrm{s}}{Q_0 V_\mathrm{OC}}.$$

Based on the linear model, the future trajectories of the SoC, the FCS power, and the battery power within the prediction horizon

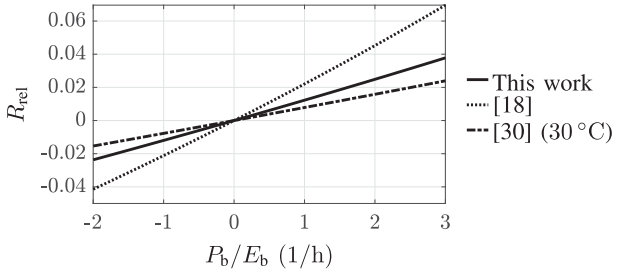

Fig. 3. Relative linearization error of the battery model as a function of the normalized battery power with respect to the nominal battery energy E_b.

can be expressed as

$$\boldsymbol{S}_k = \boldsymbol{F}_\mathrm{S}\,\boldsymbol{x}_k + \boldsymbol{\Phi}_\mathrm{S}\,\Delta\boldsymbol{U}_k + \boldsymbol{\Theta}_\mathrm{S}\boldsymbol{W}_k \tag{15}$$

$$\boldsymbol{P}_{\mathrm{FCS},k} = \boldsymbol{F}_\mathrm{F}\,\boldsymbol{x}_k + \boldsymbol{\Phi}_\mathrm{F}\,\Delta\boldsymbol{U}_k \tag{16}$$

$$\boldsymbol{P}_{\mathrm{b},k} = -\boldsymbol{F}_\mathrm{F}\,\boldsymbol{x}_k - \boldsymbol{\Phi}_\mathrm{F}\,\Delta\boldsymbol{U}_k + \boldsymbol{W}_k \tag{17}$$

and the SoC at the end of the prediction horizon can be expressed as

$$\xi_{k+N_\mathrm{p}} = \bar{\boldsymbol{F}}_\mathrm{S}\boldsymbol{x}_k + \bar{\boldsymbol{\Phi}}_\mathrm{S}\Delta\boldsymbol{U}_k + \bar{\boldsymbol{\Theta}}_\mathrm{S}\boldsymbol{W}_k \tag{18}$$

where

$$\boldsymbol{S}_k = \begin{bmatrix} \xi_{k+1} & \dots & \xi_{k+N_\mathrm{p}} \end{bmatrix}^\mathrm{T}$$

$$\boldsymbol{P}_{\mathrm{FCS},k} = \begin{bmatrix} P_{\mathrm{FCS},k} & \dots & P_{\mathrm{FCS},k+N_\mathrm{p}-1} \end{bmatrix}^\mathrm{T}$$

$$\boldsymbol{P}_{\mathrm{b},k} = \begin{bmatrix} P_{\mathrm{b},k} & \dots & P_{\mathrm{b},k+N_\mathrm{p}-1} \end{bmatrix}^\mathrm{T}$$

$$\Delta\boldsymbol{U}_k = \begin{bmatrix} \Delta P_{\mathrm{FCS},k} & \dots & \Delta P_{\mathrm{FCS},k+N_\mathrm{p}-1} \end{bmatrix}^\mathrm{T}$$

$$\boldsymbol{W}_k = \begin{bmatrix} P_{\mathrm{el},k} & \dots & P_{\mathrm{el},k+N_\mathrm{p}-1} \end{bmatrix}^\mathrm{T}.$$

These linear expressions are the basis for the formulation of the quadratic objective function. The time-invariant matrices $\boldsymbol{F}_\mathrm{S}$, $\boldsymbol{\Phi}_\mathrm{S}$, $\boldsymbol{\Theta}_\mathrm{S}$, etc., are derived from the discrete-time model as described in [29].

The linearization of the battery model implies a linearization error, which is linked to the neglected ohmic losses and, therefore, depends on the battery parameters. The relative linearization error can be computed with

$$R_\mathrm{rel}(P_\mathrm{b}) = \frac{R(P_\mathrm{b})}{f(P_\mathrm{b})} = \frac{V_\mathrm{OC} - \sqrt{V_\mathrm{OC}^2 - 4R_\mathrm{int}P_\mathrm{b}}}{2V_\mathrm{OC}}. \tag{19}$$

Fig. 3 illustrates the relative linearization errors of the battery used in the numerical study of this work and batteries from the literature [18], [30]. The approximation is good, in particular, if the battery is operated with low absolute values of the battery power. Moreover, the impact of the linearization on the SoC prediction is limited because the prediction horizon wherein an accurate short-term prediction is feasible is relatively short.

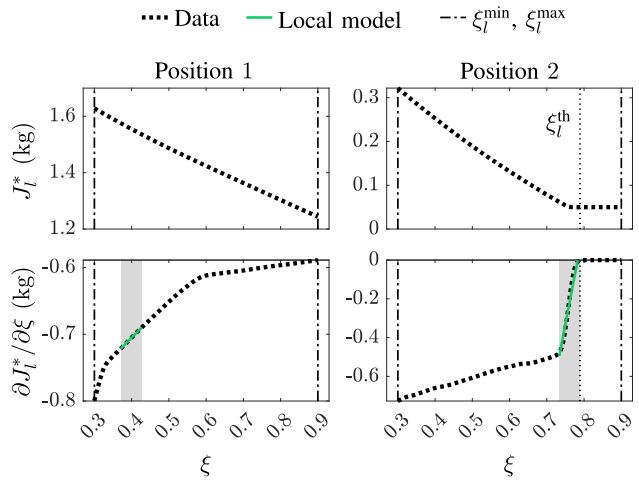

Fig. 4. The optimal cost-to-go resulting from the offline optimization and the partial derivative of the cost-to-go with respect to the SoC at two different positions of a driving cycle. The shaded areas in the lower plots indicate exemplary ranges where local linear models are fitted to. Note the differently scaled ordinates.

B. Approximation of the Cost-to-Go

The optimal cost-to-go resulting from the offline optimization is available as a discrete map $J_l^*(\xi_l)$ at each position of the distance grid and can be approximated for any position by distance-based linear interpolation. The upper plots in Fig. 4 show typical cost-to-go profiles at two different positions of a driving cycle. The cost-to-go generally decreases with an increasing SoC because more energy is stored in the battery. Under certain conditions, however, the cost-to-go remains constant if a certain threshold ξ_l^{th} is exceeded. This behavior is illustrated in the plots of position 2, which is almost at the end of the cycle, and can be explained as follows: Suppose that the minimum final SoC specified by $\mathcal{X}_1$ can be reached from the l-th position running the FCS only with the minimum feasible power according to $\mathcal{U}$ if $\xi_l = \xi_l^{\text{th}}$. Then, the minimum final SoC is exceeded if $\xi_l > \xi_l^{\text{th}}$ likewise operating the FCS with the minimum feasible power. The amount of fuel to reach the destination, i.e., the cost-to-go, is the same in either case because the fuel consumption rate is only a function of the FCS power. Consequently, the cost-to-go profile remains constant for all $\xi_l \geq \xi_l^{\text{th}}$.

The absolute value of the cost-to-go is irrelevant for the online optimization with the MPC; relevant is the partial derivative of the cost-to-go with respect to the SoC, which can be derived by numerical differentiation. Therefore, the approximation of the cost-to-go is based on a model of the derivative of the cost-to-go. Describing the derivative of the cost-to-go by a uniform function of the SoC is not possible because of the sharp changes in its slope, as the lower plots of Fig. 4 indicate (more details regarding this behavior are given in Section V-C). Consequently, the derivative of the cost-to-go at the end of the prediction horizon is described with a local linear model

$$\left.\frac{\partial \hat{J}^*_{k+N_\text{p}}}{\partial \xi}\right|_{\xi_k} = \beta_0 + \beta_1 \xi_{k+N_\text{p}} \tag{20}$$

where the two parameters β_0 and β_1 are estimated with the least-squares method within a predefined range around ξ_k (note that ξ_{k+N_p} is unknown). The range the local linear model is fitted to lies within $[\xi_l^{\min}; \xi_l^{\text{th}}]$ if the threshold is relevant, otherwise within $[\xi_l^{\min}; \xi_l^{\max}]$.

The cost-to-go at the end of the prediction horizon can then be approximated with a truncated Taylor series, where ξ_k is chosen as operating point:

$$\hat{J}^*_{k+N_\text{p}} = J^*_{k+N_\text{p}}\Big|_{\xi_k} + \left.\frac{\partial \hat{J}^*_{k+N_\text{p}}}{\partial \xi}\right|_{\xi_k} \left(\xi_{k+N_\text{p}} - \xi_k\right). \tag{21}$$

The first term in (21) is irrelevant for the optimization as it does not depend on the decision variable and, therefore, omitted. Inserting (20) gives the local quadratic approximation of the optimal cost-to-go at the end of the prediction horizon

$$\hat{J}^*_{k+N_\text{p}} = \left(\beta_0 - \beta_1 \xi_k\right) \xi_{k+N_\text{p}} + \beta_1 \xi^2_{k+N_\text{p}} \tag{22}$$

where another constant term has been omitted likewise.

C. Quadratic Objective Function

The objective function of the linear MPC considers the fuel consumption within the prediction horizon and the cost-go-to at the end of the prediction horizon. The components of the objective function are elaborated in the following.

1) Fuel Consumption Within Prediction Horizon: The quasistatic FCS model is approximated with a second-degree polynomial model:

$$\hat{\dot{m}}_{\text{H}_2} = \gamma_0 + \gamma_1 \cdot P_\text{FCS} + \gamma_2 \cdot P^2_\text{FCS}. \tag{23}$$

This allows to express the fuel consumption within the prediction horizon with a quadratic formulation based on the FCS power sequence

$$\hat{m}_{\text{H}_2,k} = \gamma_0 T_\text{s} N_\text{p} + \mathbf{q}_1^\text{T} \boldsymbol{P}_{\text{FCS},k} + \boldsymbol{P}^\text{T}_{\text{FCS},k} \mathbf{Q}_2 \boldsymbol{P}_{\text{FCS},k} \tag{24}$$

with

$$\mathbf{q}_1 = \gamma_1 T_\text{s} \begin{bmatrix} 1 & 1 & \dots & 1 \end{bmatrix}^\text{T}, \qquad \mathbf{q}_1 \in \mathbb{R}^{N_\text{p} \times 1} \tag{25}$$

$$\mathbf{Q}_2 = \gamma_2 T_\text{s} \boldsymbol{I}, \qquad \mathbf{Q}_2 \in \mathbb{R}^{N_\text{p} \times N_\text{p}} \tag{26}$$

where $\boldsymbol{I}$ denotes the identity matrix.

Since the battery model is linearized at $P_{\text{b,op}} = 0\,\text{W}$, ohmic battery losses

$$P_\Omega = R_\text{int} I_\text{b}^2 \tag{27}$$

are not considered in the linear model of the MPC. Therefore, a physically motivated equivalent fuel consumption representing the ohmic battery losses is included in the objective function, which is based on a quadratic approximation. With $I_\text{b} = -Q_0 \dot{\xi}$ and the nonlinear battery model (5) follows

$$I_\text{b}^2 = \left(\frac{V_\text{OC} - \sqrt{V_\text{OC}^2 - 4 P_\text{b} R_\text{int}}}{2 R_\text{int}}\right)^2. \tag{28}$$

16370 IEEE TRANSACTIONS ON VEHICULAR TECHNOLOGY, VOL. 73, NO. 11, NOVEMBER 2024

Truncating the Taylor series of (28) at $P_{\mathrm{b,op}} = 0\,\mathrm{W}$ after the quadratic term yields

$$I_{\mathrm{b}}^2 = \frac{P_{\mathrm{b}}^2}{V_{\mathrm{OC}}^2}. \tag{29}$$

An approximation of the ohmic battery losses can then be written after inserting (29) into (27) and assuming a mean FCS efficiency $\bar{\eta}_{\mathrm{FCS}}$

$$\dot{m}_{\mathrm{eq}} = \frac{R_{\mathrm{int}}}{V_{\mathrm{OC}}^2\,\bar{\eta}_{\mathrm{FCS}}\,H_{\mathrm{i}}} P_{\mathrm{b}}^2 \tag{30}$$

where H_{i} denotes the lower heating value of hydrogen. With that, the equivalent fuel consumption representing ohmic losses within the prediction horizon can be formulated as

$$\hat{m}_{\mathrm{eq},k} = \boldsymbol{P}_{\mathrm{b},k}^{\mathrm{T}} \mathbf{Q}_{\Omega} \boldsymbol{P}_{\mathrm{b},k} \tag{31}$$

where the matrix $\mathbf{Q}_{\Omega}$ is determined by

$$\mathbf{Q}_{\Omega} = \frac{R_{\mathrm{int}}\,T_{\mathrm{s}}}{V_{\mathrm{OC}}^2\,\bar{\eta}_{\mathrm{FCS}}\,H_{\mathrm{i}}}\boldsymbol{I}, \quad \mathbf{Q}_{\Omega} \in \mathbb{R}^{N_{\mathrm{p}} \times N_{\mathrm{p}}}. \tag{32}$$

2) Cost-to-Go: The cost-to-go at the end of the prediction horizon is considered in the form of the quadratic approximation in (22).

3) Overall Objective Function: The overall quadratic objective function is the sum of (22), (24), and (31)

$$\hat{J}_k = \hat{m}_{\mathrm{H_2},k} + \hat{m}_{\mathrm{eq},k} + \hat{J}^*_{k+N_{\mathrm{p}}} \tag{33}$$

and represents the amount of fuel required to go from the current position to the intended destination.

In each instant, the linear MPC solves the optimal control problem specified in (11) whereby J_k is replaced by $\hat{J}_k$, which turns the problem into a quadratic programming problem and reduces the computational complexity significantly. Quadratic programming problems can be solved in polynomial time, i.e., the computational time is polynomial in the length of the prediction horizon [31]. In the application, the prediction horizon is relatively short because it is limited by the accuracy of the short-term prediction, which worsens with a growing horizon.

V. NUMERICAL STUDY

In this section, the performance of the proposed EMS is analyzed and compared with an SoC reference tracking MPC based on the simulation of a real-world driving cycle. The study considers a passenger vehicle equipped with a FCS with a nominal power of 55 kW and a battery with a capacity of 9.9 kWh. The steady-state measurement data of the FCS's fuel consumption rate and the approximation with the quadratic polynomial model are shown in Fig. 5. The actual fuel consumption for the driving mission is computed by interpolating in the map of measurements, whereas the offline optimization and the online MPC operate with the polynomial model. The battery parameters were identified based on measurement data resulting in $V_{\mathrm{OC}} = 350\,\mathrm{V}$, $R_{\mathrm{int}} = 0.15\,\Omega$, and $Q_0 = 28.28\,\mathrm{Ah}$. The vehicle mass is 1950 kg.

The control-relevant system constraints are $5\,\mathrm{kW} \leq P_{\mathrm{FCS}} \leq 55\,\mathrm{kW}$, $-30\,\mathrm{kW} \leq P_{\mathrm{b}} \leq 50\,\mathrm{kW}$, $0.3 \leq \xi \leq 0.9$, and the FCS power rate is constrained with $\pm 25\,\mathrm{kW/s}$. The initial SoC is 0.7

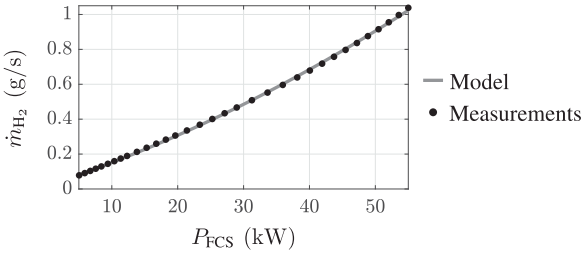

Fig. 5. Fuel consumption rate of the FCS as a function of the FCS power: steady-state measurements vs. polynomial model.

and the final SoC ≥ 0.7. The MPCs operate with a sampling time of 1 s and a prediction horizon of 30 s.

The remainder of this section is structured as follows: First, the SoC reference tracking MPC is introduced in Section V-A, followed by the description of the driving cycle and the predictions in Section V-B. The optimization based on the long-term prediction and the corresponding results are discussed in Section V-C. Finally, the performances of the MPCs are compared and evaluated in Section V-D, and the effect of the prediction horizon length is discussed in Section V-E.

A. SoC Reference Tracking MPC

The proposed cost-to-go MPC is compared with an MPC that tracks an SoC reference trajectory at the end of the prediction horizon. The linear formulation of the SoC reference tracking MPC is analogous to the formulation of the cost-to-go MPC presented in Section IV, but instead of considering the cost-to-go, the deviation from the SoC reference is penalized at the end of the prediction horizon:

$$p_{\xi,k+N_{\mathrm{p}}} = q_{\mathrm{track}} \left(\xi^{\mathrm{ref}}_{k+N_{\mathrm{p}}} - \xi_{k+N_{\mathrm{p}}} \right)^2. \tag{34}$$

Thus, the overall objective function to be minimized according to (11) is

$$J_k^{\mathrm{track}} = \hat{m}_{\mathrm{H_2},k} + \hat{m}_{\mathrm{eq},k} + p_{\xi,k+N_{\mathrm{p}}}. \tag{35}$$

The tracking weighting q_{track} is $10^3\,\mathrm{kg}$ in this study, which ensures that the SoC reference at the end of the prediction horizon is tracked sufficiently close. The remaining parameters are chosen identically as for the cost-to-go MPC.

The SoC reference is the optimal trajectory regarding the long-term prediction of the driving mission. The optimization is conducted with the DP algorithm (9), whereby the optimal control inputs $P^*_{\mathrm{FCS},l}(\xi_l)$ are stored for each position of the distance grid. After the optimization, the optimal SoC trajectory can be computed in forward direction starting at ξ_0 and linearly interpolating in the map of optimal control inputs.

B. Driving Cycle and Predictions

The velocity and altitude data of the driving cycle were recorded during a real-world drive covering 210 km, and the electric power demand was derived based on the vehicle model assuming a constant auxiliary power of 2 kW (see upper two plots of Fig. 6). The driving cycle starts and ends in urban areas

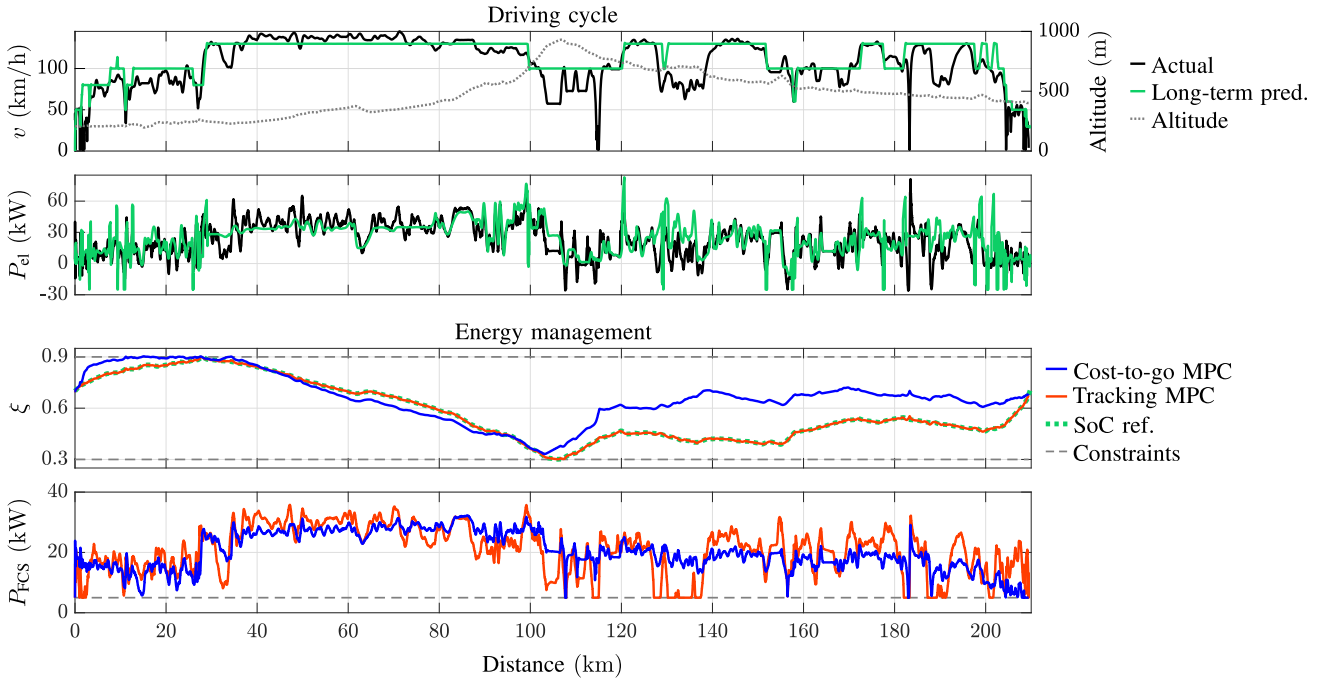

Fig. 6. Upper plots: Actual data and long-term predictions for the investigated real-world driving cycle. Lower plots: SoC and FCS power resulting from the two MPCs.

and includes rural road and highway sections. The first half of the cycle goes uphill overcoming an altitude gain of approximately 730 m. Therefore, the highway section between kilometers 30 and 100 shows a comparably high power demand.

In this study, the long-term prediction of the velocity (see Fig. 6) was retrieved from legal speed limits using *AVL Route Studio*, which is a test cycle preparation tool. The tool considers vehicle dynamics during acceleration phases and limits the cornering speed depending on the road curvature. The comparison with the actual velocity profile shows that the long-term prediction provides a good estimate of the actual velocity for a significant fraction of the driving cycle. In some sections, however, the long-term prediction deviates considerably from the actual velocity. The most obvious deviation is between kilometers 126 and 141 and was caused by roadworks on the highway.

The focus of this study is to analyze the potential of the proposed EMS and the extent to which an accurate online velocity prediction can be useful for the energy management. For this purpose, the short-term prediction is assumed to be ideal, i.e., coinciding with the actual velocity.

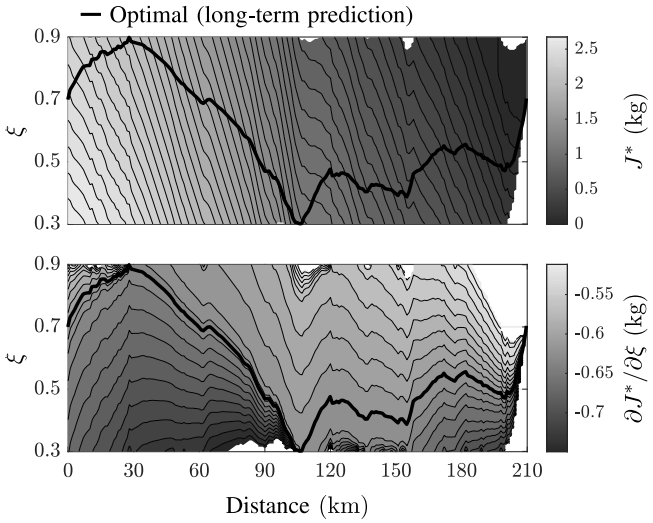

Fig. 7. Optimal cost-to-go (upper plot) and partial derivative of the optimal cost-to-go with respect to the SoC (lower plot) as a function of the position and the SoC. Both plots include the optimal SoC trajectory according to the long-term prediction. Note that extreme values are excluded in the lower plot for a better visualization.

C. *Offline Optimization*

For the offline optimization, the feasible ranges of the SoC and the FCS power are quantized with 120 and 40 grid segments, respectively, and the step size of the distance grid is chosen to be 1 km. The resulting 2-D optimal cost-to-go map depending on the position and the SoC is depicted in the upper plot of Fig. 7. It can be seen that the cost-to-go decreases with the covered distance and with an increasing SoC. White areas indicate infeasible ranges regarding the long-term prediction and the specified constraints. The plot includes the globally optimal SoC trajectory for the long-term prediction, which is used as reference trajectory for the SoC reference tracking MPC. The optimal SoC trajectory uses the whole feasible SoC range, which indicates the importance of considering state constraints in the DP.

16372 IEEE TRANSACTIONS ON VEHICULAR TECHNOLOGY, VOL. 73, NO. 11, NOVEMBER 2024

TABLE I
COMPARISON OF SPECIFIC FUEL CONSUMPTION AND EQUIVALENT NUMBER OF FCS LOAD CYCLES REGARDING THE INVESTIGATED DRIVING CYCLE

EMS	m_{fuel}	Rel. diff.	N_{eq}	Rel. diff.
Optimal	11.25 g/km	−0.3 %	14.2	+15 %
Cost-to-go MPC	11.28 g/km	0.0 %	12.4	0 %
Tracking MPC	11.32 g/km	+0.4 %	17.1	+38 %

The lower plot of Fig. 7 depicts the partial derivative of the cost-to-go with respect to the SoC. It can be shown that the derivative of the cost-to-go corresponds to the SoC-related costate in Pontryagin's minimum principle (PMP) [23]. The Hamiltonian of PMP is independent of the SoC with the chosen battery model. Consequently, the costate is constant along optimal paths within sections where no constraints are active [32]. This means that the level lines in the lower plot of Fig. 7 illustrate optimal paths for reaching the destination from any position and feasible SoC. A subset of the optimal paths meet at points where the SoC constraints are active, i.e., at the kilometers 28 and 106, causing a discontinuous change of the costate. The influence of the SoC constraints also causes the sharp changes in the slope of the $\partial J^*/\partial \xi$ profile (see lower plots of Fig. 4).

D. Performance Evaluation

The SoC and FCS power trajectories resulting from the two MPCs are depicted in the lower two plots of Fig. 6. Besides analyzing their behavior, the two MPCs are compared quantitatively based on two performance measures: the specific fuel consumption and an equivalent number of FCS load cycles [33], which is defined by

$$N_{\text{eq}} = \frac{1}{2P_{\text{FCS}}^{\max}} \int_{t_0}^{t_1} \left| \frac{\mathrm{d}P_{\text{FCS}}}{\mathrm{d}t} \right| \mathrm{d}t \tag{36}$$

and can be interpreted as a measure for degradation [34].

The SoC reference tracking MPC tracks the SoC reference at the end of the prediction horizon but can deviate from the reference within the horizon to adapt the power split according to the short-term prediction. However, the 30 s prediction horizon does not provide much freedom, and the MPC tracks the SoC reference, which is based on the long-term prediction, rather strictly. Consequently, the FCS power signal shows fluctuations depending on the deviation of the predicted power demand from the actual power demand. The fluctuating behavior stresses the FCS and affects the fuel efficiency.

Unlike the SoC tracking MPC, the proposed cost-to-go MPC is provided with optimized long-term information available for the entire SoC range and does not rely on a single reference trajectory. Thus, the cost-to-go MPC has more freedom to compensate for deviations of the long-term power demand prediction. The resulting FCS power trajectory is smoother, which improves the fuel performance and mitigates FCS degradation.

Table I compares the specific fuel consumption and the equivalent number of load cycles of the two MPCs and the overall optimal energy management minimizing the fuel consumption. For the investigated driving cycle, the cost-to-go MPC achieves a 0.4% lower fuel consumption than the SoC tracking MPC, even though the predictions are identical for both MPCs. This improvement is remarkable considering that the theoretical optimum is only 0.3% better than the result of the cost-to-go MPC. The performance advantage of the cost-to-go MPC over the SoC tracking MPC is even more impressive regarding the equivalent number of FCS load cycles, where an improvement of 38% is achieved. To sum up, the cost-to-go MPC does not only improve the fuel efficiency but also stresses the FCS considerably less, which potentially mitigates degradation. Both methods satisfy all specified constraints.

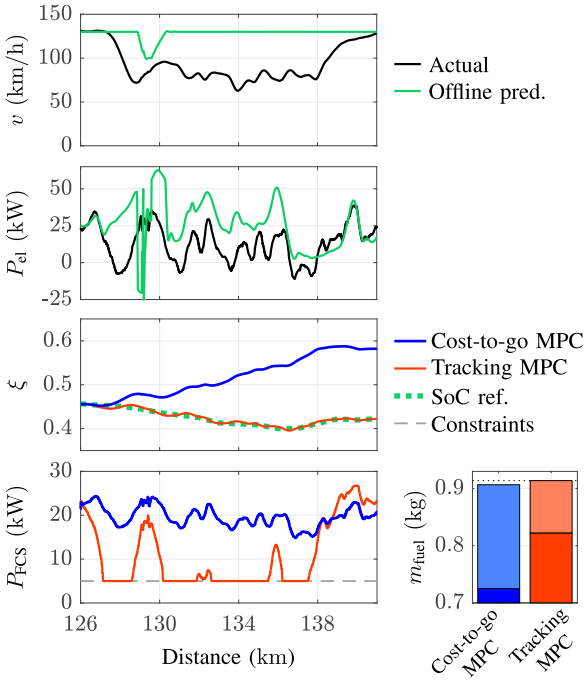

Fig. 8. Study of the two MPCs during the roadworks section, where the initial SoC is set identical for both cases. The bar chart compares the corresponding optimal costs-to-go at the end of the section (lower, dark parts), costs within the section (upper, light parts), and total costs.

The operation of the two MPCs is compared in more detail during the roadworks section between kilometers 126 and 141, where the power demand prediction based on static route data deviates considerably from the actual power demand. The comparison is shown in Fig. 8, whereby the SoC at the beginning of the section is set identical in both cases for a better illustration. The long-term prediction estimated a high power demand for the section. Therefore, the optimized SoC reference decreases meaning that the battery is expected to support the FCS. However, the actual power demand is significantly lower. The SoC tracking MPC drastically reduces the FCS power to follow the reference trajectory hitting the lower boundary on the FCS power. On the contrary, the cost-to-go MPC maintains the FCS power at a high level and even charges the battery. As the SoC rises, the cost-to-go MPC only gradually lowers the FCS power according to the optimum with the cost-to-go. Operating the FCS with a higher power implies a higher amount of fuel consumed *within* the section compared to the SoC tracking

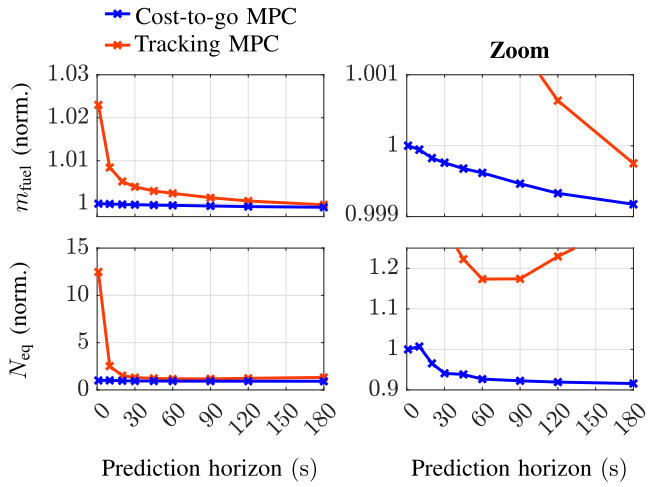

Fig. 9. Comparison of the fuel consumption and the equivalent number of FCS load cycles (both normalized) as a function of the prediction horizon length.

MPC (see upper parts of bar chart in Fig. 8). However, the cost-to-go MPC achieves a lower cost-to-go at the end of the section, which overcompensates for the higher cost within the section. Consequently, the total cost m_{fuel}, i.e., the sum of the fuel consumed within the section and the cost-to-go at the end of the section, is 7 g lower than for the SoC tracking MPC. Note that this improvement only refers to the investigated section with a length of 15 km.

E. Effect of the Prediction Horizon Length

Fig. 9 shows the comparison of the two MPCs regarding the fuel consumption and the equivalent number of FCS load cycles as a function of the prediction horizon length. The cost-to-go MPC significantly outperforms the SoC tracking MPC regarding both measures, in particular if the prediction horizon is short. For an 1-step prediction horizon, the tracking MPC has a 2.3% higher fuel consumption than the cost-to-go MPC, and the equivalent number of load cycles is even 12-fold. The tracking MPC approaches the performance of the cost-to-go MPC with an increasing prediction horizon but achieves a comparable performance only for rather long prediction horizons, where short-term predictions are expected to be less accurate.

The fuel performance of the cost-to-go MPC is already decent with an 1-step prediction horizon and improves further with growing prediction horizon. Also, the equivalent number of load cycles decreases; a 30 s prediction horizon reduces the number of load cycles by approximately 6%. The investigation indicates that the cost-to-go MPC also performs well if the prediction horizon varies throughout the driving mission, e.g., short horizons in urban areas and longer horizons on the highway.

VI. Conclusion

A predictive EMS was proposed that optimally combines a long-term prediction derived from static route information and real-time short-term predictions from vehicular communication systems. Before departure, a DP algorithm optimizes the power split between the FCS and the battery based on the long-term prediction yielding the optimal cost-to-go as a function of the position and the SoC. The online energy management is determined by an MPC that minimizes the fuel consumption considering the short-term predictions within the prediction horizon and the optimal cost-to-go as terminal cost. A linear formulation of the MPC with a physically motivated objective function was developed, which is highly beneficial for the real-time, onboard execution of the EMS.

The proposed EMS was compared with an SoC reference tracking MPC in simulation. Tracking the optimized SoC reference trajectory showed to be too restrictive to actually benefit from the short-term predictions. On the contrary, the cost-to-go MPC optimized the power split independently from the SoC based on the optimum regarding the combined long-term and short-term information. The cost-to-go MPC clearly outperformed the SoC reference tracking MPC in terms of fuel efficiency and the equivalent number of load cycles, which can be interpreted as a degradation measure, particularly if the short-term prediction horizon is short.

References

[1] S. C. De Almeida and R. Kruczan, "Effects of drivetrain hybridization on fuel economy, performance and costs of a fuel cell hybrid electric vehicle," *Int. J. Hydrogen Energy*, vol. 46, no. 79, pp. 39404–39414, 2021, doi: 10.1016/j.ijhydene.2021.09.144.

[2] P. Thounthong, V. Chunkag, P. Sethakul, B. Davat, and M. Hinaje, "Comparative study of fuel-cell vehicle hybridization with battery or supercapacitor storage device," *IEEE Trans. Veh. Technol.*, vol. 58, no. 8, pp. 3892–3904, Oct. 2009, doi: 10.1109/TVT.2009.2028571.

[3] G. G. Nassif and S. C. De Almeida, "Impact of powertrain hybridization on the performance and costs of a fuel cell electric vehicle," *Int. J. Hydrogen Energy*, vol. 45, no. 41, pp. 21722–21737, 2020, doi: 10.1016/j.ijhydene.2020.05.138.

[4] M. Koot, J. Kessels, B. De Jager, W. Heemels, P. Van Den Bosch, and M. Steinbuch, "Energy management strategies for vehicular electric power systems," *IEEE Trans. Veh. Technol.*, vol. 54, no. 3, pp. 771–782, May 2005, doi: 10.1109/TVT.2005.847211.

[5] J. Ziegmann, J. Shi, T. Schnörer, and C. Endisch, "Analysis of individual driver velocity prediction using data-driven driver models with environmental features," in *Proc. IEEE Intell. Veh. Symp.*, 2017, pp. 517–522, doi: 10.1109/IVS.2017.7995770.

[6] J. Shin and M. Sunwoo, "Vehicle speed prediction using a Markov chain with speed constraints," *IEEE Trans. Intell. Transp. Syst.*, vol. 20, no. 9, pp. 3201–3211, Sep. 2019, doi: 10.1109/TITS.2018.2877785.

[7] Z. Zhou, Z. Yang, Y. Zhang, Y. Huang, H. Chen, and Z. Yu, "A comprehensive study of speed prediction in transportation system: From vehicle to traffic," *iScience*, vol. 25, no. 3, 2022, Art. no. 103909, doi: 10.1016/j.isci.2022.103909.

[8] S. Zendegan, A. Ferrara, S. Jakubek, and C. Hametner, "Predictive battery state of charge reference generation using basic route information for optimal energy management of heavy-duty fuel cell vehicles," *IEEE Trans. Veh. Technol.*, vol. 70, no. 12, pp. 12517–12528, Dec. 2021, doi: 10.1109/TVT.2021.3121129.

[9] D. Shen, L. Lu, and S. Müller, "Utilization of predictive information to optimize driving and powertrain control of series hybrid vehicles," *Automot. Engine Technol.*, vol. 2, no. 1, pp. 39–47, 2017, doi: 10.1007/s41104-017-0016-6.

[10] S. Kelouwani, N. Henao, K. Agbossou, Y. Dube, and L. Boulon, "Two-layer energy-management architecture for a fuel cell HEV using road trip information," *IEEE Trans. Veh. Technol.*, vol. 61, no. 9, pp. 3851–3864, Nov. 2012, doi: 10.1109/TVT.2012.2214411.

[11] J. Pei, Y. Su, D. Zhang, Y. Qi, and Z. Leng, "Velocity forecasts using a combined deep learning model in hybrid electric vehicles with V2V and V2I communication," *Sci. China Technol. Sci.*, vol. 63, no. 1, pp. 55–64, 2020, doi: 10.1007/s11431-018-9396-0.

[12] W. Zhou, L. Yang, T. Ying, J. Yuan, and Y. Yang, "Velocity prediction of intelligent and connected vehicles for a traffic light distance on the urban road," *IEEE Trans. Intell. Transp. Syst.*, vol. 20, no. 11, pp. 4119–4133, Nov. 2019, doi: 10.1109/TITS.2018.2882609.

[13] Y. Li, H. He, and J. Peng, "An adaptive online prediction method with variable prediction horizon for future driving cycle of the vehicle," *IEEE Access*, vol. 6, pp. 33062–33075, 2018, doi: 10.1109/ACCESS.2018.2840536.

[14] C. Sun, S. J. Moura, X. Hu, J. K. Hedrick, and F. Sun, "Dynamic traffic feedback data enabled energy management in plug-in hybrid electric vehicles," *IEEE Trans. Control Syst. Technol.*, vol. 23, no. 3, pp. 1075–1086, May 2015, doi: 10.1109/TCST.2014.2361294.

[15] Q. Gong, Y. Li, and Z.-R. Peng, "Trip based power management of plug-in hybrid electric vehicle with two-scale dynamic programming," in *Proc. IEEE Veh. Power Propulsion Conf.*, 2007, pp. 12–19, doi: 10.1109/VPPC.2007.4544089.

[16] X. Zhang, L. Guo, N. Guo, Y. Zou, and G. Du, "Bi-level energy management of plug-in hybrid electric vehicles for fuel economy and battery lifetime with intelligent state-of-charge reference," *J. Power Sources*, vol. 481, 2021, Art. no. 228798, doi: 10.1016/j.jpowsour.2020.228798.

[17] L. Fu, Ü. Özgüner, P. Tulpule, and V. Marano, "Real-time energy management and sensitivity study for hybrid electric vehicles," in *Proc. IEEE Amer. Control Conf.*, 2011, pp. 2113–2118, doi: 10.1109/ACC.2011.5991374.

[18] V. Larsson, L. J. Mårdh, and B. Egardt, "Comparing two approaches to precompute discharge strategies for plug-in hybrid electric vehicles," *IFAC Proc. Volumes*, vol. 46, no. 21, pp. 121–126, 2013, doi: 10.3182/20130904-4-JP-2042.00114.

[19] V. Larsson, "Route optimized energy management of plug-in hybrid electric vehicles," Ph.D. dissertation, 2014. [Online]. Available: https://publications.lib.chalmers.se/records/fulltext/196399/196399.pdf

[20] L. Johannesson and B. Egardt, "A novel algorithm for predictive control of parallel hybrid powertrains based on dynamic programming," *IFAC Proc. Volumes*, vol. 40, no. 10, pp. 343–350, 2007, doi: 10.3182/20070820-3-US-2918.00047.

[21] C. Zhang and A. Vahidi, "Route preview in energy management of plug-in hybrid vehicles," *IEEE Trans. Control Syst. Technol.*, vol. 20, no. 2, pp. 546–553, Mar. 2012, doi: 10.1109/TCST.2011.2115242.

[22] S. M. Sotoudeh and B. HomChaudhuri, "Robust predictive energy management of connected power-split hybrid electric vehicles using dynamic traffic data," *J. Dyn. Syst., Meas., Control*, vol. 144, no. 1, 2022, Art. no. 014501, doi: 10.1115/1.4053291.

[23] H. Borhan, A. Vahidi, A. M. Phillips, M. L. Kuang, I. V. Kolmanovsky, and S. Di Cairano, "MPC-based energy management of a power-split hybrid electric vehicle," *IEEE Trans. Control Syst. Technol.*, vol. 20, no. 3, pp. 593–603, May 2012, doi: 10.1109/TCST.2011.2134852.

[24] D. Mayne, "Nonlinear model predictive control:Challenges and opportunities," in *Nonlinear Model Predictive Control*, F. Allgöwer and A. Zheng, Eds. Basel, Switzerland: Birkhäuser Basel, 2000, pp. 23–44, doi: 10.1007/978-3-0348-8407-5_2.

[25] L. Guzzella and A. Sciarretta, *Vehicle Propulsion Systems: Introduction to Modeling and Optimization*. Berlin, Germany: Springer 2013, doi: 10.1007/978-3-642-35913-2_2.

[26] D. E. Kirk, *Optimal Control Theory: An Introduction*. Mineola, NY, USA: Dover Publications, 2004.

[27] S. Kofler, Z. P. Du, S. Jakubek, and C. Hametner, "Adaptive step size dynamic programming for optimal energy management of fuel cell vehicles," in *Proc. IEEE Veh. Power Propulsion Conf.*, 2023, pp. 1–6, doi: 10.1109/VPPC60535.2023.10403120.

[28] F. Borrelli, A. Bemporad, and M. Morari, *Predictive Control for Linear and Hybrid Systems*. Cambridge, U.K.: Cambridge Univ. Press, 2017, doi: 10.1017/9781139061759.

[29] L. Wang, *Model Predictive Control System Design and Implementation Using MATLAB*, 1st ed. Berlin, Germany: Springer , 2009, doi: 10.1007/978-1-84882-331-0.

[30] S. Onori and L. Tribioli, "Adaptive Pontryagin's minimum principle supervisory controller design for the plug-in hybrid GM chevrolet volt," *Appl. Energy*, vol. 147, pp. 224–234, 2015, doi: 10.1016/j.apenergy.2015.01.021. [Online]. Available: https://www.sciencedirect.com/science/article/pii/S0306261915000276

[31] S. A. Vavasis, *Complexity Theory: Quadratic Programming*. Boston, MA, USA: Springer US, 2001, pp. 304–307, doi: 10.1007/0-306-48332-7_65.

[32] H. P. Geering, *Optimal Control with Engineering Applications*. Berlin, Germany: Springer, 2007, doi: 10.1007/978-3-540-69438-0.

[33] A. Ferrara, S. Jakubek, and C. Hametner, "Energy management of heavy-duty fuel cell vehicles in real-world driving scenarios: Robust design of strategies to maximize the hydrogen economy and system lifetime," *Energy Convers. Manage.*, vol. 232, 2021, Art. no. 113795, doi: 10.1016/j.enconman.2020.113795.

[34] P. Pei, Q. Chang, and T. Tang, "A quick evaluating method for automotive fuel cell lifetime," *Int. J. Hydrogen Energy*, vol. 33, no. 14, pp. 3829–3836, 2008, doi: 10.1016/j.ijhydene.2008.04.048.

Sandro Kofler (Graduate Student Member, IEEE) received the M.Sc. degree in chemical and process engineering from TU Wien, Vienna, Austria, and Universidad Politécnica de Madrid, Madrid, Spain, in 2020 and 2021, respectively. Since 2020, he has been a Project Assistant with the Institute of Mechanics and Mechatronics, TU Wien, where he is working toward the Ph.D. degree. His research focuses on modeling, control, and optimization, particularly for automotive applications.

Zhang Peng Du received the B.Sc., M.Sc., and Ph.D. degrees in mechanical engineering (management) from TU Wien, Vienna, Austria, in 2018, 2019 and 2023, respectively. From 2020 to 2024, he was a University Assistant with the Institute of Mechanics and Mechatronics, TU Wien. His research interests include nonlinear system identification, modeling, and optimization.

Stefan Jakubek received the M.Sc. degree in mechanical engineering, the Ph.D. degree in technical sciences, and the Habilitation (Professorial Qualification) degree in control theory and system dynamics from TU Wien, Vienna, Austria, in 1997, 2000 and 2007, respectively. From 2006 to 2009, he was the Head of the Development for Hybrid Powertrain Calibration and Battery Testing Technology, AVL List GmbH, Graz, Austria (automotive industry company). He is currently a Professor and Head of the Institute of Mechanics and Mechatronics, TU Wien. His research interests include fault diagnosis, nonlinear system identification, and simulation technology.

Christoph Hametner received the M.Sc. degree in mechanical engineering, the Ph.D. degree in technical sciences, and the Habilitation (Professorial Qualification) degree in control theory and system dynamics from TU Wien, Vienna, Austria, in 2005, 2007 and 2014, respectively. He is currently the Head of the Christian Doppler Laboratory for Innovative Control and Monitoring of Automotive Powertrain Systems, TU Wien. His research interests include nonlinear system identification, modeling, and control.

2.4 Publication D

Sandro Kofler, Georg Rammer, Alexander Schnabel, David Weingrill, Peter Bardosch, Stefan Jakubek, and Christoph Hametner.
Real-vehicle experimental validation of a predictive energy management strategy for fuel cell vehicles.
Journal of Power Sources, Volume 629, Number 235901, 2025.
DOI: 10.1016/j.jpowsour.2024.235901.

Contributions by the author of the dissertation[†]

- Conceptualization
- Methodology
- Software
- Validation
- Formal analysis
- Investigation
- Data curation
- Writing – original draft
- Visualization

[†]According to the Contributor Roles Taxonomy (CRediT), DOI: 10.3789/ansi.niso.z39.104-2022

Journal of Power Sources 629 (2025) 235901

Contents lists available at ScienceDirect

Journal of Power Sources

journal homepage: www.elsevier.com/locate/jpowsour

Real-vehicle experimental validation of a predictive energy management strategy for fuel cell vehicles

Sandro Kofler [a,*], Georg Rammer [b], Alexander Schnabel [b], David Weingrill [b], Peter Bardosch [b], Stefan Jakubek [a], Christoph Hametner [a]

[a] Institute of Mechanics and Mechatronics, TU Wien, Getreidemarkt 9, Vienna, 1060, Austria
[b] AVL List GmbH, Hans-List-Platz 1, Graz, 8020, Austria

HIGHLIGHTS

- Long-term predictions are used to optimize a battery SoC reference trajectory.
- Application-oriented experimental validation with a real fuel cell vehicle.
- Real driving tests on public roads affected by real-world influences such as traffic.
- Direct comparison with a nonpredictive method in reproducible dynamometer tests.
- Significant reduction in fuel consumption by 6.4 %.

ARTICLE INFO

Keywords:
Experimental validation
Fuel cell vehicle
Optimized SoC reference
Predictive energy management
Real driving test

ABSTRACT

Predictive information is highly valuable for energy management strategies (EMSs) of fuel cell vehicles. In particular, long-term predictions can significantly improve the fuel efficiency because they allow for an optimization of the energy management before departure. This potential has been demonstrated in numerous simulation studies. This work extends the literature with an extensive experimental validation of a predictive EMS that exploits route-based long-term predictions in the form of optimized reference trajectories for the battery state of charge. The experimental validation is performed with a real passenger fuel cell vehicle and strongly focuses on the real-world application where random influences such as traffic cause considerable disturbances with respect to the long-term prediction. The validation comprises two stages: First, real driving tests are repeatedly conducted on public roads, analyzing the robustness of the predictive EMS and assessing fuel efficiency gains over a nonpredictive EMS. Second, chassis dynamometer tests are performed where a selected real driving cycle is reproduced to compare the two EMSs directly. The chassis dynamometer tests confirm a significant reduction in the fuel consumption by 6.4 % compared to the nonpredictive EMS. The experimental results are analyzed quantitatively and qualitatively in detail.

1. Introduction

Fuel cell vehicles commonly have a hybrid powertrain consisting of the fuel cell system (FCS) and a battery (see Fig. 1), and the power allocation between the two power sources is determined with an energy management strategy (EMS). The EMS has a direct impact on the operating ranges of the two powertrain components and can strongly influence the fuel efficiency by avoiding inefficient operation. In addition to fuel efficiency, ensuring feasible operation is important: The requested system power must be satisfied within reasonable time, and powertrain constraints, such as constraints on the battery state of charge (SoC), must not be violated.

The optimal energy management in view of these aspects is highly specific to the power demand profile of the driving mission. Consequently, the performance of an EMS can be enhanced by considering appropriate predictive information of the driving mission. To improve the fuel efficiency by actively involving the battery in the energy management, long prediction horizons are necessary. For example, the optimal energy management for a trip including an ascent could require charging the battery already several kilometers before reaching the

* Corresponding author.
E-mail addresses: sandro.kofler@tuwien.ac.at (S. Kofler), georg.rammer@avl.com (G. Rammer), alexander.schnabel@avl.com (A. Schnabel), david.weingrill@avl.com (D. Weingrill), peter.bardosch@avl.com (P. Bardosch), stefan.jakubek@tuwien.ac.at (S. Jakubek), christoph.hametner@tuwien.ac.at (C. Hametner).

https://doi.org/10.1016/j.jpowsour.2024.235901
Received 10 September 2024; Received in revised form 10 November 2024; Accepted 18 November 2024
Available online 1 December 2024

uphill section. Long-term predictive information can be retrieved from different sources. At a basic level, long-term information can just consist of the trip length, which is often considered in predictive EMSs for plug-in hybrids to achieve an even use of battery energy throughout the driving mission [1–3]. However, the knowledge of the trip length alone does not provide information regarding the power demand profile, which is needed to optimally adapt the energy management to the driving mission. More advanced and yet simply applicable approaches consider static route information, such as the altitude profile, legal speed limits, or average segment speeds, to get long-term estimates of the power demand [4]. Even though such long-term predictions have limited accuracy, they can be highly effective for the energy management because they are available for the entire driving mission in advance. Consequently, the energy management for a planned trip can be optimized before departure, yielding predictive control information that can then be considered in the real-time EMS while driving. In the literature, optimized reference trajectories for the battery SoC have shown to be an effective way to inform the real-time EMS with the long-term prediction. Simple and yet robust strategies directly track the optimized SoC reference with basic control laws to determine the real-time power allocation between the FCS and the battery while considering powertrain constraints [5,6]. An optimization-based alternative is the adaptive equivalent consumption minimization strategy (ECMS). Here, a proportional-integral (PI) controller that tracks the SoC reference trajectory is used to determine the so-called equivalence factor, which expresses a virtual fuel consumption for using energy from the battery [7–9]. The indirect consideration of the SoC feedback combined with the continuous optimization of the equivalent fuel consumption allows for a more gradual adaption of the power allocation, which can benefit the fuel efficiency. Also, ECMS-based methods that additionally consider real-time short-term predictions while tracking the SoC reference trajectory have been developed [10–14]. Similarly, model predictive control (MPC) approaches combine short-term predictions with the long-term prediction in the form of the SoC reference while also taking into account powertrain constraints [2,15–19]. Besides SoC reference trajectories, optimized maps expressing the optimal equivalence factor or the optimal cost-to-go depending on the covered distance and SoC can be used to inform the real-time EMS with the long-term prediction. Such map-based approaches are advantageous when the long-term prediction considerably deviates because they allow the real-time EMS to continuously adapt to the actual conditions and preserve close-to-optimal fuel efficiency. EMSs based on the ECMS [20–22] and MPC [23] have been proposed to consider predictive control information in the form of optimized maps. Regardless of the approach, considering long-term power demand predictions has shown significant fuel efficiency gains over nonpredictive alternatives in simulation-based studies. However, experimental validations with real vehicles on real-world driving missions that confirm these performance benefits are not available in the literature so far.

In general, the early development and performance evaluation of EMSs, predictive and nonpredictive, happens in simulation. Simulation studies are cost and time efficient, but their outcomes deviate from reality because of modeling errors, unconsidered system behavior, and other influences. Validation with hardware-in-the-loop (HIL) testing is more realistic but found less frequently in the literature. The significance of HIL tests grows with their complexity. Simple HIL experiments only consider controller hardware to validate the real-time capability of the EMS and emulate the powertrain behavior, such as in [24–26], whereas more complex HIL setups also include small-scale powertrain components, as for example in [27–30]. Particularly HIL testing with full-scale powertrain components such as in [31–34] comes close to reality but still does not entirely cover the vehicle behavior in real-world driving.

Real driving tests with fully functional vehicles are the ultimate level of validation, but they are rare in the literature due to high cost and effort. For example, small experimental vehicles are used in real driving tests to validate nonpredictive EMSs in [35–37] and a model predictive controller considering short-term predictions in [38]. In [39–41], nonpredictive fuzzy logic strategies are demonstrated and investigated with real fuel cell trucks and buses on public roads. Similarly, extensive road tests with fuel cell buses are conducted in [42–44] to validate further nonpredictive EMSs. Whereas the real vehicle-validated strategies mentioned so far do not take into account long-term predictions, the EMS for plug-in hybrid fuel cell vehicles that was experimentally validated in [45] considers a prediction of the expected energy demand to determine the time when the FCS is turned on. To sum up, real-vehicle validations of EMSs for fuel cell vehicles in the literature were mainly conducted with buses, trucks, and small experimental vehicles and for nonpredictive strategies. In particular, EMSs exploiting long-term power demand predictions to optimize an SoC reference trajectory before departure have not been validated in real-world driving tests with real vehicles so far.

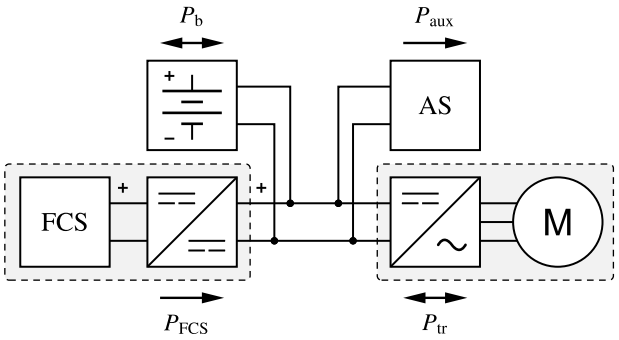

Fig. 1. Hybrid powertrain of the investigated fuel cell vehicle consisting of the FCS, battery, traction motor (M), and auxiliary systems (AS). The arrows indicate the possible directions of the power flows.
Source: The scheme is taken from [23].

The main contribution of this work is an extensive experimental validation of an EMS for fuel cell vehicles that considers a long-term prediction of the power demand to optimize SoC reference trajectories. The experimental validation is conducted with a real fuel cell vehicle and strongly focuses on real-world driving. It comprises two stages, where the performance of the predictive EMS is compared with a nonpredictive charge sustaining strategy (see Fig. 2(a)):

1. Various *real driving tests* are conducted on two routes on public roads. The real driving tests involve all random influences relevant in the actual application, such as dense traffic, traffic regulation, vehicle standstills, and varying driver behavior, which are hardly predictable over a long-term prediction horizon. In addition, the behavior of the real vehicle deviates from the prediction due to model errors. Therefore, the real driving tests evaluate the robustness of the predictive EMS against these unpredicted real-world disturbances and its feasibility regarding specified powertrain constraints. Because the power demand profile varies between individual tests due to the random influences, the performance advantage of the predictive EMS cannot be quantized directly. However, comparisons based on the equivalent fuel consumption, which takes into account differences in the battery energy and energy demand between tests, enable an indirect assessment of the fuel efficiency gains.
2. *Chassis dynamometer tests* based on measurements of a selected *real driving cycle* are conducted. Here, power demand profiles can be reproduced for multiple tests, which allows for a direct performance comparison between the predictive EMS and the nonpredictive EMS. Since the dynamometer tests are based on a real driving cycle and include the entire vehicle, the tests still cover the unpredicted real-world influences and appropriately replicate the actual application.

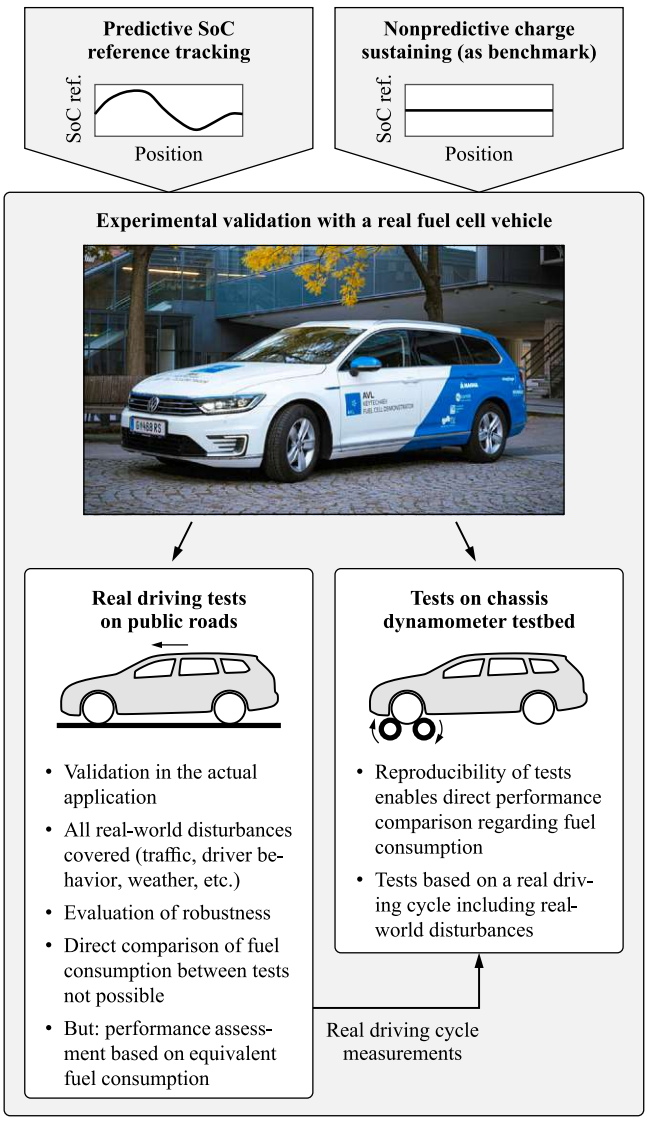

(a) Illustration of the experimental validation with a fuel cell demonstrator vehicle of AVL List GmbH.

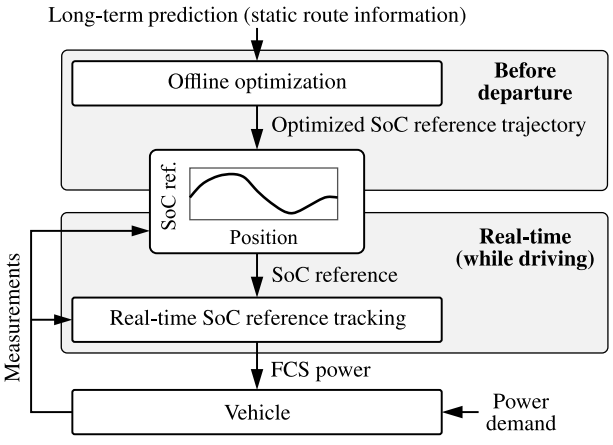

(b) Route-informed predictive SoC reference tracking.

Fig. 2. Experimental validation of predictive SoC reference tracking.

Table 1
Model parameters of the demonstrator vehicle.

Vehicle dynamics model	
Vehicle mass, m (kg)	1950
Frontal area, A_f (m^2)	2.12
Air density, ρ ($kg\,m^{-3}$)	1.204
Aerodynamic drag coefficient, c_d	0.346
Rolling friction coefficient, c_r	0.0055
Traction motor efficiency, η_m	0.87
Auxiliary power demand (estimate), P_{aux} (kW)	1
Powertrain model	
FCS idle power, P_{FCS}^{idle} (kW)	8
Max. FCS power, P_{FCS}^{max} (kW)	50
Battery energy capacity (kWh)	9.9
Battery capacity, Q_{nom} (A h)	28.28
Internal resistance, R_{int} (Ω)	0.15
Min. battery power (continuous), P_b^{min} (kW)	−20
Max. battery power (continuous), P_b^{max} (kW)	30
Min. SoC, ξ^{min}	0.2
Max. SoC, ξ^{max}	0.8

The investigated predictive EMS derives a long-term power demand prediction for a planned driving mission from easily available static route information, i.e., the altitude profile and legal speed limits. Based on the long-term prediction and a control-oriented vehicle model, a distance-based reference trajectory for the battery SoC is optimized before departure (see Fig. 2(b)). While driving, a simple real-time controller tracks the optimized SoC reference trajectory to determine the real-time power split between the FCS and the battery. The simple real-time EMS is chosen for the validation to assess the baseline for performance improvements by considering route-based power demand predictions, which might even be exceeded with more advanced methods. Moreover, the low computational complexity and robustness of the investigated EMS make it an interesting candidate for an immediate industrial application. To ensure a fair comparison, the nonpredictive charge sustaining strategy used as a benchmark is based on the same tracking controller as the proposed predictive SoC reference tracking but considers a constant SoC reference.

The remainder of this article is structured as follows. First, the fuel cell vehicle used for the validation and the control-oriented vehicle modeling are described in Section 2. Then, the predictive SoC reference tracking strategy is introduced in Section 3. In Section 4, the computation of the equivalent fuel consumption is described, which is the basis for the quantitative evaluation of the fuel efficiency. The experimental validation of the predictive SoC reference tracking based on real driving tests and dynamometer tests is presented in Section 5. A conclusion in Section 6 finalizes this article.

2. Fuel cell vehicle and control-oriented modeling

The predictive EMS investigated in this work is evaluated and compared with the nonpredictive strategy in experiments with a fuel cell demonstrator vehicle of AVL List GmbH. The demonstrator vehicle, which is shown in Fig. 2(a), is based on a Volkswagen Passat GTE and equipped with an FCS with a nominal power of 50 kW and a battery with a nominal energy capacity of 9.9 kWh.

To conduct the offline optimization of the SoC reference trajectory before departure, appropriate models of the vehicle components are required. First, a model of the vehicle longitudinal dynamics is used to derive a prediction of the power demand for the entire driving mission from static route information, i.e., the altitude profile and legal speed limits. Second, a model of the hybrid powertrain is used to optimize the energy management for the predicted power demand. To keep the computational complexity of the offline optimization low, simplified and control-oriented models are used. Nevertheless, the simplified modeling

does not affect the performance of the predictive concept because the accuracy of the long-term power demand prediction is limited in any case. In the following, the vehicle dynamics model is described first before the powertrain model is introduced.

2.1. Vehicle dynamics for power demand prediction

To estimate the power demand for the entire driving mission based on the speed limits and the altitude profile along the route, a model of the longitudinal vehicle dynamics is used. The model considers the traction force, aerodynamic drag, rolling resistance, and the gravitational force

$$m\frac{\mathrm{d}v}{\mathrm{d}t} = \eta_{\mathrm{m}}^{\operatorname{sgn} P_{\mathrm{tr}}}\frac{P_{\mathrm{tr}}}{v} - \frac{\rho A_{\mathrm{f}} c_{\mathrm{d}}}{2}v^2 - c_{\mathrm{r}} mg\cos\theta - mg\sin\theta \tag{1}$$

where m denotes the vehicle mass, v the velocity, t the time, η_{m} the traction motor efficiency, P_{tr} the traction motor power, ρ the air density, A_{f} the frontal area of the vehicle, c_{d} the aerodynamic drag coefficient, c_{r} the rolling friction coefficient, g the gravitational acceleration, and θ the road inclination angle, which can be derived from the altitude profile. The parameters are assumed to be known and summarized in the upper part of Table 1. Based on the model of the longitudinal vehicle dynamics, a prediction of the traction motor power can be derived from the speed limits and the inclination angle along the route. Here, system power constraints are considered to prevent infeasible power demands during velocity transients and uphill sections. Additionally, the vehicle velocity is saturated depending on the road curvature to prevent infeasible cornering speeds, which improves the prediction quality particularly in urban and mountainous areas.

The prediction of the overall electric power demand P_{el} can then be computed with

$$P_{\mathrm{el}} = P_{\mathrm{tr}} + P_{\mathrm{aux}} \tag{2}$$

where P_{aux} denotes the power demand of the auxiliary systems. The variation of the auxiliary power demand is hardly predictable over long-term prediction horizons, and its magnitude is relatively small compared to the traction power demand. Therefore, a constant estimate of the auxiliary power demand serves as a sufficient approximation for the prediction. The prediction of the overall power demand is the input for the offline optimization of the energy management before departure.

2.2. Powertrain model for offline optimization

The offline optimization of the SoC reference trajectory before departure is based on a model of the powertrain, which consists of the FCS and the battery (see Fig. 1). The sum of the FCS power P_{FCS} and battery power P_{b} satisfies the overall electric power demand

$$P_{\mathrm{el}} = P_{\mathrm{FCS}} + P_{\mathrm{b}} \tag{3}$$

whereby the power split between the two power sources is determined by the EMS and, therefore, the variable to be optimized. To provide the optimized SoC reference trajectory for the real-time energy management shortly after the route was determined, the offline optimization must be fast, i.e., its computational complexity must be low. Therefore, the two power sources are described with simplified, quasistatic models focusing on the characteristics relevant for the long-term optimization. Note that a consideration of more detailed power source dynamics would not necessarily improve the overall performance because the accuracy of the long-term prediction is limited and certain deviations due to real-world influences are expected.

The FCS is considered with a quadratic polynomial model describing the fuel consumption rate $\dot{m}_{\mathrm{FCS}}(P_{\mathrm{FCS}})$ as a function of the FCS power, where the compressor power demand is implicitly taken into account. In this study, the fuel consumption curve was identified based on tank measurements, which include purging losses, considering measurements of several real-world driving missions. The fuel consumption

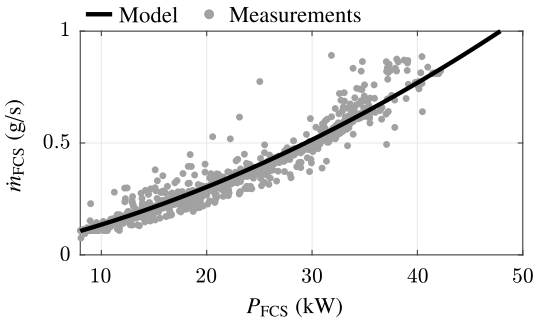

(a) Fuel consumption curve of the FCS. The $\dot{m}_{\mathrm{FCS}}$ measurements are estimated based on the measured current.

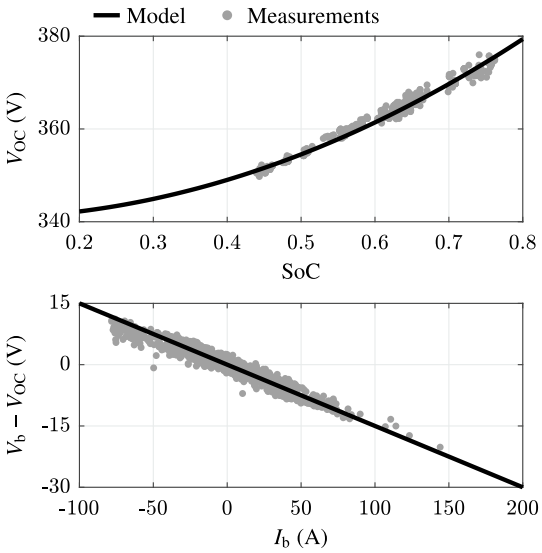

(b) Equivalent circuit model of the battery. The V_{OC} measurements in the upper plot are approximated with the measured battery voltage under small loads.

Fig. 3. Identified FCS model and battery model compared to sets of measurements.

curve is compared to a set of measurements in Fig. 3(a). The measurements deviate from the model within a certain range due to the neglected system dynamics and other influences. However, the model sufficiently describes the characteristic of the fuel consumption rate for the offline optimization based on the long-term prediction. To mitigate FCS degradation, the FCS is only operated between the idle power limit $P_{\mathrm{FCS}}^{\mathrm{idle}}$ and the maximum power limit $P_{\mathrm{FCS}}^{\mathrm{max}}$ when active. If the power request is low, the EMS can put the FCS into a stopmode where the fuel consumption rate is zero but FCS-related auxiliaries including the compressor remain active. Because the auxiliaries are not shut down, frequent switching between active operation and stopmode is possible without restrictions. The FCS power in stopmode is assumed to be zero, i.e., the electric load of the auxiliaries is neglected.

The battery behavior is approximated with an equivalent circuit model considering ohmic losses where the battery voltage V_{b} linearly depends on the battery current I_{b}:

$$V_{\mathrm{b}} = V_{\mathrm{OC}}(\xi) - R_{\mathrm{int}} I_{\mathrm{b}}. \tag{4}$$

Here, the open-circuit voltage V_{OC} varies depending on the battery SoC ξ, which is described with a quadratic polynomial, whereas the ohmic resistance R_{int} is assumed constant. In this study, the battery model was identified based on battery voltage and current measurements of several real-world driving missions. Despite the simplification, the battery fits the measurements well, as shown in Fig. 3(b). With the

equivalent circuit model, the dynamics of the battery SoC can be described as a nonlinear function of the battery power P_b with

$$\dot{\xi} = -\frac{V_\mathrm{OC} - \sqrt{V_\mathrm{OC}^2 - 4P_\mathrm{b}R_\mathrm{int}}}{2Q_\mathrm{nom}R_\mathrm{int}} \tag{5}$$

where the battery capacity Q_nom is assumed to be known. The powertrain model parameters of the demonstrator vehicle are summarized in the lower part of Table 1.

3. Predictive SoC reference tracking

The goal of the predictive EMS is to improve the fuel efficiency and ensure feasible operation by considering a long-term prediction of the driving mission that is based on easily available static route information, i.e., the altitude profile and legal speed limits. Therefore, the basic assumptions of the predictive approach are that the route is determined before departure and the mentioned static route information is accessible, e.g., through map services or the onboard navigation system. Although this kind of prediction has limited accuracy, it has shown to be highly effective for optimizing the energy management because it covers the entire driving mission and, thus, provides the long prediction horizon necessary to actively involve the battery in the energy management. Moreover, the route-based prediction is available before departure so that the predictive EMS can be divided into two stages (see Fig. 2(b)):

1. In the *offline optimization* before departure, the energy management is optimized based on the long-term power demand prediction, yielding an optimized, distance-based SoC reference trajectory. The optimization can be conducted either onboard, if the required computational resources are available, or on a cloud computing server.
2. The onboard *real-time energy management* determines the setpoint for the FCS power by tracking the optimized SoC reference trajectory considering the actual power demand and system constraints.

The significant advantage of the two-stage approach is that the real-time control can be realized with a computationally simple tracking controller because the predictive information is already processed before departure. In the following, the two stages are described in more detail.

3.1. Offline optimization before departure

To optimize the SoC reference trajectory for the planned driving mission before departure, a long-term power demand prediction is needed. The power demand prediction is derived from the altitude profile and speed limits along the route based on the vehicle dynamics model as described in Section 2.1. Due to the limited accuracy of the long-term prediction, a relatively rough discretization interval can be chosen for the offline optimization, which allows for a considerable acceleration of the optimization without affecting the overall performance of the predictive EMS. For this purpose, the power demand prediction is segmented with

$$P_{\mathrm{el},l} = \frac{\int_{t_l}^{t_{l+1}} P_\mathrm{el}\,\mathrm{d}t}{\Delta t_l} \tag{6}$$

for all $l = 1 \dots (L-1)$ before the offline optimization, where Δt_l denotes the time spent in the lth segment and $(L-1)$ is the number of segments.

The objective is to minimize the fuel consumption, which is specified in discrete-time form assuming a zero-order hold for the power demand, the FCS power, and the battery power

$$\begin{aligned} \min J = &\sum_{l=1}^{L-1} \dot{m}_\mathrm{FCS}(P_{\mathrm{FCS},l})\Delta t_l \\ \text{s.t.}\quad &\xi_1 = \xi_\mathrm{init} \\ &\xi_L \geq \xi_\mathrm{end} \\ &\xi^\mathrm{min} \leq \xi_l \leq \xi^\mathrm{max} \\ &P_\mathrm{b}^\mathrm{min} \leq P_{\mathrm{b},l} \leq P_\mathrm{b}^\mathrm{max} \\ &P_{\mathrm{FCS},l} \in \mathcal{U} \end{aligned} \tag{7}$$

where the feasible FCS power range $\mathcal{U}$ includes the stopmode

$$\mathcal{U} = \left\{ P \in \mathbb{R} : P_\mathrm{FCS}^\mathrm{idle} \leq P \leq P_\mathrm{FCS}^\mathrm{max} \vee P = 0\,\mathrm{W} \right\} \tag{8}$$

and ξ_init denotes the initial SoC, ξ_end the minimum SoC at the end of the driving mission, ξ^min the minimum SoC, and ξ^max the maximum SoC. The minimum battery power $P_\mathrm{b}^\mathrm{min}$ and maximum battery power $P_\mathrm{b}^\mathrm{max}$ are chosen conservatively according to the continuous charging and discharging current specifications of the battery to ensure feasibility of the SoC reference.

In this study, the optimal control problem is solved with dynamic programming (DP), which is a dynamic optimization method [46]. The significant advantage of DP over methods based on Pontryagin's minimum principle, a common alternative for solving optimal energy management problems, is that all specified constraints including the SoC constraints can be considered directly. Thanks to the simplified powertrain modeling, the problem includes only one state (ξ) and one control input (P_FCS). Together with the rough discretization intervals, the low dimension of the problem results in a low computational complexity, which ensures that the optimization results can be provided shortly after the route was determined. More details regarding the DP implementation for the present problem can be found in the literature, e.g., [20,23].

The output of the offline optimization is the optimized SoC reference trajectory. To limit the effects of unpredicted velocity deviations and vehicle standstills on the predictive energy management, the SoC reference trajectory $\xi^\mathrm{ref}(s)$ is specified in the distance-domain, i.e., as function of the position s along the route and not as a function of time. Consequently, unpredicted variations in the driving time that have occurred in the past do not affect the optimality of the SoC reference trajectory for the trip remainder.

3.2. Real-time SoC reference tracking

The real-time EMS determines the FCS power setpoint based on a computationally simple controller that tracks the optimized reference trajectory while driving. The position along the driving mission, which is required to access the current SoC reference value, is determined by measuring the covered distance. In this study, the real-time SoC reference tracking strategy extends an already implemented nonpredictive charge sustaining controller with a PI controller considering the deviation from the optimized SoC reference $\Delta\xi = (\xi^\mathrm{ref}(s) - \xi)$ at the current position:

$$P_\mathrm{FCS}^\mathrm{track} = k_\mathrm{P}\Delta\xi + k_\mathrm{I}\int_0^t \Delta\xi\,\mathrm{d}\tau + P_\mathrm{FCS}^\mathrm{NP}(P_\mathrm{el}, \xi). \tag{9}$$

Here, $P_\mathrm{FCS}^\mathrm{track}$ denotes the FCS power according to the tracking controller and $P_\mathrm{FCS}^\mathrm{NP}(P_\mathrm{el}, \xi)$ the nonpredictive component, which is described by a 2-D map depending on the measured power demand and SoC. The nonpredictive component, which was tuned and tested based on expert knowledge, is included to ensure reliable operation where the power demand is robustly satisfied within reasonable time in any situation. Because the SoC reference is optimized based on the power demand prediction, which is expected to deviate from the actual power demand to some extent, the PI controller gains k_P and k_I are chosen such that certain freedom for deviation from the SoC reference is provided to adapt to the unpredicted disturbances.

To prevent infeasible power requests from the FCS, the FCS power resulting from the tracking controller is saturated within the feasible power range determined by the constraints on the FCS power, FCS power increments, and battery power, which yields the FCS power setpoint $P_{\mathrm{FCS}}^{\mathrm{setp}}$:

$$\begin{aligned} P_{\mathrm{FCS}}^{\mathrm{setp}} = \min_{P_{\mathrm{FCS}}} \left| P_{\mathrm{FCS}}^{\mathrm{track}} - P_{\mathrm{FCS}} \right| + q_{\mathrm{s}} s \\ \text{s.t.} \quad 0\,\mathrm{W} \le P_{\mathrm{FCS}} \le P_{\mathrm{FCS}}^{\mathrm{max}} \\ \Delta P_{\mathrm{FCS}}^{\mathrm{min}} \le P_{\mathrm{FCS}} - P_{\mathrm{FCS}}^{\mathrm{prev}} \le \Delta P_{\mathrm{FCS}}^{\mathrm{max}} \\ \bar{P}_{\mathrm{b}}^{\mathrm{min}} - s \le P_{\mathrm{el}} - P_{\mathrm{FCS}} \le \bar{P}_{\mathrm{b}}^{\mathrm{max}} + s. \end{aligned} \tag{10}$$

Here, $P_{\mathrm{FCS}}^{\mathrm{prev}}$ denotes the FCS power in the previous instance, and $\Delta P_{\mathrm{FCS}}^{\mathrm{min}}$ and $\Delta P_{\mathrm{FCS}}^{\mathrm{max}}$ are the minimum and maximum FCS power increments per time step, respectively. The battery power constraints $\bar{P}_{\mathrm{b}}^{\mathrm{min}}$ and $\bar{P}_{\mathrm{b}}^{\mathrm{max}}$ adapt according to the battery management system in real time and are considered as soft constraints to avoid infeasibility. For this purpose, a slack variable $s \ge 0$ and a weighting coefficient $q_{\mathrm{s}} > 1$ are used. Note that the problem in Eq. (10) can be solved efficiently with a series of logical operations, see [3]. The constraints on the battery SoC are implicitly considered by tracking the optimized SoC reference trajectory.

If the resulting FCS power setpoint is considerably lower than the idle power limit, the real-time EMS puts the FCS into the stopmode where the fuel supply is stopped:

$$P_{\mathrm{FCS}} = \begin{cases} \min(P_{\mathrm{FCS}}^{\mathrm{setp}}, P_{\mathrm{FCS}}^{\mathrm{idle}}), & \text{if } P_{\mathrm{FCS}}^{\mathrm{setp}} \ge P_{\mathrm{FCS}}^{\mathrm{thr}} \\ 0\,\mathrm{W}, & \text{otherwise.} \end{cases} \tag{11}$$

Here, the power threshold $P_{\mathrm{FCS}}^{\mathrm{thr}}$ is a tuning parameter. Because FCS-related auxiliaries such as the compressor remain active in stopmode, a fast switch to active operation is possible at any time.

4. Evaluation of fuel consumption

The predictive SoC reference tracking is compared with a nonpredictive method in experiments with the real fuel cell vehicle in Section 5. The experiments include real driving tests on public roads, where variations in the power demand are inevitable due to numerous real-world influences, such as traffic, driver behavior, and weather. But also in the subsequently conducted dynamometer tests, the power demand varies within certain tolerances. Moreover, the final battery SoC generally differs from the initial SoC depending on the power demand profile because both EMSs must ensure freedom for deviation from the SoC reference to adapt to unpredicted disturbances. Consequently, the net energy contribution of the battery varies between different tests.

To allow for a performance comparison despite these variations, the experimental results are evaluated based on the equivalent fuel consumption m_{eq} that takes into account corrections for variations in the battery energy contribution Δm_{b} and the traction motor energy Δm_{tr}:

$$m_{\mathrm{eq}}(t) = m_{\mathrm{H_2}}(t) + \Delta m_{\mathrm{b}}(t) + \Delta m_{\mathrm{tr}}(t). \tag{12}$$

Here, the actual fuel consumption $m_{\mathrm{H_2}}$ is computed based on tank measurements and, thus, includes purging losses.

The correction for the battery energy is based on the deviation of the SoC from the initial SoC considering the open-circuit voltage model

$$\Delta m_{\mathrm{b}}(t) = -\frac{Q_{\mathrm{nom}}}{H_{\mathrm{i}} \bar{\eta}_{\mathrm{FCS}}} \int_{\xi_{\mathrm{init}}}^{\xi(t)} V_{\mathrm{OC}}(\xi)\,\mathrm{d}\xi \tag{13}$$

where $H_{\mathrm{i}} = 120\,\mathrm{MJ\,kg^{-1}}$ denotes the lower heating value of hydrogen. The mean FCS efficiency

$$\bar{\eta}_{\mathrm{FCS}} = \frac{\int_0^{t_{\mathrm{end}}} P_{\mathrm{FCS}}\,\mathrm{d}t}{H_{\mathrm{i}} m_{\mathrm{H_2}}} \tag{14}$$

is computed individually for each test because it strongly varies depending on the EMS.

The power demand correction takes into account variations in the traction motor power with respect to a reference test. Variations in the power demand of the auxiliaries are not considered because they depend on the EMS. This means that, for example, an increased fuel consumption due to higher cooling power demands is *not* corrected. For the dynamometer tests, where the driving times are identical, the power demand correction can be evaluated continuously over time with

$$\Delta m_{\mathrm{tr}}(t) = \frac{\int_0^t P_{\mathrm{tr}}(\tau) - P_{\mathrm{tr,ref}}(\tau)\,\mathrm{d}\tau}{H_{\mathrm{i}} \bar{\eta}_{\mathrm{FCS}}} \tag{15}$$

where $P_{\mathrm{tr,ref}}$ denotes the traction motor power of the reference test. For the real driving tests, the driving time varies depending on traffic. Therefore, the correction is only computed for the entire test with

$$\Delta m_{\mathrm{tr}} = \frac{E_{\mathrm{tr}} - E_{\mathrm{tr,ref}}}{H_{\mathrm{i}} \bar{\eta}_{\mathrm{FCS}}} \tag{16}$$

where E_{tr} and $E_{\mathrm{tr,ref}}$ denote the traction energies of the entire test and reference test, respectively.

5. Experimental results

The predictive SoC reference tracking is evaluated and compared with a nonpredictive EMS in experiments with the real fuel cell passenger vehicle. The nonpredictive EMS is a charge sustaining strategy that maintains the SoC around a constant reference value of 0.6. The nonpredictive charge sustaining is based on the same real-time tracking controller as the predictive SoC reference tracking, which allows for a fair evaluation of the fuel efficiency gains by considering route-based long-term predictions.

To ensure an application-oriented validation of the predictive EMS, the experimental evaluation puts a strong emphasis on real-world driving. Unlike synthetic driving cycles, real-world driving is affected by various random influences, such as traffic, traffic regulation, driver behavior, and weather, which cause considerable deviations from the long-term velocity prediction including vehicle standstills with varying standstill times. The experimental validation is based on two types of tests:

- *Real driving tests* were conducted on predetermined routes on public roads including urban, rural, and freeway driving. These tests are influenced by varying traffic conditions and vehicle standstills, which have an impact on the total driving time. The tests are therefore particularly interesting for analyzing the robustness of the predictive EMS against unpredicted disturbances in the real-world application.
- *Dynamometer tests* were carried out based on a *selected real driving cycle* on a chassis dynamometer testbed. In contrast to the real driving tests conducted on public roads, traction power demand profiles can be reproduced multiple times on the dynamometer testbed, which enables a direct comparison between the two EMSs and drawing more significant conclusions regarding the benefit of the predictive EMS on the fuel efficiency. Also in the dynamometer tests, the real driving cycle covers real-world disturbances including vehicle standstills, which are not considered in the speed limit-based prediction. In addition, dynamometer tests based on the "Worldwide Harmonized Light-Duty Vehicles Test Cycle" (WLTC), a standard cycle widely used in the literature, were conducted.

All tests started and ended with an SoC close to 0.6, and the small differences between the initial and the final SoC are considered in the quantitative evaluation based on the equivalent fuel consumption as described in Section 4.

The predictive strategy considers route-based predictive information, i.e., the altitude profile along the route and a speed limit-based

prediction of the velocity, to conduct the offline optimization before departure. In this work, both pieces of information were obtained from *AVL Route Studio*, a test cycle preparation tool. The tool considers longitudinal vehicle dynamics during transients and limits the velocity depending on the road curvature. In this way, feasible long-term velocity predictions can be generated conveniently for testing purposes.

In the following, the real driving tests are presented first, focusing on quantitative results. Then, the dynamometer tests are discussed, where the qualitative differences in the energy management of the two EMSs are analyzed in addition to a quantitative evaluation.

5.1. Real driving tests

The real driving tests were conducted on two different routes on public roads, which are labeled "route A" and "route B" in the following. The two routes represent day-to-day driving missions such as commuting and include shares of urban, rural, and freeway driving. On both predetermined routes, tests were repeated several times with the predictive SoC reference tracking and the nonpredictive charge sustaining. The covered distance, the altitude profile, the speed limits, and the speed limit-based prediction of the individual tests on a route are identical, whereas the velocity profile and, thus, the power demand profile and the total driving time vary because of real-world influences, such as traffic, traffic regulation, driver behavior, and weather. These influences also cause vehicle standstills with varying standstill times. The primary objective of the real driving tests is the experimental validation of the robustness of the predictive SoC reference tracking in the actual application, where unpredicted disturbances caused by the real-world influences are inevitable. For this purpose, the performance advantage over the nonpredictive EMS is assessed based on the equivalent fuel consumption. Moreover, the quality of the long-term velocity predictions is assessed with plots comparing the measured and predicted velocity profiles over distance. The distance-based plots do not reflect the effects of velocity deviations on the driving time, which is meaningful for the assessment because the predictive EMS compensates for these effects by using a distance-based SoC reference trajectory.

5.1.1. Real driving tests on route A

Route A has a length of 26 km and includes rural and urban roads. The altitude profile and the speed limit-based velocity prediction of route A are shown in Figs. 4(a) and 4(b), respectively. Based on this information, the long-term power demand prediction for the driving mission was derived, and the energy management was optimized (also see Fig. 4(a)). The optimized SoC trajectory, which is used as reference for the predictive SoC reference tracking, plans that the battery supports the FCS in the high-power uphill section and is recharged in the subsequent downhill section. In this way, the FCS is operated close to the idle power limit, where the FCS efficiency peaks, unless the power demand significantly exceeds the maximum continuous battery power limit of 30 kW.

Seven real driving tests, which are labeled A1 to A7, were performed on route A. Their measured velocity signals are compared to the long-term velocity prediction in Fig. 4(b). The speed limit-based prediction provides a good estimate but inevitably deviates because of traffic influences, particularly in the final urban part, where several stops were required.

To evaluate the potential of the predictive EMS under these varying disturbances, the route was driven twice with the nonpredictive charge sustaining (tests A1 and A2) and five times with the predictive SoC reference tracking (tests A3 to A7). The quantitative results are presented in Table 2a and 2b. The strong influence of traffic is reflected in the cumulated standstill time, which varies between 3.7 and 12.2 min and affects the total driving time. The fuel efficiency of the individual tests is evaluated based on the equivalent fuel consumption, which takes into account corrections for deviations in the traction energy and the final

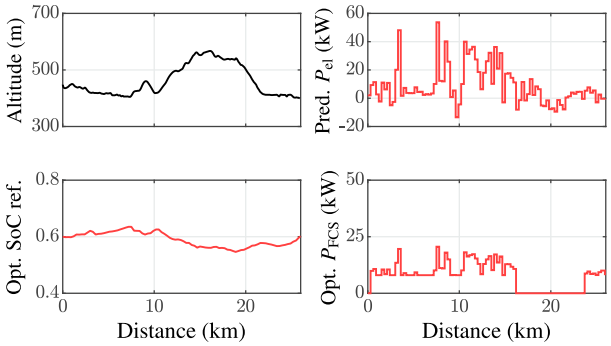

(a) Altitude profile and long-term prediction of the electric power demand of route A (upper plots) and the results of the offline optimization: optimized SoC reference trajectory and the corresponding FCS power (lower plots).

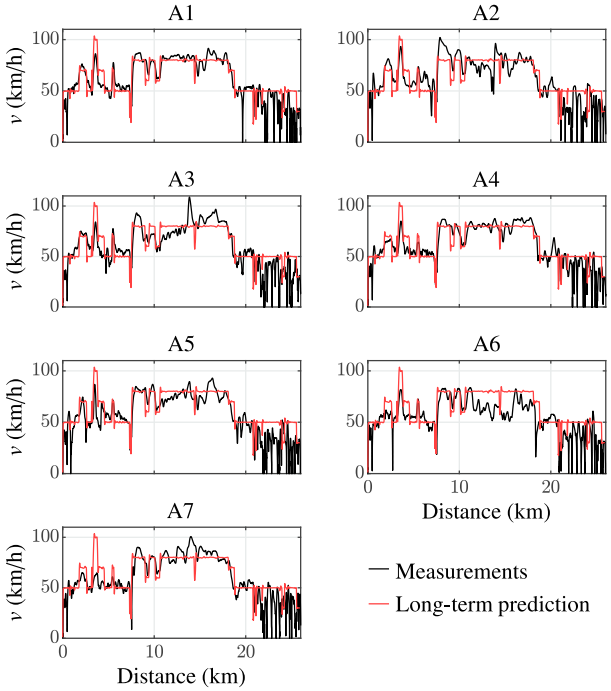

(b) Velocity measurements of the seven real driving tests compared to the speed limit-based velocity prediction of route A.

Fig. 4. Real driving tests on route A.

SoC. The two tests that applied the nonpredictive charge sustaining strategy (tests A1 and A2) showed an identical performance with an equivalent fuel consumption of 0.242 kg. Compared to this result, all tests using the predictive SoC reference tracking showed a reduced equivalent fuel consumption with improvements ranging from 0.4 % to 7.4 %. On average, the predictive SoC reference tracking yielded a considerable improvement of 4.6 %. The measurements indicate that this improvement results from an increase in the mean FCS efficiency thanks to the predictive information. Regarding the effect of the EMS on ohmic battery losses, no clear statement is possible. Feasible operation was ensured, i.e., the power demand was satisfied without violating powertrain constraints, in all tests.

Remarkably, the considerable improvements in the fuel efficiency were achieved with a rather small amplitude in the SoC reference trajectory for this route. This indicates that the results could also be achieved with a considerably smaller battery capacity.

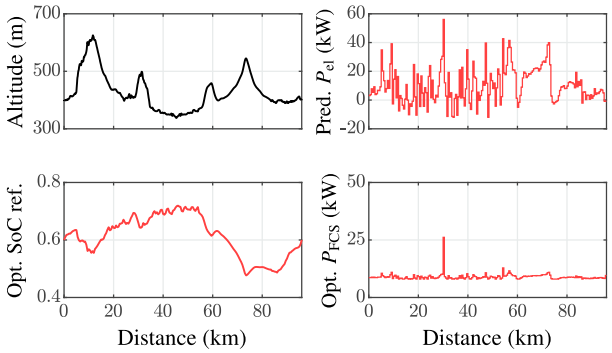

(a) Altitude profile and long-term prediction of the electric power demand of route B (upper plots) and the results of the offline optimization: optimized SoC reference trajectory and the corresponding FCS power (lower plots).

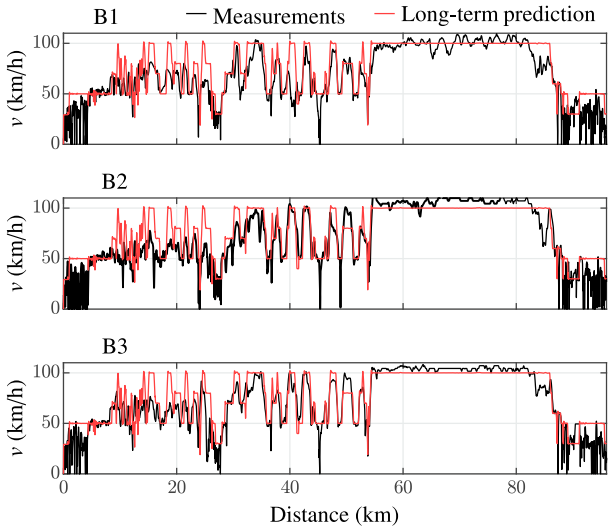

(b) Velocity measurements of the three real driving tests compared to the speed limit-based velocity prediction of route B.

Fig. 5. Real driving tests on route B.

5.1.2. Real driving tests on route B

Three tests were conducted on route B, which has a length of 96 km and covers urban, rural, and freeway driving. The route-based long-term prediction, the results of the prediction-based offline optimization, and the comparison between the predicted and the measured velocities of the three tests are shown in Fig. 5. Again, the long-term velocity prediction gives a good estimate but shows traffic-induced deviations, particularly in the urban parts of the route. Similar to the optimization outcome for route A, the optimal energy management for the predicted power demand plans a rather steady operation of the FCS in the low-power range, where the FCS efficiency is high. Consequently, most of the dynamic share of the predicted power demand is covered by the battery, which can be seen in optimized SoC profile. Due to the longer distance and the higher changes in altitude compared to route A, the optimized SoC profile shows a considerably higher amplitude here.

The first test (B1) was performed with the nonpredictive charge sustaining, and the other two tests (B2 and B3) applied the predictive SoC reference tracking. The results are presented in Table 2c. Both B2 and B3 show a considerable reduction in the equivalent fuel consumption

Table 2
Results of the real driving tests comparing the two EMSs: nonpredictive charge sustaining (CS) vs. predictive SoC reference tracking (SoC RT).

(a) Real driving tests on route A.

	A1	A2	A3	A4
EMS	**CS**	**CS**	**SoC RT**	**SoC RT**
Traction energy (kWh)	3.44	3.42	3.28	3.32
Total driving time (min)	36.7	43.5	35.8	35.3
Standstill time (min)	4.7	12.2	3.7	4.4
m_{eq} (kg)	**0.242**	**0.242**	**0.228**	**0.23**
Relative difference	**0%**	**0%**	**−5.8%**	**−5%**
Mean FCS efficiency	49.1%	49.5%	51.7%	50.8%
Battery losses (kWh)	0.061	0.088	0.069	0.046

(b) Real driving tests on route A (continuation).

	A5	A6	A7
EMS	**SoC RT**	**SoC RT**	**SoC RT**
Traction energy (kWh)	3.2	3.31	3.38
Total driving time (min)	38.7	39.8	39.1
Standstill time (min)	4.7	5.3	6.7
m_{eq} (kg)	**0.224**	**0.231**	**0.241**
Relative difference	**−7.4%**	**−4.5%**	**−0.4%**
Mean FCS efficiency	52.4%	51.4%	50.4%
Battery losses (kWh)	0.057	0.044	0.057

(c) Real driving tests on route B.

	B1	B2	B3
EMS	**CS**	**SoC RT**	**SoC RT**
Traction energy (kWh)	12.09	13.88	11.96
Total driving time (min)	120.7	120.8	112.4
Standstill time (min)	13.8	13.7	8.5
m_{eq} (kg)	**0.811**	**0.767**	**0.782**
Relative difference	**0%**	**−5.4%**	**−3.6%**
Mean FCS efficiency	51.4%	55%	55%
Battery losses (kWh)	0.163	0.262	0.25

with respect to the test applying the nonpredictive EMS with improvements of 5.4 % and 3.6 %, respectively. On average, the equivalent fuel consumption was reduced by 4.5 %. The predictive strategy caused an increase in the ohmic battery losses due to the enhanced battery use. However, the mean FCS efficiency was improved significantly from 51.4 % for the nonpredictive EMS to 55 % for the predictive strategy, which overcompensated for the increased battery losses and resulted in the significantly higher fuel efficiency. Also, feasible operation was ensured in all tests.

5.1.3. Summary of real driving tests

The evaluation based on the equivalent fuel consumption validated the robustness of the predictive SoC reference tracking for the real-world application. Even though the tests were affected by considerable disturbances with respect to the speed limit-based long-term prediction, the results of the real driving tests indicate that the predictive SoC reference tracking performs significantly better than the nonpredictive charge sustaining with average reductions in the equivalent fuel consumption of 4.6 % on route A and 4.5 % on route B. The analysis of the results also indicates that the improved fuel economy is achieved by an increase in the mean FCS efficiency, whereas influences of ohmic battery losses are less relevant.

However, the variances in the velocity and power demand profiles and the standstill times of the real driving tests do not allow for a direct comparison between the predictive SoC reference tracking and the nonpredictive charge sustaining. Therefore, dynamometer tests were conducted based on a selected real driving cycle, which are presented in the following.

5.2. Dynamometer tests

To draw more significant conclusions regarding improvements in the fuel efficiency and compare the two EMSs also qualitatively, tests were performed on the chassis dynamometer testbed, where velocity and traction power profiles can be reproduced within certain tolerances. The dynamometer tests are based on the velocity measurements of a selected real driving cycle, namely B3. Therefore, the dynamometer tests cover the significant disturbances with respect to the speed limit-based prediction that were experienced in the corresponding real driving test including vehicle standstills. Moreover, the chassis dynamometer tests involve the entire vehicle, and thus, influences of the auxiliary systems and the drivetrain are also included. In addition to the dynamometer tests based on the real driving cycle, tests based on the standard WLTC were conducted. The results are described below.

5.2.1. Dynamometer tests based on the real driving cycle

The altitude profile, velocity profile, and traction power profile of the real driving cycle B3 are shown in Fig. 6(a). The driving cycle covers urban, rural, and freeway driving and includes substantial changes in altitude, which dominate the traction power profile. The influence of the altitude profile on the traction power is particularly evident on the freeway section between 55 km and 85 km. Besides measurements, Fig. 6(a) also includes the speed limit-based velocity prediction, which considers the vehicle dynamics during transients and limits the velocity depending on the road curvature. As already discussed for the real driving tests, the long-term velocity prediction gives a good estimate of the actual velocity but inevitably deviates due to real-world influences. Particularly in the urban parts at the beginning and the end of the driving cycle, the actual velocity is affected by numerous unpredicted vehicle stops and dense traffic. Nevertheless, the long-term traction power prediction, which is derived from the predicted velocity and the altitude profile, provides a good estimate of the measured power demand except for fast dynamics, i.e., spikes in the measured traction power, which are strongly influenced by the unpredicted disturbances. Based on the power demand prediction, the energy management was optimized.

The result of the offline optimization and the comparison of the predictive SoC reference tracking and the nonpredictive charge sustaining are shown in Fig. 6(b). The optimal energy management regarding the prediction aims at operating the FCS closely to the idle power limit, where the FCS efficiency peaks, but also shows a slight power-following behavior, which reduces ohmic battery losses. Consequently, the optimized SoC reference is clearly influenced by the changes in altitude and the implicated variations in the traction power. The optimized SoC reference basically plans to charge the battery in the low-power sections of the driving cycle, e.g., during descents, and discharge the battery in the high-power sections, e.g., in the uphill freeway section starting at 55 km.

Not considering this predictive information, the charge sustaining strategy maintains the SoC around a constant reference of 0.6. Although the controller provides certain freedom for deviation from the constant reference, the charge sustaining strategy shows a clear power-following behavior, i.e., the FCS power follows the power demand. Thus, the FCS is operated in the low-power range frequently entering the stopmode in the low-power sections of the cycle and must satisfy high power requests during the high-power sections, particularly in the uphill freeway section starting at 55 km.

Unlike the charge sustaining strategy, the predictive SoC reference tracking strategy tracks the optimized SoC reference trajectory. Even though the measured FCS power of the predictive SoC reference tracking deviates from the offline solution due to the unpredicted real-world influences, the SoC follows the reference trajectory adequately. Compared to the nonpredictive strategy, the predictive SoC reference tracking requests more power from the FCS in the low-power sections of the cycle and charges the battery in this way. In return, the battery actively supports the FCS in the high-power sections of the cycle, which avoids operating the FCS in its inefficient high-power range.

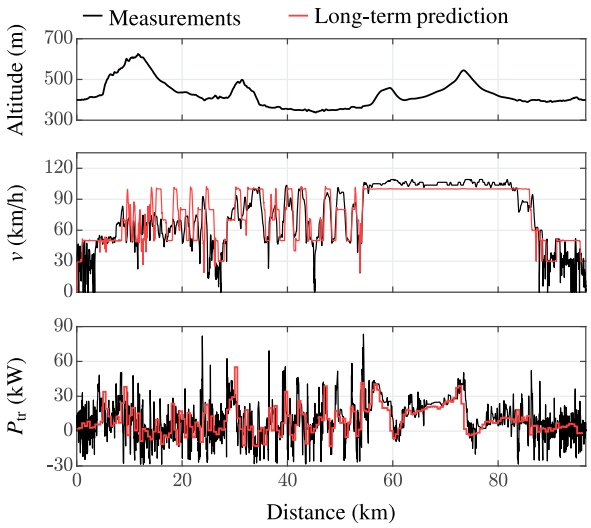

(a) Altitude, velocity, and traction motor power of the real driving cycle compared to the speed limit-based prediction.

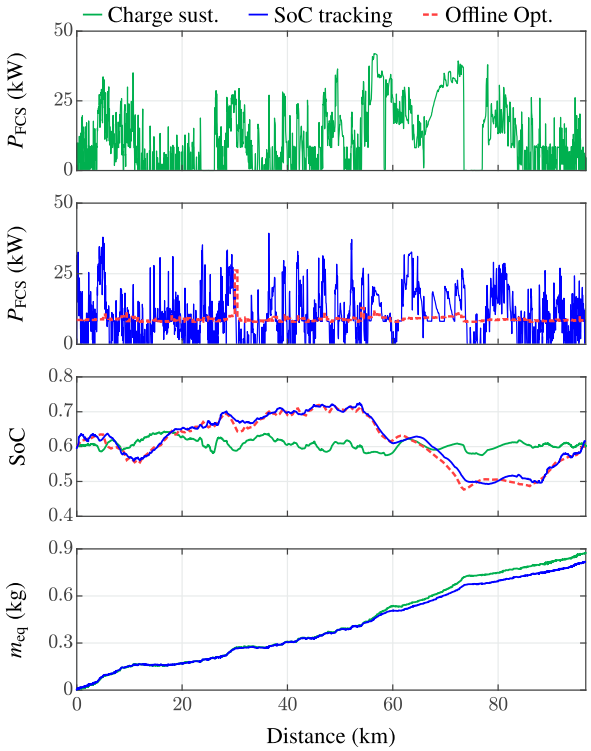

(b) Comparison of the nonpredictive charge sustaining strategy and the predictive SoC reference tracking. Additionally, the results of the offline optimization are shown.

Fig. 6. Dynamometer tests based on the real driving cycle B3.

The effects of the two EMSs on the fuel efficiency are visually compared based on the equivalent fuel consumption, which takes into account the energy stored in the battery and is also shown in Fig. 6(b). Remarkably, the time courses of the equivalent fuel consumption of the two EMSs are almost identical in the initial 55 km of the driving cycle, indicating that potentially higher battery losses due to the increased battery use of the predictive SoC reference tracking are inconsiderable.

Table 3
Results of the dynamometer tests comparing the nonpredictive charge sustaining with the predictive SoC reference tracking.

(a) Real driving cycle B3.		
	Charge sustaining	**SoC tracking**
Traction energy (kWh)	12.93	12.8
m_{eq} (kg)	**0.874**	**0.818**
Relative difference	**0%**	**−6.4%**
Mean FCS efficiency	50.1%	54.2%
Battery losses (kWh)	0.217	0.234

(b) WLTC.		
	Charge sustaining	**SoC tracking**
Traction energy (kWh)	3.46	3.45
m_{eq} (kg)	**0.225**	**0.218**
Relative difference	**0%**	**−3.1%**
Mean FCS efficiency	51.8%	53.1%
Battery losses (kWh)	0.057	0.062

However, a significant gap between the equivalent consumption trajectories of the two strategies opens up during the high-power uphill sections on the freeway starting around 55 km, where the predictive SoC reference tracking successfully avoids the inefficient high-power FCS range.

The quantitative results are summarized in Table 3a and confirm these findings. The predictive SoC reference tracking reduces the equivalent fuel consumption by remarkable 6.4 % with respect to the nonpredictive charge sustaining. The dynamometer tests confirm that the reduction in the fuel consumption is based on an improvement in the mean FCS efficiency, which is significantly increased from 50.1 % for the charge sustaining strategy to 54.2 % for the predictive SoC reference tracking strategy. Compared to the nonpredictive strategy, the predictive SoC reference tracking produces higher ohmic battery losses because of the enhanced battery use, but this increase is of minor significance regarding the overall fuel efficiency, as already observed in the real driving tests. The outcomes confirm that long-term predictions derived from easily available static route information are highly effective for improving the fuel efficiency although their prediction quality is limited due to real-world disturbances. Also, the effectiveness of the simple and easily implementable real-time SoC reference tracking controller is confirmed.

5.2.2. *Dynamometer tests based on the WLTC*

The WLTC is a standard cycle for determining fuel consumption and emission levels. As such, the WLTC is a widely used test cycle in the literature, which is why it is interesting to evaluate the performance benefit of the predictive SoC reference tracking for the WLTC. However, one must keep in mind that the official test procedure does not consider the use of predictions, and thus, the WLTC tests are hypothetical tests here. Since speed limits are also not specified for the WLTC, the actual velocity reference for the dynamometer testbed is considered as theoretical velocity prediction (see Fig. 7(a)). However, vehicle standstills are considered unpredictable and therefore *not* represented in the prediction. Because the WLTC does not consider changes in altitude, this dynamometer test also investigates the potential of the predictive EMS for driving missions where the traction power profile is dominated by the velocity.

The close-to-ideal prediction offers the possibility to evaluate the accuracy of the long-term power demand prediction based on the vehicle dynamics. The predicted traction motor power estimates the measured traction motor power well (see Fig. 7(a)), confirming the suitability of the vehicle model. Only fast dynamics, i.e., the spikes in the measured traction motor power, are not represented due to the segmentation of the prediction for the offline optimization. However,

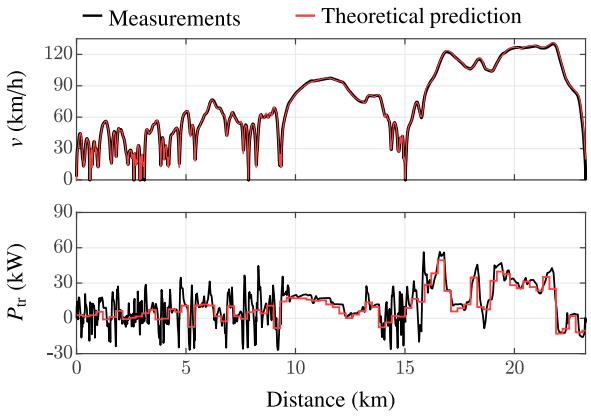

(a) Velocity and traction motor power of the WLTC. The velocity prediction coincides with the actual velocity, which is a theoretical test case.

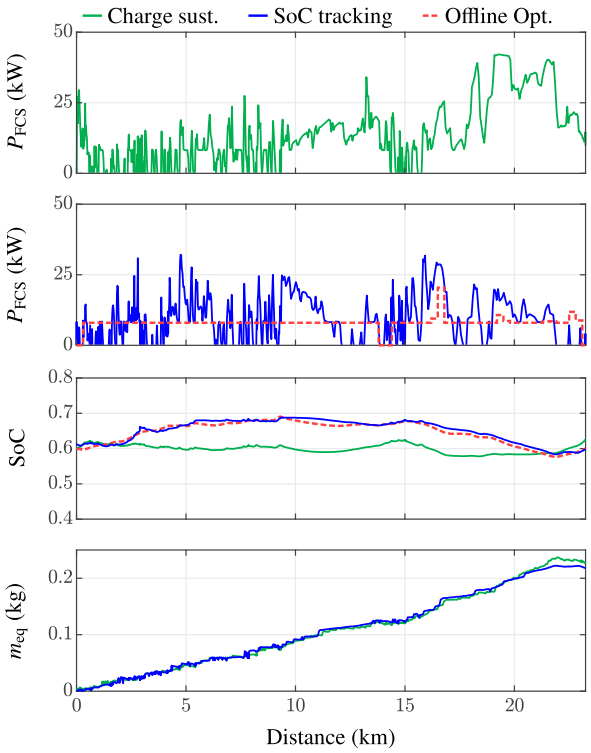

(b) Comparison of the nonpredictive charge sustaining strategy and the predictive SoC reference tracking. Additionally, the results of the offline optimization are shown.

Fig. 7. Dynamometer tests based on the WLTC.

this segmentation error does not limit the performance of the predictive concept because the real-time SoC tracking controller ensures enough freedom to deviate from the SoC reference optimized based on the prediction. Also, power demand spikes are assumed to be almost unpredictable in the real-world application.

The result of the offline optimization and the comparison of the two EMSs are shown in Fig. 7(b). Because of the relatively low mean power demand of the WLTC, the solution of the optimization indicates to operate the FCS mainly at the idle power limit. The corresponding SoC profile, which is used as reference for the predictive SoC reference tracking, basically plans to charge the battery in the initial low-power part of the cycle and discharge the battery in the final high-power part.

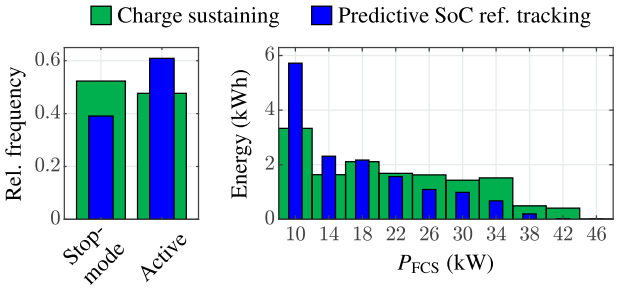

(a) Dynamometer test based on the real driving cycle B3.

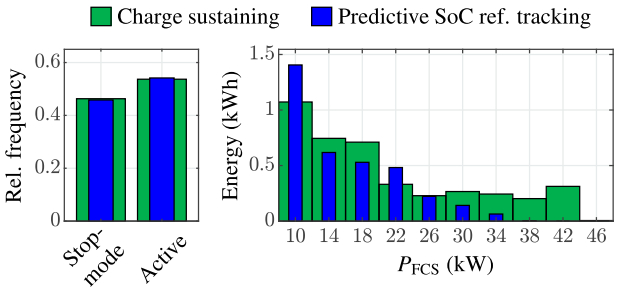

(b) Dynamometer test based on the WLTC.

Fig. 8. Effects of the EMSs on the FCS operation: relative shares of the FCS operation modes (left plots) and the energy-weighted FCS power distribution (right plots).

The qualitative differences between the nonpredictive charge sustaining and the predictive SoC reference tracking are similar to the differences observed in the test based on the real driving cycle. Tracking the optimized SoC reference, the predictive SoC reference tracking considerably reduces high-power FCS operation compared to the charge sustaining strategy thanks to the active use of the battery, particularly in the final high-power section starting around 18 km. This is also where a significant difference in the equivalent fuel consumption graphs arises. Note that the equivalent fuel consumption decreases at the end of the test cycles because the battery is charged through regenerative breaking.

The quantitative results are summarized in Table 3b. The predictive SoC reference tracking strategy decreases the equivalent fuel consumption by 3.1 % with respect to the nonpredictive strategy. This result is notable and indicates that the predictive EMS can also bring significant improvements for driving missions without changes in altitude. The improvement again results from an increase in the mean FCS efficiency.

5.2.3. Analysis of the FCS power distribution

The effect of the predictive EMS on the FCS operation is analyzed in Fig. 8 for the two dynamometer tests. The histograms illustrate the energy-weighed FCS power distribution and confirm the aforementioned findings. Compared to the charge sustaining strategy, the predictive SoC reference tracking strategy shifts energy provided by high-power operation to low-power operation in both tests. Particularly the operation in the FCS power range just above the idle power limit, where the efficiency peaks, is significantly increased with the predictive EMS. For the dynamometer test based on the real driving cycle, the predictive SoC reference tracking also considerably reduces the time spent in the stopmode, which is beneficial because the mean FCS power in active operation is decreased in this way.

6. Conclusions

This work experimentally validated an easily implementable predictive EMS considering a long-term prediction derived from static route information to optimize a distance-based SoC reference trajectory before departure. Extensive experiments were conducted with a real fuel cell passenger vehicle on public roads and on a chassis dynamometer testbed. The real driving tests on public roads proofed the robustness of the predictive SoC reference tracking strategy in real driving situations affected by unpredicted disturbances such as varying traffic. Moreover, the real driving tests indicated a considerable reduction in the fuel consumption compared to a nonpredictive charge sustaining strategy with an average reduction of around 4.5 %. Reproducible dynamometer tests based on a selected real driving cycle, which included real-world traffic influences and vehicle standstills, confirmed these findings: Although these disturbances were not considered in the prediction, the predictive SoC reference tracking reduced the fuel consumption by remarkable 6.4 % compared to the nonpredictive charge sustaining. This result confirmed that simple, route-based long-term predictions are highly effective for improving the fuel efficiency in the real-world application, even though their accuracy is limited due to unpredictable random influences. Additionally, dynamometer tests based on the WLTC revealed a reduction in the fuel consumption by 3.1 % compared to the nonpredictive EMS. This result indicated that the predictive EMS can also improve the fuel efficiency for driving missions without changes in altitude. Finally, a detailed qualitative evaluation showed that the significant improvements arose by avoiding high FCS power ranges, which considerably increased the mean FCS efficiency.

CRediT authorship contribution statement

Sandro Kofler: Writing – original draft, Visualization, Validation, Software, Methodology, Investigation, Formal analysis, Data curation, Conceptualization. **Georg Rammer:** Software. **Alexander Schnabel:** Investigation, Data curation. **David Weingrill:** Investigation. **Peter Bardosch:** Supervision, Resources, Project administration, Funding acquisition. **Stefan Jakubek:** Writing – review & editing, Funding acquisition. **Christoph Hametner:** Writing – review & editing, Supervision, Project administration, Funding acquisition, Conceptualization.

Declaration of competing interest

The authors declare that they have no known competing financial interests or personal relationships that could have appeared to influence the work reported in this paper.

Acknowledgments

This work was supported with funds from the Climate and Energy Fund, Austria and implemented in line with the “Zero Emission Mobility” Program [grant numbers 878123, 885044]. The authors acknowledge the TU Wien Bibliothek for financial support through its Open Access Funding Program.

Data availability

The authors do not have permission to share data.

References

[1] X. Lin, Y. Xia, W. Huang, H. Li, Trip distance adaptive power prediction control strategy optimization for a plug-in fuel cell electric vehicle, Energy 224 (2021) 120232, http://dx.doi.org/10.1016/j.energy.2021.120232.
[2] Y. Liu, J. Li, Z. Chen, D. Qin, Y. Zhang, Research on a multi-objective hierarchical prediction energy management strategy for range extended fuel cell vehicles, J. Power Sources 429 (2019) 55–66, http://dx.doi.org/10.1016/j.jpowsour.2019.04.118.
[3] B. Geng, J.K. Mills, D. Sun, Two-stage energy management control of fuel cell plug-in hybrid electric vehicles considering fuel cell longevity, IEEE Trans. Veh. Technol. 61 (2) (2012) 498–508, http://dx.doi.org/10.1109/TVT.2011.2177483.

[4] Y. Zhou, A. Ravey, M.-C. Péra, A survey on driving prediction techniques for predictive energy management of plug-in hybrid electric vehicles, J. Power Sources 412 (2019) 480–495, http://dx.doi.org/10.1016/j.jpowsour.2018.11.085.

[5] S. Zendegan, A. Ferrara, S. Jakubek, C. Hametner, Predictive battery state of charge reference generation using basic route information for optimal energy management of heavy-duty fuel cell vehicles, IEEE Trans. Veh. Technol. 70 (12) (2021) 12517–12528, http://dx.doi.org/10.1109/TVT.2021.3121129.

[6] A. Ferrara, S. Jakubek, C. Hametner, Energy management of heavy-duty fuel cell vehicles in real-world driving scenarios: Robust design of strategies to maximize the hydrogen economy and system lifetime, Energy Convers. Manage. 232 (2021) 113795, http://dx.doi.org/10.1016/j.enconman.2020.113795.

[7] S. Gao, Y. Zong, F. Ju, Q. Wang, W. Huo, L. Wang, T. Wang, Scenario-oriented adaptive ECMS using speed prediction for fuel cell vehicles in real-world driving, Energy 304 (2024) 132028, http://dx.doi.org/10.1016/j.energy.2024.132028.

[8] H. Gao, Z. Wang, S. Yin, J. Lu, Z. Guo, W. Ma, Adaptive real-time optimal energy management strategy based on equivalent factors optimization for hybrid fuel cell system, Int. J. Hydrog. Energy 46 (5) (2021) 4329–4338, http://dx.doi.org/10.1016/j.ijhydene.2020.10.205.

[9] T. van Keulen, B. de Jager, A. Serrarens, M. Steinbuch, Optimal energy management in hybrid electric trucks using route information, Oil Gas Sci. Technol. – Rev. IFP 65 (1) (2010) 103–113, http://dx.doi.org/10.2516/ogst/2009026.

[10] M. Piras, V. De Bellis, E. Malfi, J.M. Desantes, R. Novella, M. Lopez-Juarez, Incorporating speed forecasting and SOC planning into predictive ecms for heavy-duty fuel cell vehicles, Int. J. Hydrog. Energy 55 (2024) 1405–1421, http://dx.doi.org/10.1016/j.ijhydene.2023.11.250.

[11] T. Zeng, C. Zhang, Y. Zhang, C. Deng, D. Hao, Z. Zhu, H. Ran, D. Cao, Optimization-oriented adaptive equivalent consumption minimization strategy based on short-term demand power prediction for fuel cell hybrid vehicle, Energy 227 (2021) 120305, http://dx.doi.org/10.1016/j.energy.2021.120305.

[12] D. Chen, Y. Kim, A.G. Stefanopoulou, Predictive equivalent consumption minimization strategy with segmented traffic information, IEEE Trans. Veh. Technol. 69 (12) (2020) 14377–14390, http://dx.doi.org/10.1109/TVT.2020.3034552.

[13] F. Zhang, K. Xu, C. Zhou, S. Han, H. Pang, Y. Cui, Predictive equivalent consumption minimization strategy for hybrid electric vehicles, in: 2019 IEEE Vehicle Power and Propulsion Conference, VPPC, 2019, pp. 1–5, http://dx.doi.org/10.1109/VPPC46532.2019.8952549.

[14] X. Li, Y. Wang, D. Yang, Z. Chen, Adaptive energy management strategy for fuel cell/battery hybrid vehicles using pontryagin's minimal principle, J. Power Sources 440 (2019) 227105, http://dx.doi.org/10.1016/j.jpowsour.2019.227105.

[15] X. Lin, X. Xu, H. Lin, Predictive-ECMS based degradation protective control strategy for a fuel cell hybrid electric vehicle considering uphill condition, eTransportation 12 (2022) 100168, http://dx.doi.org/10.1016/j.etran.2022.100168.

[16] D.F. Pereira, F.d.C. Lopes, E.H. Watanabe, Nonlinear model predictive control for the energy management of fuel cell hybrid electric vehicles in real time, IEEE Trans. Ind. Electron. 68 (4) (2021) 3213–3223, http://dx.doi.org/10.1109/TIE.2020.2979528.

[17] X. Zhang, L. Guo, N. Guo, Y. Zou, G. Du, Bi-level energy management of plug-in hybrid electric vehicles for fuel economy and battery lifetime with intelligent state-of-charge reference, J. Power Sources 481 (2021) 228798, http://dx.doi.org/10.1016/j.jpowsour.2020.228798.

[18] Y. Zhou, H. Li, A. Ravey, M.-C. Péra, An integrated predictive energy management for light-duty range-extended plug-in fuel cell electric vehicle, J. Power Sources 451 (2020) 227780, http://dx.doi.org/10.1016/j.jpowsour.2020.227780.

[19] G. Li, J. Zhang, H. He, Battery SOC constraint comparison for predictive energy management of plug-in hybrid electric bus, Appl. Energy 194 (2017) 578–587, http://dx.doi.org/10.1016/j.apenergy.2016.09.071.

[20] S. Kofler, S. Jakubek, C. Hametner, Cost-to-go-based predictive equivalent consumption minimization strategy for fuel cell vehicles considering route information, in: 2024 IEEE Intelligent Vehicles Symposium, IV, 2024, pp. 2910–2916, http://dx.doi.org/10.1109/IV55156.2024.10588715.

[21] S. Kofler, S. Jakubek, C. Hametner, Predictive energy management strategy with optimal stack start/stop control for fuel cell vehicles, Appl. Energy 377 (2025) 124513, http://dx.doi.org/10.1016/j.apenergy.2024.124513.

[22] C. Zhang, A. Vahidi, Route preview in energy management of plug-in hybrid vehicles, IEEE Trans. Control Syst. Technol. 20 (2) (2012) 546–553, http://dx.doi.org/10.1109/TCST.2011.2115242.

[23] S. Kofler, Z.P. Du, S. Jakubek, C. Hametner, Predictive energy management strategy for fuel cell vehicles combining long-term and short-term forecasts, IEEE Trans. Veh. Technol. (2024) 1–11, http://dx.doi.org/10.1109/TVT.2024.3424422.

[24] W. Zou, J. Li, Q. Yang, X. Wan, Y. He, H. Lan, A real-time energy management approach with fuel cell and battery competition-synergy control for the fuel cell vehicle, Appl. Energy 334 (2023) 120667, http://dx.doi.org/10.1016/j.apenergy.2023.120667.

[25] S. Quan, Y.-X. Wang, X. Xiao, H. He, F. Sun, Real-time energy management for fuel cell electric vehicle using speed prediction-based model predictive control considering performance degradation, Appl. Energy 304 (2021) 117845, http://dx.doi.org/10.1016/j.apenergy.2021.117845.

[26] Z. Sun, Y. Wang, Z. Chen, Coordination control strategy for PEM fuel cell system considering vehicle velocity prediction information, eTransportation 18 (2023) 100287, http://dx.doi.org/10.1016/j.etran.2023.100287.

[27] M. Kandidayeni, A.O. Macias Fernandez, A. Khalatbarisoltani, L. Boulon, S. Kelouwani, H. Chaoui, An online energy management strategy for a fuel cell/battery vehicle considering the driving pattern and performance drift impacts, IEEE Trans. Veh. Technol. 68 (12) (2019) 11427–11438, http://dx.doi.org/10.1109/TVT.2019.2936713.

[28] C. Jia, W. Qiao, J. Cui, L. Qu, Adaptive model-predictive-control-based real-time energy management of fuel cell hybrid electric vehicles, IEEE Trans. Power Electron. 38 (2) (2023) 2681–2694, http://dx.doi.org/10.1109/TPEL.2022.3214782.

[29] H. Chen, J. Chen, H. Lu, C. Yan, Z. Liu, A modified MPC-based optimal strategy of power management for fuel cell hybrid vehicles, IEEE/ASME Trans. Mechatronics 25 (4) (2020) 2009–2018, http://dx.doi.org/10.1109/TMECH.2020.2993811.

[30] D. Zhou, A. Al-Durra, F. Gao, A. Ravey, I. Matraji, M. Godoy Simões, Online energy management strategy of fuel cell hybrid electric vehicles based on data fusion approach, J. Power Sources 366 (2017) 278–291, http://dx.doi.org/10.1016/j.jpowsour.2017.08.107.

[31] C. Varlese, A. Ferrara, C. Hametner, P. Hofmann, Experimental validation of a predictive energy management strategy for agricultural fuel cell electric tractors, Int. J. Hydrog. Energy 77 (2024) 1–14, http://dx.doi.org/10.1016/j.ijhydene.2024.06.097.

[32] K. Deng, H. Peng, S. Dirkes, J. Gottschalk, C. Ünlübayir, A. Thul, L. Löwenstein, S. Pischinger, K. Hameyer, An adaptive PMP-based model predictive energy management strategy for fuel cell hybrid railway vehicles, eTransportation 7 (2021) 100094, http://dx.doi.org/10.1016/j.etran.2020.100094.

[33] H. Peng, Z. Chen, K. Deng, S. Dirkes, C. Ünlübayir, A. Thul, L. Löwenstein, D.U. Sauer, S. Pischinger, K. Hameyer, A comparison of various universally applicable power distribution strategies for fuel cell hybrid trains utilizing component modeling at different levels of detail: From simulation to test bench measurement, eTransportation 9 (2021) 100120, http://dx.doi.org/10.1016/j.etran.2021.100120.

[34] A. Ravey, B. Blunier, A. Miraoui, Control strategies for fuel-cell-based hybrid electric vehicles: From offline to online and experimental results, IEEE Trans. Veh. Technol. 61 (6) (2012) 2452–2457, http://dx.doi.org/10.1109/TVT.2012.2198680.

[35] Y. Zhang, R. Ma, D. Zhao, Y. Huangfu, W. Liu, A novel energy management strategy based on dual reward function Q-learning for fuel cell hybrid electric vehicle, IEEE Trans. Ind. Electron. 69 (2) (2022) 1537–1547, http://dx.doi.org/10.1109/TIE.2021.3062273.

[36] J. Chen, C. Xu, C. Wu, W. Xu, Adaptive fuzzy logic control of fuel-cell-battery hybrid systems for electric vehicles, IEEE Trans. Ind. Inform. 14 (1) (2018) 292–300, http://dx.doi.org/10.1109/TII.2016.2618886.

[37] G. Şefkat, M.A. Özel, Experimental and numerical study of energy and thermal management system for a hydrogen fuel cell-battery hybrid electric vehicle, Energy 238 (2022) 121794, http://dx.doi.org/10.1016/j.energy.2021.121794.

[38] M. Sellali, A. Ravey, A. Betka, A. Kouzou, M. Benbouzid, A. Djerdir, R. Kennel, M. Abdelrahem, Multi-objective optimization-based health-conscious predictive energy management strategy for fuel cell hybrid electric vehicles, Energies 15 (4) (2022) http://dx.doi.org/10.3390/en15041318.

[39] D. Gao, Z. Jin, Q. Lu, Energy management strategy based on fuzzy logic for a fuel cell hybrid bus, J. Power Sources 185 (1) (2008) 311–317, http://dx.doi.org/10.1016/j.jpowsour.2008.06.083.

[40] X. Li, L. Xu, J. Hua, X. Lin, J. Li, M. Ouyang, Power management strategy for vehicular-applied hybrid fuel cell/battery power system, J. Power Sources 191 (2) (2009) 542–549, http://dx.doi.org/10.1016/j.jpowsour.2009.01.092.

[41] C. Geng, S. Mei, L. Liu, W. Ma, Q. Xue, Simulation and experimental research on energy management control strategy for fuel cell heavy-duty truck, Int. J. Hydrog. Energy 69 (2024) 1305–1318, http://dx.doi.org/10.1016/j.ijhydene.2024.05.081.

[42] Z. Hu, J. Li, L. Xu, Z. Song, C. Fang, M. Ouyang, G. Dou, G. Kou, Multi-objective energy management optimization and parameter sizing for proton exchange membrane hybrid fuel cell vehicles, Energy Convers. Manage. 129 (2016) 108–121, http://dx.doi.org/10.1016/j.enconman.2016.09.082.

[43] L. Xu, J. Li, M. Ouyang, Energy flow modeling and real-time control design basing on mean values for maximizing driving mileage of a fuel cell bus, Int. J. Hydrog. Energy 40 (43) (2015) 15052–15066, http://dx.doi.org/10.1016/j.ijhydene.2015.08.104.

[44] L. Xu, J. Li, J. Hua, X. Li, M. Ouyang, Adaptive supervisory control strategy of a fuel cell/battery-powered city bus, J. Power Sources 194 (1) (2009) 360–368, http://dx.doi.org/10.1016/j.jpowsour.2009.04.074, XIth Polish Conference on Fast Ionic Conductors 2008.

[45] P. Bubna, D. Brunner, S.G. Advani, A.K. Prasad, Prediction-based optimal power management in a fuel cell/battery plug-in hybrid vehicle, J. Power Sources 195 (19) (2010) 6699–6708, http://dx.doi.org/10.1016/j.jpowsour.2010.04.008.

[46] L. Guzzella, A. Sciarretta, Vehicle Propulsion Systems: Introduction to Modeling and Optimization, Springer, Berlin, Heidelberg, 2013, http://dx.doi.org/10.1007/978-3-642-35913-2.

List of scientific publications

International journals

- **S. Kofler**, E. Luchini, A. Schirrer, M. Fallmann, O. König, M. Kozek, C. Hametner, and S. Jakubek. Agent-based decentralized model predictive control for plants with multiple identical actuators. *IEEE Transactions on Control Systems Technology*, Volume 31, Issue 2, Pages 841–855, 2023. DOI: 10.1109/TCST.2022.3207354.

- **S. Kofler**, Z. P. Du, S. Jakubek, and C. Hametner. Predictive energy management strategy for fuel cell vehicles combining long-term and short-term forecasts. *IEEE Transactions on Vehicular Technology*, Volume 73, Issue 11, Pages 16364–16374, 2024. DOI: 10.1109/TVT.2024.3424422.

- **S. Kofler**, S. Jakubek, and C. Hametner. Predictive energy management strategy with optimal stack start/stop control for fuel cell vehicles. *Applied Energy*, Volume 377, Part B, Number 124513, 2025. DOI: 10.1016/j.apenergy.2024.124513.

- **S. Kofler**, G. Rammer, A. Schnabel, D. Weingrill, P. Bardosch, S. Jakubek, and C. Hametner. Real-vehicle experimental validation of a predictive energy management strategy for fuel cell vehicles. *Journal of Power Sources*, Volume 629, Number 235901, 2025. DOI: 10.1016/j.jpowsour.2024.235901.

International conferences

- Z. P. Du, **S. Kofler**, D. Ritzberger, S. Jakubek, and C. Hametner. Optimal Design of Experiments Model Predictive Controller. *IFAC-PapersOnLine*, Volume 56, Issue 2, Pages 11173–11178, 2023. 22nd IFAC World Congress. DOI: 10.1016/j.ifacol.2023.10.839.

- **S. Kofler**, Z. P. Du, S. Jakubek and C. Hametner. Adaptive step size dynamic programming for optimal energy management of fuel cell vehicles. *2023 IEEE Vehicle Power and Propulsion Conference (VPPC)*, Pages 1–6, 2023. DOI: 10.1109/VPPC60535.2023.10403120.

- **S. Kofler**, S. Jakubek, and C. Hametner. Cost-to-go-based predictive equivalent consumption minimization strategy for fuel cell vehicles considering route information. *2024 IEEE Intelligent Vehicles Symposium (IV)*, Pages 2910–2916, 2024. DOI: 10.1109/IV55156.2024.10588715.

Book contributions

- S. Daume, **S. Kofler**, J. Kager, P. Kroll, and C. Herwig. Generic workflow for the setup of mechanistic process models. In *Animal Cell Biotechnology. Methods in Molecular Biology*, Pages 189–211, Springer US, New York, NY, 2020. DOI: 10.1007/978-1-0716-0191-4_11.